POLITECNICO
MILANO 1863

SCUOLA DI INGEGNERIA INDUSTRIALE
E DELL'INFORMAZIONE

A State Observer Design for a Direct-Drive Wind Energy Conversion System

TESI DI LAUREA MAGISTRALE IN
ELECTRICAL ENGINEERING - INGEGNERIA ELETTRICA

Author: **Matteo Deponti**

Student ID: 978305
Advisor: Prof. Roberto Perini
Co-advisors: Dr. Dejan Pejovski
Academic Year: 2022-23

Abstract

In every drive-train, in which two or multiple rotating masses are mounted on the same shaft, torsional vibrations arise, due to the shaft's finite stiffness. The amplitude of the oscillations depends on the torque components acting on the system: if the latter ones have a frequency close to one of the system's torsional natural frequencies, a mechanical resonance condition is reached, which causes fatigue stress and decreases the system's reliability. A way to suppress torsional vibrations in a drive train is represented by the design of a PI-based State Space (SS) control scheme. This control needs a state observer for its operation, which is a mathematical tool that estimates all the system's state variables based on the available measurements.
In this thesis, the design of a state observer for a two Degree-of-Freedom (DOF) Wind Energy Conversion Systems (WECS), comprising a wind turbine directly connected to a Permanent Magnet Synchronous Generator (PMSG), is carried out. The aim is to reconstruct the state variables based on the information of the PMSG rotor's angular position and the direct and quadrature stator current components.
The mechanical and electrical models are derived first and an analysis of the torque harmonics produced by a Variable Frequency Drive (VFD) consisting of a Voltage Source Converter (VSC) with Pulse Width Modulation (PWM) is provided.
Then, the design of two different typologies of state observer is presented and a methodology to deal with the system's nonlinearities is proposed.
The first observer is represented by a Non-Linear Extended State Observer (NLESO): in this case, the system is linearized around the nominal operating point. After a subsystem decomposition, needed to transform the Multi-Input Multi-Output (MIMO) system into different Multi-Input Single-Output (MISO) ones, a procedure for state variables' estimates reconstruction based on a relative-degree analysis is defined. Also, a method to prove the convergence of the estimation error is provided. The observer's performance is evaluated based on computer simulation results from a Matlab Simulink model of the system.
The second type of observer consists of a Luenberger-based Lipschitz Observer. Its formulation is less cumbersome compared to the Non-Linear Extended State Observer

(NLESO) and deals directly with the nonlinear system, without any linearization. Also in this case, the observer is tested through computer simulations; the observers are compared based on simulation results and design complexity.

Keywords: Nonlinear, State Observer, Permanent Magnet Synchronous Generator, Wind Energy Conversion System

Abstract in lingua italiana

In ogni trasmissione, dove due o più masse rotanti sono calettate sullo stesso albero, le vibrazioni torsionali entrano in gioco a causa della finita rigidezza dell'albero. L'intensità di queste oscillazioni dipende dalle coppie meccaniche a cui il sistema è sottoposto: se queste hanno una frequenza vicina ad una delle frequenze naturali torsionali del sistema, una condizione di risonanza meccanica è raggiunta e ciò causa sforzi di fatica nell'albero e diminuisce la affidabilità del sistema. Un metodo per eliminare le vibrazioni torsionali in una trasmissione è rappresentato da un controllore Proporzionale-Integrativo (PI) in Spazio di Stato (SS). Questo tipo di controllore ha bisogno di un osservatore dello stato per il suo corretto funzionamento, ossia di un modello matematico che stima le variabili di stato basandosi sulle misure disponibili.
In questa tesi è effettuata la progettazione di un osservatore dello stato, per un sistema di conversione dell'energia eolica a due gradi di libertà, formato da una turbina eolica in collegamento diretto ad un generatore sincrono a magneti permanenti. L'obiettivo è quello di ricostruire le variabili di stato attraverso le misure di posizione angolare del rotore del generatore e delle componenti diretta e in quadratura delle correnti statoriche.
In primo luogo sono definiti il modello elettrico e meccanico ed è fornita un'analisi delle armoniche di coppia generate da un variatore di frequenza, formato da un inverter con modulazione PWM. Dopodichè è presentata la progettazione di due diverse tipologie di osservatore dello stato con una metodologia per gestire le nonlinearità presenti nel sistema.
Il primo è un Non-Linear Extended State Observer (NLESO): in questo caso, il sistema è linearizzato attorno al punto di lavoro nominale. Dopo una decomposizione in sottosistemi, necessaria per portare il sistema da una forma Multi-Input Multi-Output (MIMO) ad una Multi-Input Single-Output (MISO), è proposta una procedura per la ricostruzione delle stime delle variabili di stato basato sul cosiddetto grado relativo, così come un metodo per dimostrare la convergenza dell'errore di stima. Le prestazioni dell'osservatore sono valutate attraverso i risultati delle simulazioni a computer eseguite su un modello del sistema nell'ambiente Matlab Simulink.

Il secondo consiste in un osservatore Lipschitz basato sul modello di Luenberger. La sua formulazione è meno complessa rispetto a quella del Non-Linear Extended State Observer (NLESO) e opera direttamente con il sistema in forma nonlineare, quindi senza bisogno di una linearizzazione. Anche in questo caso le prestazioni dell'osservatore sono testate attraverso simulazioni a computer; viene poi fatto un confronto tra le due tipologie proposte, valutando i risultati ottenuti e la complessità di progettazione.

Parole chiave: Osservatore dello stato, Nonlineare, Generatore sincrono a magneti permanenti, Sistemi di conversione dell'energia eolica

Contents

Introduction

In recent years, renewable energy sources have come under increasing attention, mainly due to environmental concerns about global warming and de-carbonization policies. Among them, wind energy is becoming competitive with conventional sources of energy, with a cumulative installed capacity continuously increasing worldwide. In Wind Energy Conversion Systems (WECS), Permanent Magnet Synchronous Generators (PMSGs) are usually implemented in the so-called Type 4 configuration, where the generator is connected to the grid via a fully-rated power converter, constituting a Variable Frequency Drive (VFD). Regarding the PMSG topology, Multi-Modular Axial-Flux Permanent Magnet Synchronous Generators (MMAFPMSGs) are gaining attention for wind applications due to their relatively low aspect ratio (ratio between machine length and diameter) and high power densities, compared to the conventional Radial Flux Permanent Magnet (RFPM) machines.
In a multi-mass drive system, as in the case of an MMAFPMSG, the shaft's finite stiffness allows torsional oscillation between each rotating mass: if a torsional natural frequency is excited, a mechanical resonance condition occurs. Without a proper mitigation technique, torsional vibrations cause fatigue stress in the drive train and reliability issues.
Several methods to detect and mitigate torsional vibrations can be found in the literature and will be briefly introduced in the thesis. Among them, PI-based State Space control enhances the capability of a PI control implementing a state observer, which is a mathematical model that, based on the available system measurements, provides an estimate of the system's state variables. Beyond the implementation in a PI-based State Space control, a state observer allows estimating the variables that are physically difficult to measure, avoiding potentially complex and expensive measurement systems. This can be the case of a Multi-Modular Axial-Flux Permanent Magnet Synchronous Generator (MMAFPMSG), in which the measure of the inner rotors' angular positions represents a challenge: the little space available between the stator and rotor's disks, needed to keep a small air-gap, results in an unfeasible sensor implementation. It also increases the system's reliability: in fact, if designed properly, by comparing the esti-

mated values with the measured ones, sensors' faults can be detected.

Aim of the thesis

This thesis aims at designing a state observer for a two Degree-of-Freedom (DOF) drive system comprising a PMSG directly connected to a wind turbine. The mechanical and electrical models of the system are derived first. Two state observers will be proposed, each with its own formulation and performance analysis.

Structure of the thesis

The work will be divided into the following chapters:

1. State of the art: a brief overview of the thesis' main topics is proposed. First an introduction to Multi-Modular Axial-Flux Permanent Magnet (MMAFPM) machines is given, followed by the definition of the electrical model of a generic PMSG. Then, the torsional vibration concept from a theoretical point of view is introduced, together with the main methods for torsional vibration suppression present in the literature. Finally, a brief overview of the state observers is given.
2. Two Degree-of-Freedom System Definition: first, the overall system setup is presented. Then, the free vibration analysis of the mechanical system is carried out and the torsional natural frequencies are calculated. Moreover, the overall system is transformed into a per unit equivalent. A torque harmonic analysis is also provided.
3. Non-Linear Extended-State Observer: a Non-Linear Extended State Observer (NLESO) is designed for the system. To deal with the nonlinearities, a linearization around the nominal working point of the system is proposed, through a small perturbation analysis. After a complete observer design, its performance and observation accuracy are evaluated through simulation results.
4. Luenberger-based Lipschitz Observer: the design of a Lipschitz Observer is carried out in this chapter. Its stability properties are discussed and the performance is evaluated and compared to the NLESO, based on simulation results.

1 | State of the art

In this chapter, a brief overview of the main topics of this work is provided: first, an overall description of the Axial Flux Permanent Magnet Synchronous Generator (AFPMSG) is given, followed by an introduction to the problem of torsional vibrations. Finally, the concept of State Observer (SO) is summarized with a description of the most common observers.

1.1. Axial Flux Permanent Magnet Synchronous Generators

1.1.1. Machine Description

In recent years, Permanent Magnet Synchronous Generators (PMSGs) have received more attention in Wind Energy Conversion Systems (WECS), which play a key role in renewable power generation worldwide. The greater availability and decreasing cost of high-energy permanent-magnet materials, such as NdFeB magnets, have pushed the development and employment of these types of machines. PM machines feature higher efficiencies than machines with excitation windings due to the absence of field winding losses, also leading to less weight and a higher power factor. The use of PMs avoids the necessity to supply the magnetizing current to the rotor for constant air-gap flux. Moreover, the use of PMSG allows obtaining a direct-drive variable-speed WECS that does not require a gearbox, which implies a less efficient and less reliable system [9]. Completing the system, the power generated is then fed to the grid through a converter with an intermediate DC bus, which permits the generation at different speed levels separating the machine frequency from the grid one. It must be noted that directly driven Synchronous Generators (SGs) imply the presence of a larger number of pole pairs if compared to a mechanical transmission system configuration. An example of direct drive PMSG WECS design can be found in [23]: Figure 1.1 shows the schematic working principle.

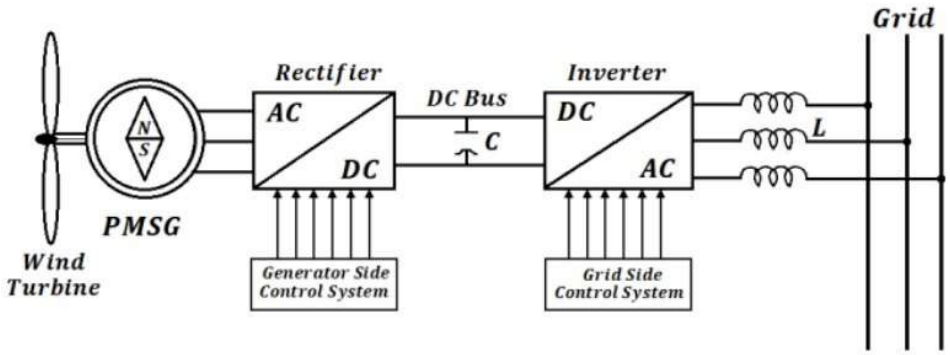

Figure 1.1: Electric scheme of a variable speed direct-drive PMSG WECS design.

The Axial Flux Permanent Magnet (AFPM) machine represents an attractive alternative to the classical Radial Flux Permanent Magnet (RFPM) one: in papers from the recent years, apart from the structural analyses of AFPM generators used in WECS, it is shown how this technology is used in several sectors [16]. Since a large number of poles can be accommodated on the rotor, these machines are ideal for low-speed applications [10].

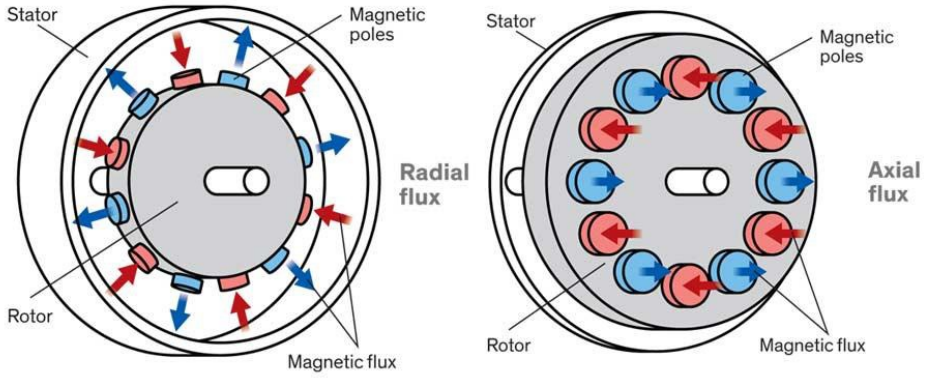

Figure 1.2: Simple scheme of an RFPM machine (left) and an AFPM machine (right)

Differently from the conventional radial flux machine in which the magnetic field is directed radially to the shaft axis, in an axial flux machine the field is parallel to it, as shown in Figure 1.2. In practice, axial flux machines are limited to three types: induction machines, PM DC commutator machines, and PM brushless DC and AC machines [10].
Brushless AFPM machines can be designed in different ways from a construction point of view, as it is well explained in [10]: they can be single-sided or double-sided, with

and without armature slots and armature cores, with internal or external PM rotors, with surface mounted or interior PMs, single stage or multi-stage machines.

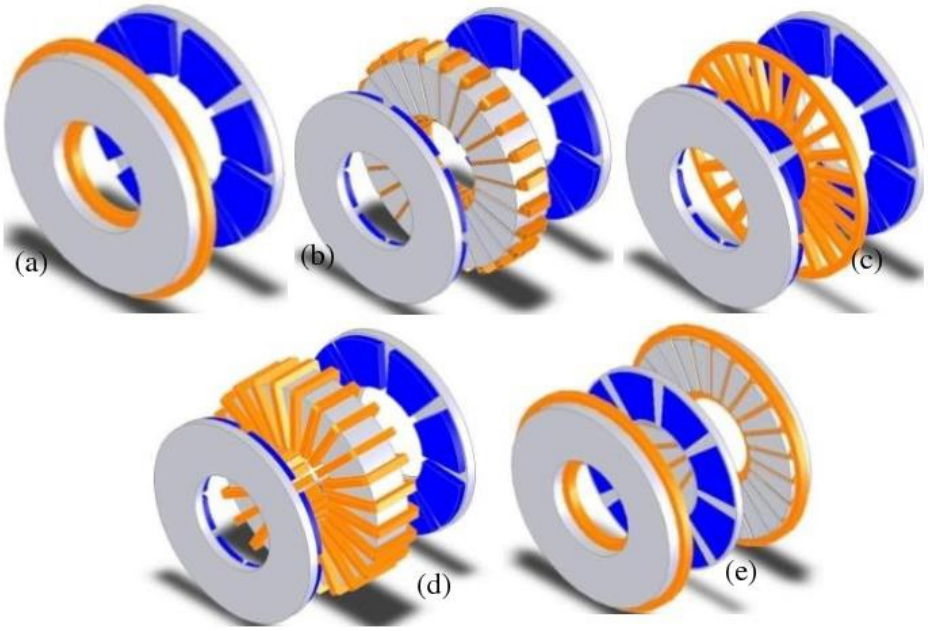

Figure 1.3: different types of AFPM machines: (a) 1-stator-1-rotor, (b) 1-stator-2-rotor (also called slotted TORUS type), (c) coreless 1-stator-2-rotor, (d) slotless TORUS and (e) 2-stator-1-rotor (also called AFIR type)

The different types of stators, rotors, and winding arrangements can be seen in Figure 1.3. The slotless winding configuration shows a much larger air gap; moreover, compared to a slotted winding one, it has the advantages of being simpler to assemble, it eliminates the problem of the cogging torque and it reduces rotor surface losses, magnetic saturation, and acoustic noises. The disadvantages are the need for more PM material and significant eddy current losses. Slotless AFPM machines are often classified to their winding arrangement and coil shapes: toroidal, trapezoidal, and rhomboidal forms. For what concerns the coreless configuration, it has the pro of eliminating eddy current and hysteresis core losses, also resulting in no magnetic attraction forces between the stator and rotor [10]. In [19], a performance comparison between traditional RFPM and different AFPM brushless machines is carried out, showing how the latter architecture provides a higher power density, thanks to the design which requires a lower volume, a lower rotor moment of inertia, mainly due to the shorter shaft needed, and less mass of iron. Moreover, in [3] a conventional RFPM and a two-stator-one-rotor AFPM synchronous motors for low-speed direct drive applications are

compared, concluding that the axial flux machine is an attractive solution for designs that require a high number of poles and short machine axial length.

1.1.2. Electrical Model

A brief introduction to the electrical model of a generic PMSG is here reported. For a three-phase PMSG, generic phase i stator line voltage equation is defined as:

$$v_{s,i} = R_s i_{s,i} + \frac{d\psi_{s,i}}{dt} \quad | \, i = a, b, c \tag{1.1}$$

where $v_{s,i}$ represents the stator phase voltage, $i_{s,i}$ the stator current, $\psi_{s,i}$ the stator flux linkage, and R_s the stator resistance. The flux linkage component can be defined as the sum of a leakage flux and a mutual flux:

$$\psi_{s,i} = L_\sigma i_{s,i} + \psi_{m,i} \quad | \, i = a, b, c \tag{1.2}$$

assuming that:

- $L_\sigma = L_{\sigma,i} \quad | \, i = a, b, c$;
- leakage flux links to only one winding at a time.

Thus, replacing (1.2) in (1.1):

$$v_{s,i} = R_s i_{s,i} + L_\sigma \frac{di_{s,i}}{dt} + \frac{d\psi_{m,i}}{dt} \quad | \, i = a, b, c \tag{1.3}$$

The mutual flux $\psi_{m,i}$ term could be derived considering the expression of the flux density in the air-gap, which is the sum of the flux density produced by the stator currents $i_{s,i}$ and the flux density produced by the Permanent Magnets (PMs) installed on the rotor. However, the latter analysis will not be reported here since it is out of the scope of this thesis: for a deeper examination please refer to [14]. For a generic three-phase electrical variable $f_i \quad | \, i = 1, 2, 3$, its space vector is defined as:

$$\mathbf{f} = k \left(f_1 + f_2 e^{j\frac{2\pi}{3}} + f_3 e^{-j\frac{2\pi}{3}} \right) \tag{1.4}$$

where k is an arbitrary constant and:

$$\begin{cases} f_\alpha = \mathfrak{Re}\{\mathbf{f}\} \\ f_\beta = \mathfrak{Im}\{\mathbf{f}\} \end{cases} \tag{1.5}$$

This change of coordinate is also known as $\alpha\beta$ or Clarke transformation. In this thesis, $k = \sqrt{\frac{2}{3}}$ is selected, which defines a power invariant transformation. Considering an isotropic machine, where the air gap is constant along the rotor, the expression of the stator voltage in space vector components is:

$$\mathbf{v}_s = R_s \mathbf{i}_s + L_s \frac{d\mathbf{i}_s}{dt} + \frac{d\psi_{\mathbf{PM}}}{dt} = R_s \mathbf{i}_s + L_s \frac{d\mathbf{i}_s}{dt} + j n_p \omega_m \, \psi_{PM} e^{j n_p \theta_m} \tag{1.6}$$

where:

- $L_s = L_\sigma + L_m \quad | \, L_m$: stator winding mutual inductance ;
- θ_m: rotor mechanical angular position;
- $n_p = \frac{p}{2}$: machine number of pole pairs, where p is the number of poles;
- $\psi_{\mathbf{PM}}$: space vector of the flux linkage due to the rotor PMs.

At the same time, the torque expression could be derived based on the Lorentz force that arises from the interaction between the stator current distribution and the flux density distribution inside the air gap: again, the complete derivation can be found in [14]. The electromagnetic torque produced by the machine is given by:

$$T = n_p \mathfrak{Im}\{\mathbf{i}_s \, {\psi_{\mathbf{PM}}}^*\} \tag{1.7}$$

Eventually, starting from (1.6) and multiplying both sides by $e^{-jp\theta_m}$ the space vector model can be referred to a coordinate system that rotates at the rotor speed, with the horizontal axis, namely the d-axis, parallel with the rotor flux vector $\psi_{\mathbf{PM}}$ and the vertical axis, or q-axis, perpendicular to it. Equation 1.6 can be split into the projections on the d-q axis, obtaining the so-called d-q stator voltage equations:

$$\begin{cases} v_{sd} = R_s i_{sd} + L_s \frac{di_{sd}}{dt} - n_p \omega_m L_s i_{sq} \\ v_{sq} = R_s i_{sq} + L_s \frac{di_{sq}}{dt} + n_p \omega_m L_s i_{sd} + n_p \omega_m \psi_{PM} \end{cases} \tag{1.8}$$

This latter change of coordinate is called dq or Park transformation.
Analogously, the torque expression in dq components is given by:

$$T = n_p \mathfrak{Im}\{\mathbf{i}_{sdq} \, {\psi_{\mathbf{PM}}}^*\} = n_p \mathfrak{Im}\{\mathbf{i}_{sdq} \, \psi_{PM} \, e^{-j n_p \theta_m}\} = n_p i_{sq} \psi_{PM} \tag{1.9}$$

This last relation leads to the conclusion that, for an isotropic PM machine, the torque is maximized when the stator current magnetic axis is perpendicular to the rotor PMs'

magnetic axis: for this reason, in Maximum Torque per Ampere (MTPA) control technique, the direct current i_{sd} reference value is kept equal to zero.

1.2. Torsional vibrations: problem definition and suppressing methods

1.2.1. Torsional vibrations fundamentals

Torsional vibration is a relative angular motion around the rotating axis between different points of a shaft. This deformation phenomenon is due to the shaft's finite stiffness: taking into consideration the simple example of a uniform beam, fixed on one end, subject to an external torque T, as shown in Figure 1.4, the angular displacement θ in [rad] on the free end will be given by:

$$\theta = T \frac{L}{G I_p} \tag{1.10}$$

where G is the material shear modulus, I_p is the polar moment of inertia and L is the length of the shaft.

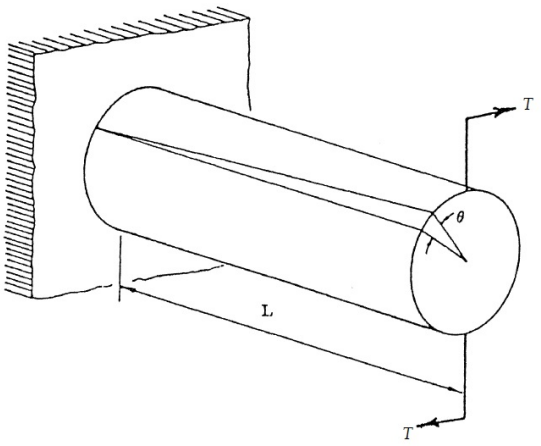

Figure 1.4: Torsional deformation of a beam subject to an external torque

Moreover, studying the free torsional vibration of the one Degree-of-Freedom (DOF) system above, which is described by the homogeneous second-order linear differential equation, called equation of motion, in the absence of the external torque and neglecting damping:

$$J\ddot{\theta} + K\theta = 0 \tag{1.11}$$

where J is the moment of inertia of the shaft and K its stiffness. The natural angular

frequency of the system is defined as:

$$\omega_n = \sqrt{\frac{K}{J}} \tag{1.12}$$

which is the angular frequency at which the undamped free response of the system occurs. The free vibration analysis for a one-degree of freedom system is well explained in [17]. The natural angular frequency concept is of utmost importance in the study of forced vibrations, so in the presence of an external forcing term acting on the system: in fact, a time-varying forcing term with a frequency equal to the system's natural one will lead to strong mechanical vibrations. A resonant condition happens when the forcing term frequency matches the natural frequency of the system: the harmonic response in this condition is only limited by the damping coefficient, and it tends to infinite for undamped systems.
These concepts can be extended to the analysis of an n-degrees-of-freedom system. A dynamic system has as many natural frequencies and modes of vibration as the number of degrees of freedom [17]. In each mode of vibration, the different system motions oscillate with their relative amplitude depending on the system properties.
Let us consider a direct drive WECS composed by a wind turbine and an AFPMSG, where the turbine and the different rotors are mounted onto the same shaft: this system can be modeled with a series of lumped torsional inertias, the rotating masses, connected by torsional springs and dissipative components which represent the shaft stiffness and damping coefficient, as it can be seen in Figure 1.5.

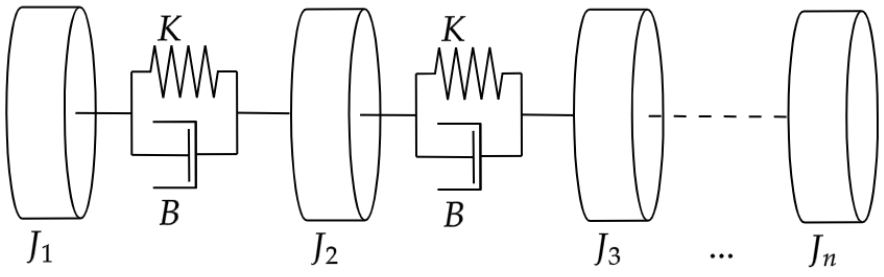

Figure 1.5: schematic representation of a multi-mass torsional system, where the shaft is represented by an equivalent torsional spring and dissipative component

By writing the equation of motion for each mass, neglecting damping and external forcing terms, a system of homogeneous second-order linear differential equations can be written. From this system, the characteristic equation can be obtained, which gives as solutions the natural angular frequencies of the system. The mathematical proce-

dure to find these last quantities is explained in detail in [17]. As in the case of the one DOF case, resonance occurs when the system is perturbed by a forcing term whose frequency corresponds to a natural angular frequency of the system. The presence of a torsional resonant vibration can lead to a shaft fault or to a fatigue failure if persistent in time, certainly depending on the mechanical stress intensity caused by the vibration.

1.2.2. Source of resonance in an electric machine system

In [21], different sources of resonance in a train traction system are discussed: in addition to mechanical vibrations caused by several mechanical components present in the system, the attention is brought to torque harmonics produced by the Variable Frequency Drive (VFD) of the motor. The rotational speed of an AC motor is dependent on the frequency of the electrical power supplied, which is controlled by the VFD. Thus, it is highlighted how pulsating torque components are caused by voltage and current harmonics and inter-harmonics coming from the VFD. If the pulsating torque frequencies coincide with the mechanical system's torsional natural frequencies, mechanical resonance occurs. Torsional vibration can also be intensified by cutting-load excitation with violent grid perturbations [11], in case generators connected to the transmission system. Considering the wind power generation sector, nowadays wind farms are asked to provide ancillary services such as voltage and frequency control, in order to improve the voltage and rotor angle stability of the system. In this situation, disturbances of the grid frequency can be a source of torsional vibrations, which can excite some resonant frequency [25].

1.2.3. Methods to suppress torsional vibrations

In the literature, several papers propose different methods to suppress torsional vibrations in a drive train.
A common solution in mitigating torsional oscillations is the use of a Band-pass Filter (BP): the generator speed value is fed to a BP to generate a torque ripple with appropriate frequency and phase. This ripple is then added to the torque reference and the vibration can be compensated [4].
Another way to damp torsional vibrations can be obtained using a Static Synchronous Compensator (STATCOM), particularly those due to grid voltage disturbances: in [28], a solution comprising a STATCOM and an Energy Storage System (ESS) is studied, to deal with torsional vibrations caused both by voltage sags and frequency devia-

tions. In [4], a Linear Quadratic Gaussian (LQG) control algorithm controller is used to suppress torsional vibrations: the controller modifies the generator torque reference inserting a specific damping torque. This latter one is derived by combining a Linear Quadratic Regulator (LQR) and a Kalman Filter (KF) for state estimation, working on the angular displacement and velocity differences between the rotating masses.
In [22], different control methods for damping torsional vibrations are briefly introduced, such as Sliding Mode Control (SMC), H_∞ control, Flatness-based Control (FBC) and Model Predictive-based Control (MPBC). Moreover, PI controllers, which are commonly used for the speed or position control of the drive system, can be tuned to reduce mechanical oscillations. However, the pole placement of the closed-loop system is very limited, resulting in not effective damping of torsional vibrations [22]. This is no more true if the control system is provided with complete information on the system state variables: indeed, in this case, the controller designer can set freely the poles of the system, as it is explained in [1]. This type of control is called State Space (SS) control. In SS control, the complete information on the state variables of the system is needed: however, the measurement of all the system states is not always possible in practical applications. For this reason, SOs are used, that is mathematical models that, taking as input the few measurements available from the system, give as output the estimate of each system's state variable.

1.3. State Observers

Considering a generic linear system of n states $\mathbf{x}(t) \in \mathbb{R}^n$, p inputs $\mathbf{u}(t) \in \mathbb{R}^p$ and q outputs $\mathbf{y}(t) \in \mathbb{R}^q$, its state space representation will be:

$$\begin{aligned} \dot{\mathbf{x}} &= \mathbf{A}\mathbf{x} + \mathbf{B}\mathbf{u} \\ \mathbf{y} &= \mathbf{C}\mathbf{x} + \mathbf{D}\mathbf{u} \end{aligned} \tag{1.13}$$

where $\mathbf{A} \in \mathbb{R}^{nxn}$, $\mathbf{B} \in \mathbb{R}^{nxp}$, $\mathbf{C} \in \mathbb{R}^{qxn}$ and $\mathbf{D} \in \mathbb{R}^{qxp}$.

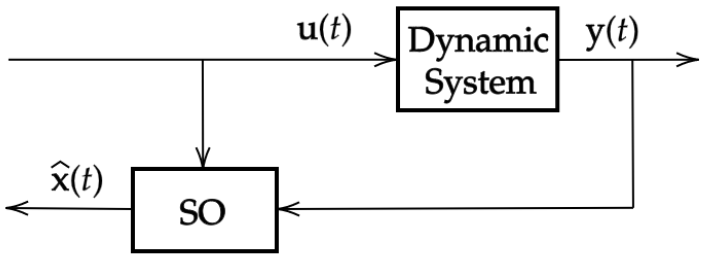

Figure 1.6: Simple block scheme of a SO

The SO is a system which, having as inputs $\mathbf{u}(t)$ and $\mathbf{y}(t)$, gives as output an estimation of the state variables $\hat{\mathbf{x}}(t)$, as shown in Figure 1.6; the quality of the estimation is measured through the observation error given by:

$$\mathbf{e} = \hat{\mathbf{x}} - \mathbf{x} \tag{1.14}$$

Different types of state observers exist, each of them with different robustness and mathematical model: in the following some typologies will be briefly introduced.

1.3.1. Trivial Observer

To understand better how a state observer works it is useful to start introducing the most trivial observer type, hence the copy of the State Space (SS) model of the system:

$$\dot{\hat{\mathbf{x}}} = \mathbf{A}\hat{\mathbf{x}} + \mathbf{B}\mathbf{u} \quad | \, \hat{\mathbf{x}}(0) = \hat{\mathbf{x}}_0 \tag{1.15}$$

where the value $\hat{\mathbf{x}}_0$ is the a priori estimate of the initial state; it must be noticed how this observer does not need the output information $y(t)$.

If the initial state was exactly known, such that:

$$\hat{\mathbf{x}}_0 = \mathbf{x}_0 \tag{1.16}$$

and if there was no uncertainty on the system matrices' parameters, this observer would be able to estimate the state variables' evolution. If (1.16) is not satisfied, then the estimation error defined in (1.14) would evolve according to the following differential equation:

$$\dot{\mathbf{e}} = \mathbf{A}\mathbf{e} \quad | \, \mathbf{e}(0) = \hat{\mathbf{x}}_0 - \mathbf{x}_0 \tag{1.17}$$

It is clear how the control design does not affect on the estimation error dynamics, which only depends on matrix $\mathbf{A}$, thus merely on the system properties: this is the main disadvantage that makes this type of observer unfeasible in practical application [1].

1.3.2. Luenberger Observer

The Luenberger observer formulation is given by:

$$\begin{aligned} \dot{\hat{\mathbf{x}}} &= \mathbf{A}\hat{\mathbf{x}} + \mathbf{B}\mathbf{u} + \mathbf{H}\left(\hat{\mathbf{y}} - \mathbf{y}\right) \quad | \, \hat{\mathbf{x}}(0) = \hat{\mathbf{x}}_0 \\ \hat{\mathbf{y}} &= \mathbf{C}\hat{\mathbf{x}} + \mathbf{D}\mathbf{u} \end{aligned} \tag{1.18}$$

where the matrix $\mathbf{H} \in \mathbb{R}^{nxq}$ is called the observer gain matrix and it represents a set of free parameters.
Now, following the observation error definition expressed in (1.14), subtracting (1.13) from (1.18) the observation error dynamic is obtained:

$$\begin{aligned} \dot{\mathbf{e}} &= \dot{\hat{\mathbf{x}}} - \dot{\mathbf{x}} \\ &= \mathbf{A}\hat{\mathbf{x}} + \mathbf{B}\mathbf{u} + \mathbf{H}\left(\hat{\mathbf{y}} - \mathbf{y}\right) - \mathbf{A}\mathbf{x} - \mathbf{B}\mathbf{u} \\ &= \mathbf{A}\hat{\mathbf{x}} + \mathbf{B}\mathbf{u} + \mathbf{H}\left(\mathbf{C}\hat{\mathbf{x}} - \mathbf{C}\mathbf{x}\right) - \mathbf{A}\mathbf{x} - \mathbf{B}\mathbf{u} \\ &= \left(\mathbf{A} + \mathbf{H}\mathbf{C}\right)\mathbf{e} \end{aligned} \tag{1.19}$$

It is clear how, choosing a correct gain matrix it is possible to select the correct pole placement working on the eigenvalues of matrix $\mathbf{N} = (\mathbf{A} + \mathbf{H}\mathbf{C}) \in \mathbb{R}^{nxn}$. If all the eigenvalues of $\mathbf{N}$ have a negative real part then the observation error tends to zero in a finite time. A necessary and sufficient condition for this observer is for the couple $(\mathbf{A}\ \mathbf{C})$ to be completely observable. This observer design is heavily dependent on the accuracy of the initial guess $\hat{\mathbf{x}}_0$ and of the mathematical model of the system, thus

of matrix **A**, **B**, **C** and, when present, **D**. This makes the Luenberger Observer not effective in system with high level of noise and uncertainty. [24]

1.3.3. Extended State Observer

In [8], a state observer for a Single-Input Single-Output (SISO) system in integral chain form with large uncertainty is defined, hence for a system of the kind:

$$\begin{cases} \dot{x}_1(t) = x_2(t); \\ \dot{x}_2(t) = x_3(t); \\ ... \\ \dot{x}_n(t) = f(t, x_1(t), x_2(t), ..., x_n(t)) + w(t) + u(t); \\ y = x_1 \end{cases} \tag{1.20}$$

where $w(t) \in \mathbb{R}$ is an external disturbance and $f : \mathbb{R}^{n+1} \to \mathbb{R}$ a possibly unknown system function. Defining the extended state and its derivative as:

$$\begin{cases} x_{n+1}(t) = f(t, x_1(t), x_2(t), ..., x_n(t)) + w(t); \\ \dot{x}_{n+1} = h(t) \end{cases} \tag{1.21}$$

and substituting (1.21) in (1.20), the following extended state system is obtained:

$$\begin{cases} \dot{x}_1(t) = x_2(t); \\ \dot{x}_2(t) = x_3(t); \\ ... \\ \dot{x}_n(t) = x_{n+1}(t) + u(t); \\ \dot{x}_{n+1} = h(t) \\ y = x_1 \end{cases} \tag{1.22}$$

Finally, the Extended State Observer (ESO) takes the form:

$$\begin{cases} \dot{\hat{x}}_1(t) = \hat{x}_2(t) - \alpha_1 g_1\left(\hat{y}_1 - y_1\right); \\ \dot{\hat{x}}_2(t) = \hat{x}_3(t) - \alpha_2 g_2\left(\hat{y}_1 - y_1\right); \\ \dots \\ \dot{\hat{x}}_n(t) = \hat{x}_{n+1}(t) - \alpha_n g_n\left(\hat{y}_1 - y_1\right) + u(t); \\ \dot{\hat{x}}_{n+1} = -\alpha_{n+1} g_{n+1}\left(\hat{y}_1 - y_1\right) \\ \hat{y_1} = \hat{x}_1 \end{cases} \tag{1.23}$$

where $\alpha_i \quad i = 1, ..., n, n+1$ are the observer gain coefficients and $g(.) : \mathbb{R} \to \mathbb{R}$ is a function that can be chosen linear or nonlinear: in the first case, the observer is called Linear Extended State Observer (LESO), while in the second case NLESO.
In the literature, several studies show that, for some nonlinear functions $g(.)$ and gains α_i, the ESO performs well in terms of adaptability, robustness, and anti-chattering. However, the estimation error system stability proof for the ESO is not an easy task: as an example, in [7] this last problem is addressed.

1.3.4. Other State Observers

In addition to the previously introduced observers, there are many other types of observers that can be found in the literature.
In [5], an Extended Kalman Filter (EKF) is used as a state observer in the control of a Permanent Magnet Synchronous Motor (PMSM). The EKF is an optimal algorithm which minimizes the mean square error of the estimated variables, considering the model inaccuracies and measurement noises. Although it guarantees good results, complex online computations performed on matrices makes this algorithm a time consuming process.
In [13], a Sliding Mode Observer (SMO) for the sensorless speed control of a PMSM is implemented. A good advantage of this state observer is that it is low affected by disturbances, under the assumption that the latter ones are bounded. Anyway, the observer does not provide a global state estimation convergence. Further information and details about this state observer can be found in [18].

2 | Two-Degree of Freedom System Definition

In this chapter, the system's setup and its mechanical and electrical model are defined. First, the overall system is shown, defining the main components composing it and the control scheme. Then, the system will be defined and analyzed from a mechanical point of view, through a free-vibration analysis to find its mechanical natural frequencies. To get all the state variables of the same order of magnitude, the model will be transformed into a per unit (p.u.) equivalent. Eventually, a torque harmonic analysis will be performed, considering that the PMSG is fed by a Voltage Source Converter (VSC) with Pulse Width Modulation (PWM).

2.1. System Setup

The overall system setup is shown in Figure 2.1. The PMSG, which produces an electromagnetic torque T_{elm}, is directly connected to the wind turbine, responsible for T_t. The generator feeds a Voltage Source Converter (VSC) with Pulse Width Modulation (PWM): the DC-bus voltage V_{DC} is controlled by a Grid Side Converter that keeps it at a constant value; its control and configuration are not considered in this work. The system control is made by an inner current control loop and an outer speed control loop:

- the current control loop comprises two current PI regulators, operating in the dq frame:
  - the stator current direct component's reference i_{sd}^{ref} is set to 0 based on a Maximum Torque per Ampere (MTPA) control;
  - the stator current quadrature component's reference i_{sd}^{ref} is given by the electromagnetic torque reference T_{elm}^{ref}, following the relation given in (1.9).

  The current loop cut-off frequency is set to $\omega_{cI} = 30\ [\frac{rad}{s}]$;

- the speed control loop follows a prescribed reference ω_1^{ref}. In this case, the cut-off frequency is set to $\omega_{c\Omega} = 3\,[\frac{rad}{s}]$

The control loops cut-off frequencies are chosen so that the control response in mechanical resonance condition is limited: in this way, the torsional vibrations are not damped by the control and the observers' performance can be properly evaluated in this condition, as it will be shown in the next chapters.
It is assumed that the 3-phase stator currents i_{abc} and the PMSG angular position θ_1 and velocity ω_1 are measured through specific sensors, without any noise and errors in the measurements.

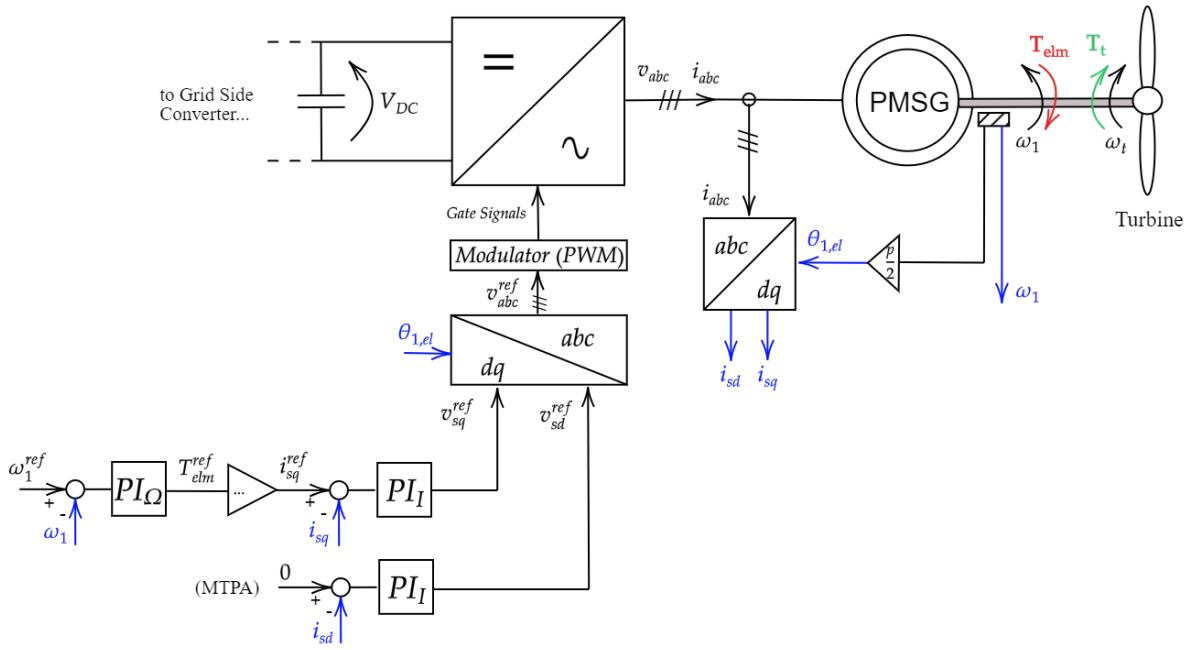

Figure 2.1: system setup comprising the control scheme with the speed and current control loops, electronic converter, PMSG directly connected to the wind turbine.

2.2. System mechanical and electrical model

2.2.1. Free Vibration analysis

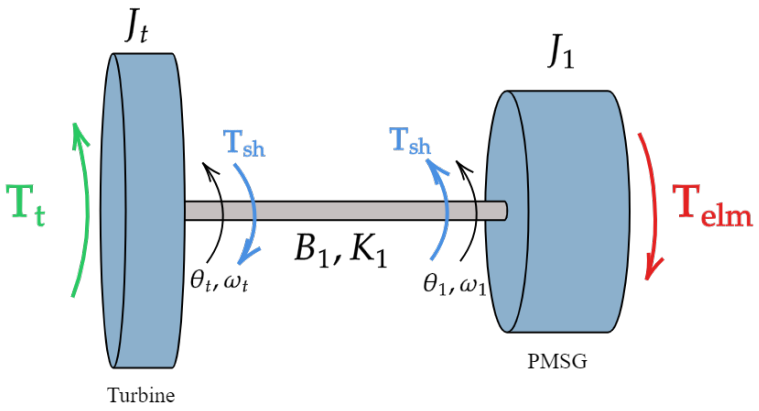

Figure 2.2: 2DOF system sketch; subscript t stands for turbine, while 1 refers to the rotor of the PMSG

The system comprises a wind turbine, working as a motor and producing a torque T_t, and a PMSG mounted on the same shaft, responsible for the electromagnetic torque T_{elm}: the system sketch can be seen in Figure 2.2. In particular, the shaft torque T_{sh}, defined as:

$$T_{sh} = K_1(\theta_t - \theta_1)$$

represent the torque that arises from the relative torsional motion between the two rotating masses. Its evaluation is important to assess the shaft's torsional stress, especially during mechanical resonance conditions, in which the difference $\theta_t - \theta_1$ reaches high values.
The system's mechanical and electrical parameters are listed in Table 2.1.

Table 2.1: PMSG and turbine parameters

PMSG and turbine parameters	
$P_n\ [MW]$	1.0
$T_n\ [Nm]$	$561{*}10^3$
$I_n\ [A]$	713
$V_{n,ph}\ [V]$	435
$f_n\ [Hz]$	14.73
$\Psi_{PM}\ [Wb]$	8.147
$poles\ (p)\ ;\ n_p = \frac{p}{2}$	104 ; 52
$R_s\ [m\Omega]$	14.59
$L_s\ [mH]$	4.321
$D_{out,stator}\ [mm]$	5586
$D_{out,rotor}\ [mm]$	5262
$K_{shaft} = K_1\ [\frac{Nm}{rad}]$	$1.2{*}10^{11}$
$J_{turbine} = J_t\ [kg\,m^2]$	$3{*}10^6$
$J_{rotor} = J_1\ [kg\,m^2]$	$3.36{*}10^6$

Let us first analyze the mechanical behavior of the system; in the following, the damping torque term in the dynamic equations will be neglected, its value being negligible compared to the others in the equation.
The equations of motion of the unforced 2DOF mechanical system are:

$$\begin{cases} J_t\dot{\omega}_t + K_1(\theta_t - \theta_1) = 0 \\ J_1\dot{\omega}_1 - K_1(\theta_t - \theta_1) = 0 \end{cases} \tag{2.1}$$

which, in matrix form can be expressed as:

$$[J][\ddot{\theta}] + [K][\theta] = 0 \tag{2.2}$$

where:

$$[\theta] = \begin{bmatrix} \theta_t \\ \theta_1 \end{bmatrix}; [J] = \begin{bmatrix} J_t & 0 \\ 0 & J_1 \end{bmatrix}; [K] = \begin{bmatrix} K_1 & -K_1 \\ -K_1 & K_1 \end{bmatrix}$$

Considering a simple harmonic motion as the solution of (2.1) [17], hence:

$$[\theta] = \begin{bmatrix} \theta_t \\ \theta_1 \end{bmatrix} = \begin{bmatrix} \hat{\theta}_t \cos(\omega t + \varphi) \\ \hat{\theta}_1 \cos(\omega t + \varphi) \end{bmatrix} \tag{2.3}$$

Now, substituting (2.3) in (2.2):

$$\begin{bmatrix} -J_t\omega^2 + K_1 & -K_1 \\ -K_1 & -J_1\omega^2 + K_1 \end{bmatrix} \begin{bmatrix} \hat{\theta}_t \cos(\omega t + \varphi) \\ \hat{\theta}_1 \cos(\omega t + \varphi) \end{bmatrix} = 0 \tag{2.4}$$

Simplifying the $cos()$ term of both rows, the natural frequencies of the system will be the solution of the characteristic equation, i.e.:

$$\det \begin{bmatrix} -J_t\omega^2 + K_1 & -K_1 \\ -K_1 & -J_1\omega^2 + K_1 \end{bmatrix} = 0 \tag{2.5}$$

Solving (2.5), the natural frequencies of the system are:

$$|f_{res}| = \left|\frac{\omega_{res}}{2\pi}\right| = \begin{bmatrix} 0 \\ 302.45 \end{bmatrix} [Hz] \tag{2.6}$$

2.2.2. Electrical and Mechanical model per unit transformation

In order to deal with mechanical and electrical state variables of similar order of magnitude, the entire system model is transformed into a p.u. equivalent model.
In the following, first both system models will be introduced denoting with superscript $*$ the variable original value, i.e. with dimensions. Then, once the p.u. transformation is fully defined, the superscript pu, firstly used to name the homonymous variables, will be neglected.
Starting from the mechanical model part, the base parameter for the transformation are:

- $\omega_{b,el} = 2\pi f_n = 92.55 \ \left[\frac{rad}{s}\right]$;
- $\omega_{b,mech} = \frac{\omega_{b,el}}{n_p} = 1.78 \ \left[\frac{rad}{s}\right]$;
- $T_b = T_n = 561 * 10^3 \ [Nm]$.

The mechanical system is given by the following equations of motion:

$$\begin{cases} J_t\dot{\omega_t^*} = -B_1(\omega_t^* - \omega_1^*) - K_1(\theta_t - \theta_1) + T_t \\ J_1\dot{\omega_1^*} = B_1(\omega_t^* - \omega_1^*) + K_1(\theta_t - \theta_1) - T_{elm} \end{cases} \tag{2.7}$$

The angular variables are not denoted with a superscript since they are already dimensionless.
Now, dividing all terms of (2.7) by $T_b = T_n$:

$$\begin{cases} \frac{J_t}{T_n}\dot{\omega_t^*} = -\frac{B_1}{T_n}(\omega_t^* - \omega_1^*) - \frac{K_1}{T_n}(\theta_t - \theta_1) + \frac{T_t}{T_n} \\ \frac{J_1}{T_n}\dot{\omega_t^*} = \frac{B_1}{T_n}(\omega_t^* - \omega_1^*) + \frac{K_1}{T_n}(\theta_t - \theta_1) - \frac{T_{elm}}{T_n} \end{cases} \tag{2.8}$$

and defining the inertia constant H_i as:

$$H_i = \frac{1}{2}\frac{J_i\omega_{b,mech}^2}{T_n\omega_{b,mech}} \quad | \, i = 1, t; \;\; \rightarrow \begin{cases} H_t = \frac{1}{2}\frac{J_t\omega_{b,mech}^2}{T_n\omega_{b,mech}} = 4.76 \;\; [s] \\ H_1 = \frac{1}{2}\frac{J_1\omega_{b,mech}^2}{T_n\omega_{b,mech}} = 0.053 \;\; [s] \end{cases} \tag{2.9}$$

the following system is obtained:

$$\begin{cases} \frac{2H_t}{\omega_{b,mech}}\dot{\omega_t^*} = -\frac{B_1}{T_n}(\omega_t^* - \omega_1^*) - \frac{K_1}{T_n}(\theta_t - \theta_1) + \frac{T_t}{T_n} \\ \frac{2H_1}{\omega_{b,mech}}\dot{\omega_1^*} = \frac{B_1}{T_n}(\omega_t^* - \omega_1^*) + \frac{K_1}{T_n}(\theta_t - \theta_1) - \frac{T_{elm}}{T_n} \end{cases} \tag{2.10}$$

Considering:

$$\omega_i^{pu} = \frac{\omega_i^*}{\omega_{b,mech}} \quad | \, i = 1, t; \tag{2.11}$$

and substituting (2.11) in system (2.10) it becomes:

$$\begin{cases} 2H_t\dot{\omega_t^{pu}} = -\frac{B_1\omega_{b,mech}}{T_n}(\omega_t^{pu} - \omega_1^{pu}) - \frac{K_1}{T_n}(\theta_t - \theta_1) + \frac{T_t}{T_n} \\ 2H_1\dot{\omega_1^{pu}} = \frac{B_1\omega_{b,mech}}{T_n}(\omega_t^{pu} - \omega_1^{pu}) + \frac{K_1}{T_n}(\theta_t - \theta_1) - \frac{T_{elm}}{T_n} \end{cases} \\ \begin{cases} \dot{\omega_t^{pu}} = -\frac{B_1\omega_{b,mech}}{2H_tT_n}(\omega_t^{pu} - \omega_1^{pu}) - \frac{K_1}{2H_tT_n}(\theta_t - \theta_1) + \frac{T_t}{2H_tT_n} \\ \dot{\omega_1^{pu}} = \frac{B_1\omega_{b,mech}}{2H_1T_n}(\omega_t^{pu} - \omega_1^{pu}) + \frac{K_1}{2H_1T_n}(\theta_t - \theta_1) - \frac{T_{elm}}{2H_1T_n} \end{cases} \tag{2.12}$$

As it was explained before, to simplify the writing the apex p.u. will not be shown in the following; hence, the mechanical p.u. system is defined as:

$$\begin{cases} \dot{\omega}_t = -\frac{B_1\omega_{b,mech}}{2H_tT_n}(\omega_t - \omega_1) - \frac{K_1}{2H_tT_n}(\theta_t - \theta_1) + \frac{T_t}{2H_tT_n} \\ \dot{\omega}_1 = \frac{B_1\omega_{b,mech}}{2H_1T_n}(\omega_t - \omega_1) + \frac{K_1}{2H_1T_n}(\theta_t - \theta_1) - \frac{T_{elm}}{2H_1T_n} \end{cases} \tag{2.13}$$

The base parameters for the electrical model p.u. transformation are:

- $V_b^{dq} = \sqrt[2]{3}V_{n,phase}^{abc} = 753.44 \;\; [V]$
- $I_b^{dq} = \sqrt[2]{3}I_n^{abc} = 1.23 * 10^3 \;\; [A]$
- $Z_b = \frac{V_b^{dq}}{I_b^{dq}} = 0.61 \;\; [\Omega]$

- $\omega_b = \omega_{b,el}$
- $L_b = \frac{Z_b}{\omega_b} = 6.6 * 10^{-3}\ [H]$
- $\psi_b = \frac{V_b^{dq}}{\omega_b} = 8.14\ [Wb]$

The electrical model comprises the d-q stator voltage equations of the PMSG, as found in Section 1.1.2. Thus, rewriting (1.8) denoting the state variables with apex $*$ and referring the mechanical quantities to the rotor of the PMSG, the original electrical model is:

$$\begin{cases} v_{sd}^* = R_s i_{sd}^* + L_s \frac{di_{sd}^*}{dt} - n_p \omega_1^* L_s i_{sq}^* \\ v_{sq}^* = R_s i_{sq}^* + L_s \frac{di_{sq}^*}{dt} + n_p \omega_1^* L_s i_{sd} + n_p \omega_1^* \psi_{PM}^* \end{cases} \tag{2.14}$$

To perform the p.u. transformation, first of all both equations of (2.14) are divided by V_b^{dq}, getting:

$$\begin{cases} \frac{v_{sd}^*}{V_b^{dq}} = \frac{R_s i_{sd}^*}{V_b^{dq}} + L_s \frac{di_{sd}^*}{dt} \frac{1}{V_b^{dq}} - \frac{n_p \omega_1^* L_s i_{sq}^*}{V_b^{dq}} \\ \frac{v_{sq}^*}{V_b^{dq}} = \frac{R_s i_{sq}^*}{V_b^{dq}} + L_s \frac{di_{sq}^*}{dt} \frac{1}{V_b^{dq}} + \frac{n_p \omega_1^* L_s i_{sd}}{V_b^{dq}} + \frac{n_p \omega_1^* \psi_{PM}^*}{V_b^{dq}} \end{cases} \tag{2.15}$$

Then, considering that:

- $\frac{v_{sdq}^*}{V_b^{dq}} = v_{sdq}^{pu}$;
- $\frac{R_s i_{sdq}^*}{V_b^{dq}} = \frac{R_s i_{sdq}^*}{V_b^{dq}} \frac{I_b^{dq}}{I_b^{dq}} = \frac{R_s}{Z_b} \frac{i_{sdq}^*}{I_b^{dq}} = r_s^{pu} i_{sdq}^{pu}$;
- $L_s \frac{di_{sdq}^*}{dt} \frac{1}{V_b^{dq}} = L_s \frac{di_{sdq}^*}{dt} \frac{1}{V_b^{dq}} \frac{I_b^{dq}}{I_b^{dq}} \frac{\omega_b}{\omega_b} = \frac{L_s}{L_b} \frac{di_{sdq}^*}{dt} \frac{1}{I_b^{dq}} \frac{1}{\omega_b} = \frac{l_s^{pu}}{\omega_b} \frac{di_{sdq}^{pu}}{dt}$;
- $\frac{n_p \omega_1^* L_s i_{sdq}^*}{V_b^{dq}} = \frac{n_p \omega_1^* L_s i_{sdq}^*}{V_b^{dq}} \frac{I_b^{dq}}{I_b^{dq}} \frac{\omega_b}{\omega_b} = \frac{n_p \omega_1^*}{\omega_b} \frac{L_s}{L_b} \frac{i_{sdq}^*}{I_b^{dq}} = \omega_1^{pu} l_s^{pu} i_{sdq}^{pu}$;
- $\frac{n_p \omega_1^* \psi_{PM}^*}{V_b^{dq}} = \frac{n_p \omega_1^* \psi_{PM}^*}{V_b^{dq}} \frac{\omega_b}{\omega_b} = \frac{n_p \omega_1^*}{\omega_b} \frac{\psi_{PM}^*}{\psi_b} = \omega_1^{pu} \psi_{PM}^{pu}$;

it follows that system (2.15) becomes:

$$\begin{cases} v_{sd}^{pu} = r_s^{pu} i_{sd}^{pu} + \frac{l_s^{pu}}{\omega_b} \frac{di_{sd}^{pu}}{dt} - \omega_1^{pu} l_s^{pu} i_{sq}^{pu} \\ v_{sq}^{pu} = r_s^{pu} i_{sq}^{pu} + \frac{l_s^{pu}}{\omega_b} \frac{di_{sq}^{pu}}{dt} + \omega_1^{pu} l_s^{pu} i_{sd}^{pu} + \omega_1^{pu} \psi_{PM}^{pu} \end{cases} \tag{2.16}$$

Considering that to simplify the writing the apex p.u. will not be shown in the following and rearranging the terms to make $\frac{di_{sdq}}{dt} = \dot{i_{sdq}}$ explicit, the following system is obtained:

$$\begin{cases} \dot{i_{sd}} = -r_s \frac{\omega_b}{l_s} i_{sd} + \omega_b i_{sq} \omega_1 + \frac{\omega_b}{l_s} v_{sd} \\ \dot{i_{sq}} = -r_s \frac{\omega_b}{l_s} i_{sq} - \omega_b i_{sd} \omega_1 - \frac{\omega_b}{l_s} \psi_{PM} \omega_1 + \frac{\omega_b}{l_s} v_{sq} \end{cases} \tag{2.17}$$

Eventually, the complete system of differential equations, comprising the mechanical and electrical p.u. models, is:

$$\begin{cases} \dot{\omega}_t = -\frac{B_1\omega_{b,mech}}{2H_tT_n}(\omega_t - \omega_1) - \frac{K_1}{2H_tT_n}(\theta_t - \theta_1) + \frac{T_t}{2H_tT_n} \\ \dot{\omega}_1 = \frac{B_1\omega_{b,mech}}{2H_1T_n}(\omega_t - \omega_1) + \frac{K_1}{2H_1T_n}(\theta_t - \theta_1) - \frac{T_{elm}}{2H_1T_n} \\ \dot{i_{sd}} = -r_s\frac{\omega_b}{l_s}i_{sd} + \omega_b i_{sq}\omega_1 + \frac{\omega_b}{l_s}v_{sd} \\ \dot{i_{sq}} = -r_s\frac{\omega_b}{l_s}i_{sq} - \omega_b i_{sd}\omega_1 - \frac{\omega_b}{l_s}\psi_{PM}\omega_1 + \frac{\omega_b}{l_s}v_{sq} \end{cases} \tag{2.18}$$

Taking into consideration that:

- $\dot{\theta}_t = \omega_{b,mech}\omega_t$;
- $\dot{\theta}_1 = \omega_{b,mech}\omega_1$;
- the measurements of θ_1, i_{sd} and i_{sq} are available from the system;

system (2.18) can be updated, denoting with y the measured state variables:

$$\begin{cases} \dot{\theta}_t = \omega_{b,mech}\omega_t \\ \dot{\theta}_1 = \omega_{b,mech}\omega_1 \\ \dot{\omega}_t = -\frac{B_1\omega_{b,mech}}{2H_tT_n}(\omega_t - \omega_1) - \frac{K_1}{2H_tT_n}(\theta_t - \theta_1) + \frac{T_t}{2H_tT_n} \\ \dot{\omega}_1 = \frac{B_1\omega_{b,mech}}{2H_1T_n}(\omega_t - \omega_1) + \frac{K_1}{2H_1T_n}(\theta_t - \theta_1) - \frac{T_{elm}}{2H_1T_n} \\ \dot{i_{sd}} = -r_s\frac{\omega_b}{l_s}i_{sd} + \omega_b i_{sq}\omega_1 + \frac{\omega_b}{l_s}v_{sd} \\ \dot{i_{sq}} = -r_s\frac{\omega_b}{l_s}i_{sq} - \omega_b i_{sd}\omega_1 - \frac{\omega_b}{l_s}\psi_{PM}\omega_1 + \frac{\omega_b}{l_s}v_{sq} \\ y_1 = \theta_1 \\ y_2 = i_{sd} \\ y_3 = i_{sq} \end{cases} \tag{2.19}$$

2.2.3. Torque harmonics analysis

As already discussed in Section 1.2.2, pulsating torque components are caused by harmonics and inter-harmonics coming from the VFD which supplies the machine. The analytical derivation of harmonic torque components generated by the interaction between stator voltage and current harmonics is provided in Appendix A.1.
In the case under analysis, the following hypotheses are made:

- the PMSG stator is supplied with a 3-phase VSC with PWM;
- modulation frequency ratio: $m_f = \frac{f_{sw}}{f_c} = 33$ where:
  - f_{sw} is the switching frequency;

  - f_c is the carrier signal frequency;

- the VSC operates in linear modulation and produces only voltage harmonics of order:

$$h_v = m\, m_f + n \quad | \, m \in \mathbb{N}, n \in \mathbb{Z}$$

  where:

  - if m is even then n is odd;
  - if m is odd then n is even;

- since the machine is a synchronous generator, the fundamental angular frequency of the stator voltage ω_{fund} corresponds to the rotor electrical angular frequency $\omega_{r,el}$:

$$\omega_{fund} = \omega_{r,el} = \frac{p}{2}\omega_{r,mech} \quad | \, \omega_{r,mech} = \text{rotor mechanical angular frequency}$$

  - in this analysis: $\omega_{r,mech} = \omega_1$;

- the machine operates in the range: $\omega_{r,el} \in [0.3\omega_n \, ; \, \omega_n]$.

The voltage harmonics spectrum of a PWM VSC for $h_v > 1$ is characterized by higher order harmonics divided into m groups each one composed of n components that rapidly decay in magnitude as $|n|$ increases. Being the torque harmonic's amplitude directly related to the voltage harmonic's one, just the following indices were considered:

- $m = 1, 2, 3, 4$;
- $n = 0, \pm1, \pm2, \pm3, \pm4$

Based on the previous assumptions, the harmonic indexes h_v present in the stator voltage are listed in Table 2.2.

Table 2.2: Stator voltage harmonic indexes h_v for the considered m and n when $m_f = 33$

Stator voltage harmonic indexes

h_v		n								
		0	±1		±2		±3		±4	
m	1	33	0	0	35	31	0	0	37	29
	2	0	67	65	0	0	69	63	0	0
	3	99	0	0	101	97	0	0	103	95
	4	0	133	131	0	0	135	129	0	0

Now, the voltage harmonic of index h_v generates a torque harmonic component of index h_T given by the following relation:

$$\begin{cases} h_T = h_v - 1 & \text{if the stator voltage harmonic of order } h_v \text{ is a positive sequence harmonic} \\ h_T = h_v + 1 & \text{if the stator voltage harmonic of order } h_v \text{ is a negative sequence harmonic} \\ \text{Null torque} & \text{if the stator voltage harmonic of order } h_v \text{ is a zero sequence harmonic} \end{cases}$$

Therefore, by identifying the harmonic sequence typology through the following rules:

- h_v represents a positive sequence harmonic if: $h_v = 6k + 1 \quad | k \in \mathbb{N}$;
- h_v represents a negative sequence harmonic if: $h_v = 6k - 1 \quad | k \in \mathbb{N}$;
- h_v represents a zero sequence harmonic if: $h_v = 3k \quad | k \in \mathbb{N}$;

the torque harmonic indexes given by a h_v voltage component defined by a specific m and n are listed in Table 2.3

Table 2.3: Torque harmonic indexes h_T produced by a specific h_v, defined by specific values of m and n when $m_f = 33$

Stator voltage harmonic indexes

h_T		n								
		0	±1		±2		±3		±4	
m	1	0	0	0	36	30	0	0	36	30
	2	0	66	66	0	0	0	0	0	0
	3	0	0	0	102	96	0	0	102	96
	4	0	132	132	0	0	0	0	0	0

Recalling that this analysis aims to detect the torque harmonic components that excite the resonance frequency of the system, a useful tool to be used is the Campbell diagram, in which the forcing terms' frequencies acting on the system are plotted together with the natural frequencies of the system, in $[Hz]$, as a function of the machine rotating speed, usually in $[rpm]$.
In this case, the forcing terms are represented by the torque harmonic components previously described. Defining with f_{exc,h_T} the excitation frequency component related to the torque harmonic of order h_T, and reminding that, for a synchronous machine, the stator voltage fundamental frequency f_{fund} is related to the rotor angular speed through:

$$f_{fund} = \frac{\omega_{r,el}}{2\pi}$$

f_{exc,h_T} can be calculated as:

$$f_{exc,h_T} = h_T f_{fund} = h_T \frac{\omega_{r,el}}{2\pi} = h_T \frac{p\omega_{r,mech}}{4\pi} = h_T \frac{p\omega_1}{4\pi}$$

which puts in evidence the relation between the f_{exc,h_T} and the rotor angular speed. Concerning the system's natural frequencies, they are depicted by horizontal lines in the diagram, being independent of the machine speed; in this case, the natural frequencies of the system were found in Section 2.2.1:

$$|f_{res}| = \left|\frac{\omega_{res}}{2\pi}\right| = \begin{bmatrix} 0 \\ 302.45 \end{bmatrix} [Hz]$$

Typically, in the Campbell diagram, the operating region of the machine is defined drawing two vertical lines, which represent the speed range of the machine; in this case it was assumed that the machine operates within 30% and 100% of the nominal speed $\omega_{n,mech}$:

$$\omega_{n,mech} = \frac{2}{p}\omega_{n,el} = \frac{4\pi f_n}{p} = \frac{4\pi 14.73}{104} = 1.78\left[\frac{rad}{s}\right] \approx 17\,[rpm]$$

The Campbell diagram of the system under analysis is shown in Figure 2.3.

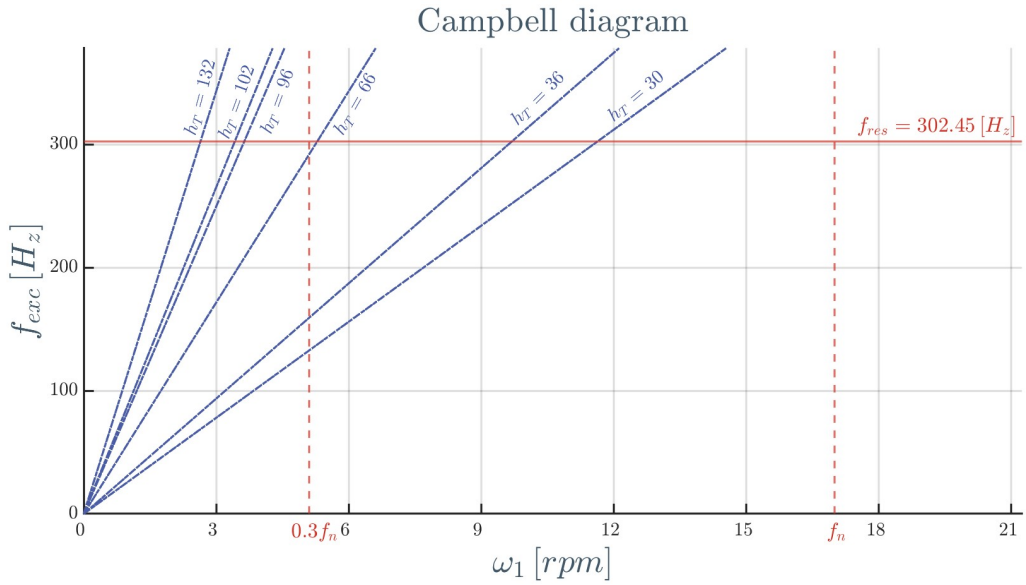

Figure 2.3: Campbell diagram showing the VSC produced torque harmonics which excite the resonance frequency of the system

Based on what is shown in the diagram, the torque harmonics' components h_T exciting the resonance frequency in the operating region are:

- $h_T = 30$ when the rotor spins at: $\omega_{r,mech} = \omega_1 = \frac{4\pi}{p}\frac{f_{res}}{h_T} = 1.22\left[\frac{rad}{s}\right] = 11.6\,[rpm]$;
- $h_T = 36$ when the rotor spins at: $\omega_{r,mech} = \omega_1 = \frac{4\pi}{p}\frac{f_{res}}{h_T} = 1.01\left[\frac{rad}{s}\right] = 9.69\,[rpm]$;
- $h_T = 66$ when the rotor spins at: $\omega_{r,mech} = \omega_1 = \frac{4\pi}{p}\frac{f_{res}}{h_T} = 0.55\left[\frac{rad}{s}\right] = 5.29\,[rpm]$;

3 | Non-Linear Extended State Observer

In this chapter, the design of a Non-Linear Extended State Observer (NLESO) for the system is carried out. To deal with the system's nonlinearities and to properly design the observer, the model is linearized around the nominal working point. Then, the system is divided into three different Multi-Input Single-Output (MISO) subsystems, each one with a dedicated state observer: the different estimates are then processed to extract the best state estimations. The design of a NLESO is important to estimate all the linearized system's state variables, including the non-measured ones, and to evaluate the shaft torque T_{sh} component during mechanical resonance conditions. The observer's performance is evaluated through a computer simulation by examining the estimates' accuracy.

3.1. Non-Linear Extended State Observer design

3.1.1. System Linearization

As it can be seen from (2.19), the system is nonlinear due to the following terms:

- i_{sd} equation: $\omega_b i_{sq} \omega_1$;
- i_{sq} equation: $\omega_b i_{sd} \omega_1$.

The first strategy adopted, accordant to what is usually done when dealing with non-linear systems, is to linearize the system around a working point, thus working with a linear system instead.
Therefore, the idea is to start linearizing the system around a specific working point and then transform it into an integral-chain form through a state variable transformation, needed for the design of NLESO (see Section 1.3.3).
The linearization follows a small perturbation analysis concept: in fact, as already discussed in Section 1.2.3, the state observer implementation aims to estimate the tor-

sional vibrations occurring on the shaft, which consist of oscillating phenomena. This last concept permits to split a generic state variable $x(t)$ into the sum of a continuous steady state term x_0 and an oscillating one (small perturbation) $\Delta x(t)$:

$$x(t) = x_0 + \Delta x(t) \tag{3.1}$$

Following this concept, system (2.19) can be seen as:

$$\begin{cases} \dot{\theta_{t0}} + \Delta\dot{\theta}_t = (\omega_{t0} + \Delta\omega_t)\,\omega_{b,mech} \\ \dot{\theta}_{10} + \Delta\dot{\theta}_1 = (\omega_{10} + \Delta\omega_1)\,\omega_{b,mech} \\ (\dot{\omega_{t0}} + \Delta\dot{\omega}_t) = -\frac{K_1}{2H_tT_n}\,(\theta_{t0} + \Delta\theta_t - \theta_{10} - \Delta\theta_1) + \frac{1}{2H_tT_n}\,(T_{t0} + \Delta T_t) \\ (\dot{\omega_{10}} + \Delta\dot{\omega}_1) = \frac{K_1}{2H_1T_n}\,(\theta_{t0} + \Delta\theta_t - \theta_{10} - \Delta\theta_1) - \frac{n_p(I_b\psi_b)\psi_{PM}}{2H_1T_n}\,(i_{sq0} + \Delta i_{sq}) \\ \left(\dot{i}_{sd0} + \Delta\dot{i}_{sd}\right) = -r_s\frac{\omega_b}{l_s}\,(i_{sd0} + \Delta i_{sd}) + \omega_b\,(i_{sq0} + \Delta i_{sq})\,(\omega_{10} + \Delta\omega_1) + \\ \qquad +\frac{\omega_b}{l_s}\,(v_{sd0} + \Delta v_{sd}) \\ \left(\dot{i_{sq0}} + \Delta\dot{i}_{sq}\right) = -r_s\frac{\omega_b}{l_s}\,(i_{sq0} + \Delta i_{sq}) - \omega_b\,(i_{sd0} + \Delta i_{sd})\,(\omega_{10} + \Delta\omega_1) - \\ \qquad -\frac{\omega_b}{l_s}\psi_{PM}\,(\omega_{10} + \Delta\omega_1) + \frac{\omega_b}{l_s}\,(v_{sq0} + \Delta v_{sq}) \\ y_1 = y_{10} + \Delta y_1 = \theta_1 = \theta_{10} + \Delta\theta_1 \\ y_2 = y_{20} + \Delta y_2 = i_{sd} = i_{sd0} + \Delta \mathrm{i}_{sd} \\ y_3 = y_{30} + \Delta y_3 = i_{sq} = i_{sq0} + \Delta i_{sq} \end{cases} \tag{3.2}$$

Now, splitting (3.2) with respect to the continuous and oscillating terms, two subsystems can be obtained:

$$\text{Steady State} \begin{cases} \dot{\theta_{t0}} = \omega_{b,mech}\omega_{t0} \\ \dot{\theta_{10}} = \omega_{b,mech}\omega_{10} \\ \dot{\omega_{t0}} = -\frac{K_1}{2H_tT_n}\,(\theta_{t0} - \theta_{10}) + \frac{T_{t0}}{2H_tT_n} \\ \dot{\omega_{10}} = \frac{K_1}{2H_1T_n}\,(\theta_{t0} - \theta_{10}) - \frac{n_p(I_b\psi_b)\psi_{PM}}{2H_1T_n}i_{sq0} \\ \dot{i_{sd0}} = -r_s\frac{\omega_b}{l_s}i_{sd0} + \omega_b\omega_{10}i_{sq0} + \frac{\omega_b}{l_s}v_{sd0} \\ \dot{i_{sq0}} = -r_s\frac{\omega_b}{l_s}i_{sq0} - \omega_b\omega_{10}i_{sd0} - \frac{\omega_b}{l_s}\psi_{PM}\omega_{10} + \frac{\omega_b}{l_s}v_{sq0} \\ y_{10} = \theta_{10} \\ y_{20} = i_{sd0} \\ y_{30} = i_{sq0} \end{cases} \tag{3.3}$$

$$\text{Small Perurbations } (\Delta) \begin{cases} \dot{\Delta\theta_t} = \omega_{b,mech}\Delta\omega_t \\ \dot{\Delta\theta_1} = \omega_{b,mech}\Delta\omega_1 \\ \dot{\Delta\omega_t} = -\frac{K_1}{2H_tT_n}\left(\Delta\theta_t - \Delta\theta_1\right) + \frac{\Delta T_t}{2H_tT_n} \\ \dot{\Delta\omega_1} = \frac{K_1}{2H_1T_n}\left(\Delta\theta_t - \Delta\theta_1\right) - \frac{n_p(I_b\psi_b)\psi_{PM}}{2H_1T_n}\Delta i_{sq} \\ \dot{\Delta i_{sd}} = -r_s\frac{\omega_b}{l_s}\Delta i_{sd} + \omega_b\omega_{10}\Delta i_{sq} + \omega_b i_{sq0}\Delta\omega_1 + \\ \qquad +\omega_b\Delta i_{sq}\Delta\omega_1 + \frac{\omega_b}{l_s}\Delta v_{sd} \\ \dot{\Delta i_{sq}} = -r_s\frac{\omega_b}{l_s}\Delta i_{sq} - \omega_b\omega_{10}\Delta i_{sd} - \omega_b i_{sd0}\Delta\omega_1 - \\ \qquad -\omega_b\Delta\omega_1\Delta i_{sd} - \frac{\omega_b}{l_s}\psi_{PM}\Delta\omega_1 + \frac{\omega_b}{l_s}\Delta v_{sq} \\ \Delta y_1 = \Delta\theta_1 \\ \Delta y_2 = \Delta i_{sd} \\ \Delta y_3 = \Delta \mathrm{i_{sq}} \end{cases} \tag{3.4}$$

Assuming that:

1. at steady state:
   (a) $\dot{\omega_{10}} = \dot{\omega_{t0}} = 0$ with $\omega_{t0} = \omega_{10} = \omega_{ref,SS}$;
   (b) $\dot{i_{sd0}} = 0$ with $i_{sd0} = 0$ (MTPA);
   (c) $\dot{i_{sq0}} = 0$ with $i_{sq0} = \frac{T_{elm,0}}{n_p(I_b\psi_b)\psi_{PM}}$;
2. for generic state variables x_i and x_j: $|\Delta x_i \Delta x_j| << |x_{i0}\Delta x_j| \quad |\, \forall i, j$;
3. $\Delta T_t \approx 0 \leftrightarrow T_{t0} = T_t$: no oscillating torque acting on the turbine;

the two systems in (3.4) become:

$$\text{Steady State } \begin{cases} \dot{\theta_{t0}} = \omega_{b,mech}\omega_{t0} \\ \dot{\theta_{10}} = \omega_{b,mech}\omega_{10} \\ 0 = -\frac{K_1}{2H_tT_n}\left(\theta_{t0} - \theta_{10}\right) + \frac{T_{t0}}{2H_tT_n} \\ 0 = \frac{K_1}{2H_1T_n}\left(\theta_{t0} - \theta_{10}\right) - \frac{T_{elm,0}}{2H_1T_n} \\ 0 = \omega_b\omega_{10}i_{sq0} + \frac{\omega_b}{l_s}v_{sd0} \\ 0 = -r_s\frac{\omega_b}{l_s}i_{sq0} - \frac{\omega_b}{l_s}\psi_{PM}\omega_{10} + \frac{\omega_b}{l_s}v_{sq0} \\ y_{10} = \theta_{10} \\ y_{20} = i_{sd0} \\ y_{30} = i_{sq0} \end{cases} \tag{3.5}$$

$$\text{Small pert. } (\Delta) \begin{cases} \dot{\Delta\theta_t} = \omega_{b,mech}\Delta\omega_t \\ \dot{\Delta\theta_1} = \omega_{b,mech}\Delta\omega_1 \\ \dot{\Delta\omega_t} = -\frac{K_1}{2H_tT_n}\left(\Delta\theta_t - \Delta\theta_1\right) \\ \dot{\Delta\omega_1} = \frac{K_1}{2H_1T_n}\left(\Delta\theta_t - \Delta\theta_1\right) - \frac{n_p(I_b\psi_b)\psi_{PM}}{2H_1T_n}\Delta i_{sq} \\ \dot{\Delta i_{sd}} = -r_s\frac{\omega_b}{l_s}\Delta i_{sd} + \omega_b\omega_{10}\Delta i_{sq} + \omega_b i_{sq0}\Delta\omega_1 + \frac{\omega_b}{l_s}\Delta v_{sd} \\ \dot{\Delta i_{sq}} = -r_s\frac{\omega_b}{l_s}\Delta i_{sq} - \omega_b\omega_{10}\Delta i_{sd} - \frac{\omega_b}{l_s}\psi_{PM}\Delta\omega_1 + \frac{\omega_b}{l_s}\Delta v_{sq} \\ \Delta y_1 = \Delta\theta_1 \\ \Delta y_2 = \Delta i_{sd} \\ \Delta y_3 = \Delta \mathrm{i_{sq}} \end{cases} \tag{3.6}$$

From the equations of (3.5) it can be found that:

- $T_{t0} = T_t = K_1\left(\theta_{t0} - \theta_{10}\right) = T_{elm,0}$;
- $v_{sd0} = -l_s\omega_{10}i_{sq0}$;
- $v_{sq0} = r_s i_{sq0} + \psi_{PM}\omega_{10}$.

From now on in this section, the focus will be entirely on (3.6), the oscillating (or Δ) system that, as expected, is linear. Therefore, the observer designed for this system will aim at estimating the oscillating terms of the state variables, which contain the evolution of the resonant phenomenon of interest.
The linearization should be performed around the working point of the system; however, this would mean calculating each time a linearized model based on the operating condition under analysis. For this reason, a single linearization is considered and performed once around the nominal working point of the system, i.e. when:

$$\omega_{n,mech} = \frac{2}{p}\omega_{n,el} = \frac{4\pi f_n}{p} = \frac{4\pi 14.73}{104} = 1.78\left[\frac{rad}{s}\right] \approx 17\,[rpm]$$

A wind turbine, rotating at Ω and operating under a wind speed v_{wind}, produces a torque given by:

$$T_t = \frac{1}{2}\,\rho\,\frac{C_p(\lambda_{tip-speed})}{\frac{2}{D_t}\lambda_{tip-speed}}\,\frac{\pi D_t^2}{4}\,v_{wind}^2$$

where ρ is the air density, D_t is the turbine diameter, $\lambda_{tip-speed} = \frac{\frac{D}{2}\Omega}{v_{wind}}$ is the tip-speed ratio and $C_p(\lambda)$ is the power coefficient as a function of $\lambda_{tip-speed}$.
At $\omega_{n,mech}$, the wind turbine torque is assumed to be:

$$T_{t0} = T_{elm,0} = 7.87 * 10^5\,[Nm]$$

Hence, the following variables can be calculated:

- $\omega_{10} = \frac{\omega_{n,mech}}{\omega_{b,mech}} = 1\ [p.u.]$;
- $i_{sd0} = 0$ (MTPA operation);
- $i_{sq0} = \frac{T_{elm,0}}{n_p(I_b\psi_b)\psi_{PM}} = 1.5\ [p.u.]$

System (3.6) can be represented in matrix form:

$$\underbrace{\begin{bmatrix} \Delta\dot{\theta}_t \\ \Delta\dot{\theta}_1 \\ \Delta\dot{\omega}_t \\ \Delta\dot{\omega}_1 \\ \Delta\dot{i}_{sd} \\ \Delta\dot{i}_{sq} \end{bmatrix}}_{\mathbf{\Delta\dot{x}}} = \underbrace{\begin{bmatrix} 0 & 0 & \omega_{b,mech} & 0 & 0 & 0 \\ 0 & 0 & 0 & \omega_{b,mech} & 0 & 0 \\ -\frac{K_1}{2H_tT_n} & \frac{K_1}{2H_tT_n} & 0 & 0 & 0 & 0 \\ \frac{K_1}{2H_1T_n} & -\frac{K_1}{2H_1T_n} & 0 & 0 & 0 & -\frac{n_p(I_b*\psi_b)\psi_{PM}}{2H_1T_n} \\ 0 & 0 & 0 & \omega_b i_{sq0} & -r_s\frac{\omega_b}{l_s} & \omega_b\omega_{10} \\ 0 & 0 & 0 & -\frac{\omega_b}{l_s}\psi_{PM} & -\omega_b\omega_{10} & -r_s\frac{\omega_b}{l_s} \end{bmatrix}}_{\mathbf{\Delta A}} \underbrace{\begin{bmatrix} \Delta\theta_t \\ \Delta\theta_1 \\ \Delta\omega_t \\ \Delta\omega_1 \\ \Delta i_{sd} \\ \Delta i_{sq} \end{bmatrix}}_{\mathbf{\Delta x}} +$$

$$+ \underbrace{\begin{bmatrix} 0 & 0 \\ 0 & 0 \\ 0 & 0 \\ 0 & 0 \\ \frac{\omega_b}{l_s} & 0 \\ 0 & \frac{\omega_b}{l_s} \end{bmatrix}}_{\mathbf{\Delta B}} \underbrace{\begin{bmatrix} \Delta v_{sd} \\ \Delta v_{sq} \end{bmatrix}}_{\mathbf{\Delta u}}$$

$$\underbrace{\begin{bmatrix} \Delta y_1 \\ \Delta y_2 \\ \Delta y_3 \end{bmatrix}}_{\mathbf{\Delta y}} = \underbrace{\begin{bmatrix} 0 & 1 & 0 & 0 & 0 & 0 \\ 0 & 0 & 0 & 0 & 1 & 0 \\ 0 & 0 & 0 & 0 & 0 & 1 \end{bmatrix}}_{\mathbf{\Delta C}} \underbrace{\begin{bmatrix} \Delta\theta_t \\ \Delta\theta_1 \\ \Delta\omega_t \\ \Delta\omega_1 \\ \Delta i_{sd} \\ \Delta i_{sq} \end{bmatrix}}_{\mathbf{\Delta x}} = \begin{bmatrix} \Delta\theta_1 \\ \Delta i_{sd} \\ \Delta i_{sq} \end{bmatrix}$$

where $\mathbf{\Delta x} \in \mathbb{R}^n$, $\mathbf{\Delta y} \in \mathbb{R}^q$, $\mathbf{\Delta A} \in \mathbb{R}^{nxn}$, $\mathbf{\Delta B} \in \mathbb{R}^{nxp}$ and $\mathbf{\Delta C} \in \mathbb{R}^{qxn}$, with $n = 6$, $p = 2$ and $q = 3$.

If the system is completely observable with a given set of outputs then it is possible to estimate the state variables through a state observer. Following [1], considering the generic system in state space form defined in Section 1.3:

$$\dot{\mathbf{x}} = \mathbf{Ax} + \mathbf{Bu}$$
$$\mathbf{y} = \mathbf{Cx} + \mathbf{Du}$$

it is completely observable if the pair $(\mathbf{C}, \mathbf{A})$ is completely observable, so if the observability matrix $\mathbf{M_O}$ defined as:

$$\mathbf{M_O} = \begin{bmatrix} \mathbf{C} \\ \mathbf{CA} \\ \mathbf{CA}^2 \\ \dots \\ \mathbf{CA}^{n-1} \end{bmatrix} \tag{3.7}$$

is full rank, so if:

$$\rho = \text{rank}\,(\mathbf{M_O}) = n \tag{3.8}$$

In this case, the observability matrix is:

$$\mathbf{\Delta M_O} = \begin{bmatrix} \mathbf{\Delta C} \\ \mathbf{\Delta C} * \mathbf{\Delta A} \\ \mathbf{\Delta C} * \mathbf{\Delta A}^2 \\ \dots \\ \mathbf{\Delta C} * \mathbf{\Delta A}^{n-1} \end{bmatrix} \tag{3.9}$$

and applying (3.8):

$$\rho = \text{rank}\,(\mathbf{\Delta M_O}) = 6 \tag{3.10}$$

hence the system (3.6) is completely observable. All the observability matrices that are defined in the thesis can be found in Appendix A.2 and A.4.

3.1.2. Subsystem Decomposition

Referring to Section 1.3.3, the NLESO is defined for a single output system. To implement an observer of this type for the Multi-Input Multi-Output (MIMO) system defined in the previous section, a MISO subsystem decomposition is performed. In other words, q MISO subsystems are created starting from the original MIMO one, each of them referring to a specific output. At this point, a NLESO will be designed for each subsystem and all the estimates collected will be processed together to obtain the best one.
While matrices $\mathbf{\Delta A}$ and $\mathbf{\Delta B}$ remain the same, as the MIMO system is just divided according to the outputs $\Delta \mathbf{y}$, matrix $\mathbf{\Delta C}$ changes for each subsystem, becoming a single row vector; hence:

- Subsystem 1: $\mathbf{\Delta y} = \Delta y_1 = \Delta\theta_1$

$$\mathbf{\Delta C_1} = \begin{bmatrix} 0 & 1 & 0 & 0 & 0 & 0 \end{bmatrix}$$

  while: $\mathbf{\Delta A_1} = \mathbf{\Delta A}$, $\mathbf{\Delta B_1} = \mathbf{\Delta B}$, $\mathbf{\Delta u_1} = \mathbf{\Delta u}$, $\mathbf{\Delta x_1} = \mathbf{\Delta x}$

- Subsystem 2: $\mathbf{\Delta y} = \Delta y_2 = \Delta i_{sd}$

$$\mathbf{\Delta C_2} = \begin{bmatrix} 0 & 0 & 0 & 0 & 1 & 0 \end{bmatrix}$$

  while: $\mathbf{\Delta A_2} = \mathbf{\Delta A}$, $\mathbf{\Delta B_2} = \mathbf{\Delta B}$, $\mathbf{\Delta u_2} = \mathbf{\Delta u}$, $\mathbf{\Delta x_2} = \mathbf{\Delta x}$

- Subsystem 3: $\mathbf{\Delta y} = \Delta y_3 = \Delta i_{sq}$

$$\mathbf{\Delta C_3} = \begin{bmatrix} 0 & 0 & 0 & 0 & 0 & 1 \end{bmatrix}$$

  while: $\mathbf{\Delta A_3} = \mathbf{\Delta A}$, $\mathbf{\Delta B_3} = \mathbf{\Delta B}$, $\mathbf{\Delta u_3} = \mathbf{\Delta u}$, $\mathbf{\Delta x_3} = \mathbf{\Delta x}$

Before moving on, the observability of each subsystem, i.e. of each pair $(\mathbf{\Delta C_i}, \mathbf{\Delta A})\,|i = 1, 2, 3$, must be assessed, being a necessary condition for the implementation of a state observer. Following the definition of observability matrix defined in (3.7), the observability matrix subsystem i $\mathbf{\Delta M_{Oi}}$ is defined as:

$$\mathbf{\Delta M_{Oi}} = \begin{bmatrix} \mathbf{\Delta C_i} \\ \mathbf{\Delta C_i} * \mathbf{\Delta A} \\ \mathbf{\Delta C_i} * \mathbf{\Delta A}^2 \\ \dots \\ \mathbf{\Delta C_i} * \mathbf{\Delta A}^{n-1} \end{bmatrix} \quad | \, i = 1, 2, 3 \tag{3.11}$$

All the observability matrices can be found in Appendix A.2; the following results are obtained:

- Subsystem 1: rank $(\mathbf{\Delta M_{O1}}) = 6 = n \;\rightarrow$ Subsystem 1 is completely observable;
- Subsystem 2: rank $(\mathbf{\Delta M_{O2}}) = 5 \neq n \;\rightarrow$ Subsystem 2 is not completely observable;
- Subsystem 3: rank $(\mathbf{\Delta M_{O3}}) = 5 \neq n \;\rightarrow$ Subsystem 3 is not completely observable.

It is clear how, in the actual form, a state observer cannot be applied to subsystem 2 and 3.
Based on [6], for a generic state space system with observability matrix $\mathbf{M_O}$, the non-observable states subspace $\mathbf{x}_{null}$ is defined as the kernel of $\mathbf{M_O}$, that is:

$$\mathbf{x}_{null} = \ker(\mathbf{M_O}) \tag{3.12}$$

Before moving on, let us revise the concept of the kernel of a matrix and how it is calculated. By the definition from [2], the kernel of a linear map $L(\mathbf{x}) : \mathbb{R}^{n'} \rightarrow \mathbb{R}^{m'}$ is the set of vectors $\mathbf{x} \in \mathbb{R}^{n'}$ which have as image the null vector of $\mathbb{R}^{m'}$, i.e.:

$$\ker(L) = \left\{ \mathbf{x} \in \mathbb{R}^{n'} \mid L(\mathbf{x}) = \mathbf{0} \in \mathbb{R}^{m'} \right\} \tag{3.13}$$

An example of kernel calculation is provided for completeness in Appendix B.1.
Now, calculating the kernel of the observability matrices related to the non-observable subsystems, through a Matlab script using function $null()$, the following result is obtained:

- Subsystem 2:

$$\ker\left(\mathbf{\Delta M_{02}}\right) = \begin{bmatrix} \Delta\theta_t \\ \Delta\theta_1 \\ 0 \\ 0 \\ 0 \\ 0 \end{bmatrix}$$

- Subsystem 3:

$$\ker\left(\mathbf{\Delta M_{03}}\right) = \begin{bmatrix} \Delta\theta_t \\ \Delta\theta_1 \\ 0 \\ 0 \\ 0 \\ 0 \end{bmatrix}$$

Apparently, the non-observability property of subsystems 2 and 3 is related to $\Delta\theta_t$ and $\Delta\theta_1$. These last two state variables can be merged to form a single state variable, that is:

$$\Delta\theta_t \text{ and } \Delta\theta_1 \rightarrow \Delta\theta_t - \Delta\theta_1 \tag{3.14}$$

Redefining subsystems 2 and 3 with (3.14), the new system matrices become:

$$\mathbf{\Delta x_2} = \mathbf{\Delta x_3} = \begin{bmatrix} \Delta\theta_t - \Delta\theta_1 \\ \Delta\omega_t \\ \Delta\omega_1 \\ \Delta i_{sd} \\ \Delta i_{sq} \end{bmatrix};$$

$$\mathbf{\Delta A_2} = \mathbf{\Delta A_3} = \begin{bmatrix} 0 & \omega_{b,mech} & -\omega_{b,mech} & 0 & 0 \\ -\frac{K_1}{2H_tT_n} & 0 & 0 & 0 & 0 \\ \frac{K_1}{2H_1T_n} & 0 & 0 & 0 & -\frac{n_p(I_b*\psi_b)\psi_{PM}}{2H_1T_n} \\ 0 & 0 & \omega_b i_{sq0} & -\frac{r\omega_b}{l_s} & \omega_b\omega_{10} \\ 0 & 0 & -\frac{\omega_b}{l_s}\psi_{PM} & -\omega_b\omega_{10} & -\frac{r\omega_b}{l_s} \end{bmatrix};$$

$$\mathbf{\Delta B_2} = \mathbf{\Delta B_3} = \begin{bmatrix} 0 & 0 \\ 0 & 0 \\ 0 & 0 \\ \frac{\omega_b}{l_s} & 0 \\ 0 & \frac{\omega_b}{l_s} \end{bmatrix};$$

$$\mathbf{\Delta C_2} = \begin{bmatrix} 0 & 0 & 0 & 1 & 0 \end{bmatrix}; \qquad \mathbf{\Delta C_3} = \begin{bmatrix} 0 & 0 & 0 & 0 & 1 \end{bmatrix}.$$

It must be noticed that now $\mathbf{\Delta x_2} \in \mathbb{R}^{n_2}$, $\mathbf{\Delta x_3} \in \mathbb{R}^{n_3}$ with $n_2 = n_3 = 5$. If now the observability of the two latter subsystems is re-addressed, it can be found that:

- Subsystem 2:

$$\mathbf{\Delta M^1_{O2}} = \begin{bmatrix} \mathbf{\Delta C_2} \\ \mathbf{\Delta C_2} * \mathbf{\Delta A_2} \\ \mathbf{\Delta C_2} * \mathbf{\Delta A_2}^2 \\ \dots \\ \mathbf{\Delta C_2} * \mathbf{\Delta A_2}^{n_2-1} \end{bmatrix} \rightarrow \text{rank}\left(\mathbf{\Delta M^1_{O2}}\right) = 5 = n_2\,;$$

- Subsystem 3:

$$\mathbf{\Delta M^1_{O3}} = \begin{bmatrix} \mathbf{\Delta C_3} \\ \mathbf{\Delta C_3} * \mathbf{\Delta A_3} \\ \mathbf{\Delta C_3} * \mathbf{\Delta A_3}^2 \\ \dots \\ \mathbf{\Delta C_3} * \mathbf{\Delta A_3}^{n_3-1} \end{bmatrix} \rightarrow \text{rank}\left(\mathbf{\Delta M^1_{O3}}\right) = 5 = n_3\,.$$

Eventually, the original MIMO system is decomposed into $q = 3$ observable MISO subsystems defined as:

Subsystem 1

$$\underbrace{\begin{bmatrix} \Delta\dot{\theta}_t \\ \Delta\dot{\theta}_1 \\ \Delta\dot{\omega}_t \\ \Delta\dot{\omega}_1 \\ \Delta\dot{i}_{sd} \\ \Delta\dot{i}_{sq} \end{bmatrix}}_{\mathbf{\Delta\dot{x}_1}} = \underbrace{\begin{bmatrix} 0 & 0 & \omega_{b,mech} & 0 & 0 & 0 \\ 0 & 0 & 0 & \omega_{b,mech} & 0 & 0 \\ -\frac{K_1}{2H_tT_n} & \frac{K_1}{2H_tT_n} & 0 & 0 & 0 & 0 \\ \frac{K_1}{2H_1T_n} & -\frac{K_1}{2H_1T_n} & 0 & 0 & 0 & -\frac{n_p(I_b*\psi_b)\psi_{PM}}{2H_1T_n} \\ 0 & 0 & 0 & \omega_b i_{sq0} & -\frac{r\omega_b}{l_s} & \omega_b\omega_{10} \\ 0 & 0 & 0 & -\frac{\omega_b}{l_s}\psi_{PM} & -\omega_b\omega_{10} & -\frac{r\omega_b}{l_s} \end{bmatrix}}_{\mathbf{\Delta A_1}} \underbrace{\begin{bmatrix} \Delta\theta_t \\ \Delta\theta_1 \\ \Delta\omega_t \\ \Delta\omega_1 \\ \Delta i_{sd} \\ \Delta i_{sq} \end{bmatrix}}_{\mathbf{\Delta x_1}}$$

$$+ \underbrace{\begin{bmatrix} 0 & 0 \\ 0 & 0 \\ 0 & 0 \\ 0 & 0 \\ \frac{\omega_b}{l_s} & 0 \\ 0 & \frac{\omega_b}{l_s} \end{bmatrix}}_{\mathbf{\Delta B_1}} \underbrace{\begin{bmatrix} \Delta v_{sd} \\ \Delta v_{sq} \end{bmatrix}}_{\mathbf{\Delta u_1}}$$

$$\Delta y_1 = \underbrace{\begin{bmatrix} 0 & 1 & 0 & 0 & 0 & 0 \end{bmatrix}}_{\mathbf{\Delta C_1}} \underbrace{\begin{bmatrix} \Delta\theta_t \\ \Delta\theta_1 \\ \Delta\omega_t \\ \Delta\omega_1 \\ \Delta i_{sd} \\ \Delta i_{sq} \end{bmatrix}}_{\mathbf{\Delta x_1}} = \Delta\theta_1 \tag{3.15}$$

Subsystem 2

$$\underbrace{\begin{bmatrix} \Delta\dot{\theta}_t - \Delta\dot{\theta}_1 \\ \Delta\dot{\omega}_t \\ \Delta\dot{\omega}_1 \\ \Delta\dot{i}_{sd} \\ \Delta\dot{i}_{sq} \end{bmatrix}}_{\mathbf{\Delta\dot{x}_2}} = \underbrace{\begin{bmatrix} 0 & \omega_{b,mech} & -\omega_{b,mech} & 0 & 0 \\ -\frac{K_1}{2H_tT_n} & 0 & 0 & 0 & 0 \\ \frac{K_1}{2H_1T_n} & 0 & 0 & 0 & -\frac{n_p(I_b*\psi_b)\psi_{PM}}{2H_1T_n} \\ 0 & 0 & \omega_b i_{sq0} & -\frac{r\omega_b}{l_s} & \omega_b\omega_{10} \\ 0 & 0 & -\frac{\omega_b}{l_s}\psi_{PM} & -\omega_b\omega_{10} & -\frac{r\omega_b}{l_s} \end{bmatrix}}_{\mathbf{\Delta A_2}} \underbrace{\begin{bmatrix} \Delta\theta_t - \Delta\theta_1 \\ \Delta\omega_t \\ \Delta\omega_1 \\ \Delta i_{sd} \\ \Delta i_{sq} \end{bmatrix}}_{\mathbf{\Delta x_2}} + \underbrace{\begin{bmatrix} 0 & 0 \\ 0 & 0 \\ 0 & 0 \\ \frac{\omega_b}{l_s} & 0 \\ 0 & \frac{\omega_b}{l_s} \end{bmatrix}}_{\mathbf{\Delta B_2}} \underbrace{\begin{bmatrix} \Delta v_{sd} \\ \Delta v_{sq} \end{bmatrix}}_{\mathbf{\Delta u_2}}$$

$$\Delta y_2 = \underbrace{\begin{bmatrix} 0 & 0 & 0 & 1 & 0 \end{bmatrix}}_{\mathbf{\Delta C_2}} \underbrace{\begin{bmatrix} \Delta\theta_t - \Delta\theta_1 \\ \Delta\omega_t \\ \Delta\omega_1 \\ \Delta i_{sd} \\ \Delta i_{sq} \end{bmatrix}}_{\mathbf{\Delta x_2}} = \Delta i_{sd} \tag{3.16}$$

Subsystem 3

$$\underbrace{\begin{bmatrix} \Delta\dot{\theta}_t - \Delta\dot{\theta}_1 \\ \Delta\dot{\omega}_t \\ \Delta\dot{\omega}_1 \\ \Delta\dot{i}_{sd} \\ \Delta\dot{i}_{sq} \end{bmatrix}}_{\mathbf{\Delta\dot{x}_3}} = \underbrace{\begin{bmatrix} 0 & \omega_{b,mech} & -\omega_{b,mech} & 0 & 0 \\ -\frac{K_1}{2H_tT_n} & 0 & 0 & 0 & 0 \\ \frac{K_1}{2H_1T_n} & 0 & 0 & 0 & -\frac{n_p(I_b*\psi_b)\psi_{PM}}{2H_1T_n} \\ 0 & 0 & \omega_b i_{sq0} & -\frac{r\omega_b}{l_s} & \omega_b\omega_{10} \\ 0 & 0 & -\frac{\omega_b}{l_s}\psi_{PM} & -\omega_b\omega_{10} & -\frac{r\omega_b}{l_s} \end{bmatrix}}_{\mathbf{\Delta A_3}} \underbrace{\begin{bmatrix} \Delta\theta_t - \Delta\theta_1 \\ \Delta\omega_t \\ \Delta\omega_1 \\ \Delta i_{sd} \\ \Delta i_{sq} \end{bmatrix}}_{\mathbf{\Delta x_3}} + \underbrace{\begin{bmatrix} 0 & 0 \\ 0 & 0 \\ 0 & 0 \\ \frac{\omega_b}{l_s} & 0 \\ 0 & \frac{\omega_b}{l_s} \end{bmatrix}}_{\mathbf{\Delta B_3}} \underbrace{\begin{bmatrix} \Delta v_{sd} \\ \Delta v_{sq} \end{bmatrix}}_{\mathbf{\Delta u_3}}$$

$$\Delta y_3 = \underbrace{\begin{bmatrix} 0 & 0 & 0 & 0 & 1 \end{bmatrix}}_{\mathbf{\Delta C_3}} \underbrace{\begin{bmatrix} \Delta\theta_t - \Delta\theta_1 \\ \Delta\omega_t \\ \Delta\omega_1 \\ \Delta i_{sd} \\ \Delta i_{sq} \end{bmatrix}}_{\mathbf{\Delta x_3}} = \Delta i_{sq} \tag{3.17}$$

3.1.3. Relative-Degree based estimate selection

In [26], a systematic procedure for distributed state estimation in nonlinear systems is presented. Particularly, a relative degree analysis, with which the closeness between states and outputs can be evaluated, is provided. Based on this analysis, it is assumed that the closer the state to the output used as the observer input, the more accurate the estimation of the state variable.
A generic MISO system can be expressed in the form:

$$\begin{cases} \dot{\mathbf{x}} = \mathbf{f}(\mathbf{x}) + \mathbf{g}(\mathbf{u}) \\ y = \mathbf{h}(\mathbf{x}) \end{cases} \tag{3.18}$$

where $\mathbf{x} \in \mathbb{R}^n$, $\mathbf{u} \in \mathbb{R}^p$, $y \in \mathbb{R}$ state variables.
Let us start defining matrix $\mathbf{F}$ as:

$$\mathbf{F} = \frac{\partial \mathbf{f}}{\partial \mathbf{x}} = \begin{bmatrix} \mathbf{F_1} & \mathbf{F_2} & \dots & \mathbf{F_n} \end{bmatrix} \tag{3.19}$$

where $\mathbf{F_i} \mid i = 1, ..., n$ are column vectors.
Another useful concept to be introduced is the Lie derivative [12] of $\mathbf{h}(\mathbf{x})$ along $\mathbf{F_i} \mid i = 1, ..., n$, defined as:

$$L_{\mathbf{F_i}}\mathbf{h}(\mathbf{x}) \triangleq \frac{\partial \mathbf{h}(\mathbf{x})}{\partial \mathbf{x}} * \mathbf{F_i}(\mathbf{x}) \tag{3.20}$$

The closeness between the output y and the generic subsystem variable $x_i \in \mathbf{x} \mid i = 1, ..., n$ is evaluated calculating D_i:

$$D_i = \begin{cases} 0 & \text{if} \quad \frac{\partial \mathbf{h}}{\partial x_i} \neq 0 \\ 1 & \text{if} \quad \frac{\partial \mathbf{h}}{\partial x_i} = 0 \quad \& \quad L_{\mathbf{F_i}}\mathbf{h}(\mathbf{x}) \neq 0 \\ d_i & \text{if} \quad \frac{\partial \mathbf{h}}{\partial x_i} = 0 \quad \& \quad L_{\mathbf{F_i}}L_{\mathbf{f}}^{k-1}\mathbf{h}(\mathbf{x}) = 0 \quad \& \\ & \qquad\qquad L_{\mathbf{F_i}}L_{\mathbf{f}}^{d_i-1}\mathbf{h}(\mathbf{x}) \neq 0 \quad \mid k = 0, 1, ..., d_i - 1 \\ \infty & \text{if} \quad d_i \to \infty \end{cases} \tag{3.21}$$

The lower D_i the closer is the state variable $x_i \mid i = 1, ..., n$ to the output y. However, calculations get a little simpler if a generic linear system is considered, that is again the one defined in (1.13):

$$\dot{\mathbf{x}} = \mathbf{Ax} + \mathbf{Bu}$$
$$\mathbf{y} = \mathbf{Cx} + \mathbf{Du}$$

Indeed, in this case, assuming $\mathbf{D} = 0$ and a MISO system with $\mathbf{C} \in \mathbb{R}^{qxn} \mid q = 1$:

- $\frac{\partial \mathbf{h}}{\partial \mathbf{x}} = \frac{\partial(\mathbf{Cx})}{\partial \mathbf{x}} = \mathbf{C}$;
- $\frac{\partial \mathbf{h}}{\partial x_i} = \frac{\partial(\mathbf{Cx})}{\partial x_i} = C_i \in \mathbb{R}$: element i of matrix $\mathbf{C}$;
- $\mathbf{F} = \frac{\partial \mathbf{f}}{\partial \mathbf{x}} = \frac{\partial \mathbf{Ax}}{\partial \mathbf{x}} = \mathbf{A} = \begin{bmatrix} \mathbf{A_1} & \mathbf{A_2} & ... & \mathbf{A_n} \end{bmatrix}$
  - $\mathbf{A_i} \mid i = 1, ..., n$ is the column vector i of matrix $\mathbf{A}$;
- $L_{\mathbf{F_i}}\mathbf{h}(\mathbf{x}) = \frac{\partial \mathbf{h}}{\partial \mathbf{x}} * \mathbf{F_i} = \mathbf{CA_i} \mid i = 1, ..., n$;
- $L_{\mathbf{F_i}} L_{\mathbf{f}}^{k-1}\mathbf{h}(\mathbf{x}) = \mathbf{CA}^{k-1}\mathbf{A_i} \mid i = 1, ..., n;\ k \in \mathbb{R}$.

The above procedure must be applied to each subsystem; for a better understanding, let us carry out for subsystem 1 the closeness between the output $\Delta y_1 = \Delta\theta_1$ and some of the state variables of $\mathbf{\Delta x_1}$:

1. $\Delta\theta_t$:
   (a) $\frac{\partial \mathbf{h}}{\partial x_1} =$

$$= \frac{\partial\left(\mathbf{\Delta C_1 \Delta x_1}\right)}{\partial \Delta\theta_t} = \frac{\partial\left\{\begin{bmatrix} 0 & 1 & 0 & 0 & 0 & 0 \end{bmatrix}\begin{bmatrix} \Delta\theta_t \\ \Delta\theta_1 \\ \Delta\omega_t \\ \Delta\omega_1 \\ \Delta i_{sd} \\ \Delta i_{sq} \end{bmatrix}\right\}}{\partial \Delta\theta_t} = 0;$$

(b) $L_{\mathbf{F_1}}\mathbf{h}(\mathbf{x}) =$

$$= \frac{\partial \mathbf{h}}{\partial \mathbf{x}} * \mathbf{F_1} = \frac{\partial \left\{ \begin{bmatrix} 0 & 1 & 0 & 0 & 0 & 0 \end{bmatrix} \begin{bmatrix} \Delta\theta_t \\ \Delta\theta_1 \\ \Delta\omega_t \\ \Delta\omega_1 \\ \Delta i_{sd} \\ \Delta i_{sq} \end{bmatrix} \right\}}{\partial \left\{ \begin{bmatrix} \Delta\theta_t \\ \Delta\theta_1 \\ \Delta\omega_t \\ \Delta\omega_1 \\ \Delta i_{sd} \\ \Delta i_{sq} \end{bmatrix} \right\}} \mathbf{\Delta A_{11}} =$$

$$= \mathbf{\Delta C_1 \Delta A_1} = \begin{bmatrix} 0 & 1 & 0 & 0 & 0 & 0 \end{bmatrix} \begin{bmatrix} 0 \\ 0 \\ -\frac{K_1}{2H_tT_n} \\ \frac{K_1}{2H_1T_n} \\ 0 \\ 0 \end{bmatrix} = 0;$$

(c) $L_{\mathbf{F_1}} L_{\mathbf{f}}^{2-1}\mathbf{h}(\mathbf{x}) = \frac{\partial\left(\frac{\partial \mathbf{h}}{\partial \mathbf{x}}\right) * \mathbf{f}}{\partial \mathbf{x}} * \mathbf{F_1}$

i. $\left(\frac{\partial \mathbf{h}}{\partial \mathbf{x}}\right) * \mathbf{f} = \left(\frac{\partial(\mathbf{C\Delta x})}{\partial \mathbf{\Delta x}}\right) \mathbf{\Delta A_1 \Delta x_1} = \mathbf{\Delta C_1 \Delta A_1 \Delta x_1} = \begin{bmatrix} 0 & 0 & 0 & \omega_{b,mech} & 0 & 0 \end{bmatrix} \mathbf{\Delta x_1};$

ii. $\frac{\partial\left(\frac{\partial \mathbf{h}}{\partial \mathbf{x}}\right) * \mathbf{f}}{\partial \mathbf{x}} * \mathbf{F_1} = \frac{\partial \left\{ \begin{bmatrix} 0 & 0 & 0 & \omega_{b,mech} & 0 & 0 \end{bmatrix} \mathbf{\Delta x_1} \right\}}{\partial \mathbf{\Delta x_1}} \mathbf{\Delta A_{11}} =$

$$= \begin{bmatrix} 0 & 0 & 0 & \omega_{b,mech} & 0 & 0 \end{bmatrix} \begin{bmatrix} 0 \\ 0 \\ -\frac{K_1}{2H_tT_n} \\ \frac{K_1}{2H_1T_n} \\ 0 \\ 0 \end{bmatrix} \neq 0;$$

Thus: $D_{11} = 2$.

2. $\Delta\theta_1$:

   (a) $\frac{\partial \mathbf{h}}{\partial x_2} = \frac{\partial(\mathbf{\Delta C_1 \Delta x_1})}{\partial \Delta\theta_1} = \frac{\partial\left\{\begin{bmatrix} 0 & 1 & 0 & 0 & 0 & 0 \end{bmatrix} \begin{bmatrix} \Delta\theta_t \\ \Delta\theta_1 \\ \Delta\omega_t \\ \Delta\omega_1 \\ \Delta i_{sd} \\ \Delta i_{sq} \end{bmatrix}\right\}}{\partial \Delta\theta_1} \neq 0$

   Thus: $D_{12} = 0$.

3. $\Delta x_{13} = \Delta\omega_t$:

   (a) ...

... and so on and so forth for each state variable, for each subsystem.
In Table 3.1 the results of this analysis are listed.

Table 3.1: Relative degrees between the state variables and each subsystem's output. D_{ji} is the relative degree between the MISO Subsystem j's output and the state variable i of state vector $\mathbf{\Delta x}_j$, with $j = 1, 2, 3$ (subsystem number)

Relative Degrees

Subsystem 1 $i = 1, ..., n_1$		Subsystem 2 $i = 1, ..., n_2$		Subsystem 3 $i = 1, ..., n_3$	
$\mathbf{\Delta x_1}$	D_{1i}	$\mathbf{\Delta x_2}$	D_{2i}	$\mathbf{\Delta x_3}$	D_{3i}
$\Delta\theta_t$	2	$\Delta\theta_t - \Delta\theta_1$	2	$\Delta\theta_t - \Delta\theta_1$	2
$\Delta\theta_1$	0				
$\Delta\omega_t$	3	$\Delta\omega_t$	3	$\Delta\omega_t$	3
$\Delta\omega_1$	1	$\Delta\omega_1$	1	$\Delta\omega_1$	1
Δi_{sd}	3	Δi_{sd}	0	Δi_{sd}	1
Δi_{sq}	2	Δi_{sq}	1	Δi_{sq}	0

As already mentioned, the estimates of the state variables showing the lowest relative degree between each subsystem will be kept.
By looking at Table 3.1 the choice for some variables appears straightforward, that is:

- $D_{12} = 0$: the estimate of $\Delta\theta_1$ will be taken from subsystem 1 observer;
- $D_{24} = 0$: the estimate of Δi_{sd} will be taken from subsystem 2 observer;
- $D_{35} = 0$: the estimate of Δi_{sq} will be taken from subsystem 3 observer;

For what concerns the other state variables:

- $\Delta\omega_t$ and $\Delta\omega_1$ show the same relative degree in each subsystem: in this case, the average of the three estimates is taken for each variable;
- $\Delta\theta_t$ for subsystem 1 and $(\Delta\theta_t - \Delta\theta_1)$ for subsystems 2 and 3 show the same relative degree: in this case, $\Delta\theta_1$ estimate, taken from subsystem 1, is summed to $(\Delta\theta_t - \Delta\theta_1)$ expression to find two distinct estimates of $\Delta\theta_t$ from subsystem 2 and 3; then, the average of the three estimates of $\Delta\theta_t$ is taken.

Summarizing, a simple block scheme of the steps from the MISO subsystem decomposition to the estimate reconstruction is provided in Figure 3.1.

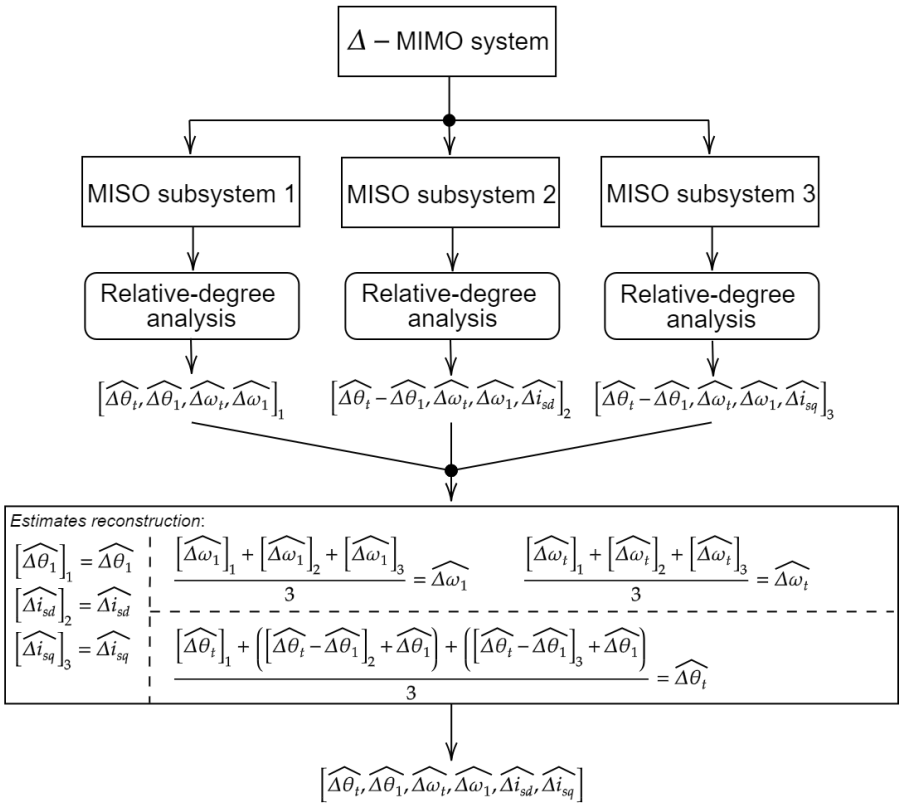

Figure 3.1: simple block scheme of the steps taken from subsystem decomposition to estimates reconstruction.

The vector:

$$\left[\begin{array}{cccccc} \widehat{\Delta\theta_t} & \widehat{\Delta\theta_1} & \widehat{\Delta\omega_t} & \widehat{\Delta\omega_1} & \widehat{\Delta i_{sd}} & \widehat{\Delta i_{sq}} \end{array} \right] \tag{3.22}$$

represent the final estimations of the linearized system's state variables. Therefore, each MISO subsystem's observer, the design of which is carried out in the next chapter, provides a set of estimates that contributes to getting the final state variables' estimations, which are obtained by processing all the subsystems' estimates based on the above analysis.

3.1.4. NLESO Definition

Subsystems transformation

In this section a NLESO is designed for each of the subsystems defined in Section 3.1.2. As discussed in Section 1.3.3, in order to apply an ESO the system must be in integral chain form: to do this, a state variable transformation must be performed for each subsystem. However, the transformation follows several steps that remain the same in each case: for this reason, first the procedure is presented for a general MISO system and then the resultant subsystems are shown.
Let us introduce again the general linear system (1.13), considering in this case $\mathbf{D} = \mathbf{0}$ and $q = 1$, that is:

$$\begin{aligned} \dot{\mathbf{x}} &= \mathbf{A}\mathbf{x} + \mathbf{B}\mathbf{u} \\ y &= \mathbf{C}\mathbf{x} \end{aligned}$$

where $\mathbf{A} \in \mathbb{R}^{nxn}$, $\mathbf{B} \in \mathbb{R}^{nxp}$, $\mathbf{C} \in \mathbb{R}^{1xn}$.
For this system, a transformation matrix $\mathbf{T} \in \mathbb{R}^{nxn}$ can be defined [6] such that:

$$\mathbf{z} = \mathbf{T}\mathbf{x} \tag{3.23}$$

where $\mathbf{z} \in \mathbb{R}^n$ is the vector of the new state variables and provided that $\mathbf{T}$ is invertible. The new (or transformed) system will have the form:

$$\begin{aligned} \dot{\mathbf{z}} &= \mathbf{A}_\mathbf{z}\mathbf{z} + \mathbf{B}_\mathbf{z}\mathbf{u} \\ y &= \mathbf{C}_\mathbf{z}\mathbf{z} \end{aligned} \tag{3.24}$$

with:

$$\mathbf{A}_\mathbf{z} = \mathbf{T}\mathbf{A}\mathbf{T}^{-1} \quad ; \quad \mathbf{B}_\mathbf{z} = \mathbf{T}\mathbf{B} \quad ; \quad \mathbf{C}_\mathbf{z} = \mathbf{C}\mathbf{T}^{-1} \quad .$$

The following steps to build $\mathbf{T}$ are made:

1. find the system transfer function matrix between the p inputs and the $q = 1$ output:
   - $\mathbf{W}(s) = \mathbf{C}\left(s\mathbf{I} - \mathbf{A}\right)^{-1}\mathbf{B}$;
   - $\mathbf{W}(s) \in \mathbb{R}^{qxp}$;
2. find the minimum polynomial $qW(s)$ of $\mathbf{W}(s)$ [6]:
   - first verify that $\mathbf{W}(s)$ is a proper rational matrix, so that each element of $\mathbf{W}(s)$ is a rational function of s, where the degree of the numerator is lower than the degree of the denominator;
   - the minimum polynomial $qW(s)$ is defined as the least common multiple of the denominators of the elements of $\mathbf{W}(s)$;
     - Example:

$$\mathbf{W_{example}}(s) = \begin{bmatrix} \frac{1}{s+1} \\ \frac{s+2}{(s+1)(s+5)} \end{bmatrix} \rightarrow qW_{example}(s) = s + 1$$

   - $qW(s)$ will be in the form: $qW(s) = s^{\bar{m}} + \sum_{i=0}^{\bar{m}-1} \gamma_i s^i$
3. find $\mathbf{A_z}$, the realization of the observable canonical form [6]:
   - in this case $\bar{m} = n$, being $q = 1$;
   - $qW(s) = s^n + \sum_{i=0}^{n-1} \gamma_i s^i$;
   -

$$\mathbf{A_z} = \begin{bmatrix} 0 & 1 & 0 & 0 & ... & 0 \\ 0 & 0 & 1 & 0 & ... & 0 \\ ... & .... & ... & ... & ... & ... \\ 0 & 0 & 0 & 0 & ... & 1 \\ -\gamma_0 & -\gamma_1 & -\gamma_2 & -\gamma_3 & ... & -\gamma_{n-1} \end{bmatrix}$$

4. find $\mathbf{B_z}$:
   - define:
     - $\mathbf{W_0}(s) = \mathbf{W(s)}$;
     - $\overline{\mathbf{W_0}} = \lim_{s \to +\infty} \mathbf{W_0}(s)$;

- define, for $1 \leq h \leq n$:
  - $\mathbf{W_h}(s) = s\left(\mathbf{W_{h-1}}(s) - \overline{\mathbf{W}}_{\mathbf{h-1}}\right)$;
  - $\overline{\mathbf{W}}_{\mathbf{h}} = \lim_{s \to +\infty} \mathbf{W_h}(s)$;
- $\mathbf{B_z}$ can be built:

$$\mathbf{B_z} = \begin{bmatrix} \overline{\mathbf{W}}_{\mathbf{1}} \\ \overline{\mathbf{W}}_{\mathbf{2}} \\ \dots \\ \overline{\mathbf{W}}_{\mathbf{n}} \end{bmatrix} \in \mathbb{R}^{nxp}$$

5. build matrix $\mathbf{T}$ starting from the controllability matrices of the original and of the transformed systems, using only one column of $\mathbf{B}$ and $\mathbf{B_z}$ respectively:
   - build controllability matrix $\mathbf{P}$ for the original system using only one column of $\mathbf{B}$;
     - $\mathbf{B} = \begin{bmatrix} \mathbf{B_1} & \mathbf{B_2} & \dots & \mathbf{B_p} \end{bmatrix}$;
     - $\mathbf{P} = \begin{bmatrix} \mathbf{B_1} & \mathbf{AB_1} & \mathbf{A}^2\mathbf{B_1} & \dots & \mathbf{A}^{n-1}\mathbf{B_1} \end{bmatrix}$;
   - build controllability matrix $\mathbf{P_z}$ for the transformed system using only one column of $\mathbf{B_z}$;
     - $\mathbf{B_z} = \begin{bmatrix} \mathbf{B_{z1}} & \mathbf{B_{z2}} & \dots & \mathbf{B_{zp}} \end{bmatrix}$;
     - $\mathbf{P_z} = \begin{bmatrix} \mathbf{B_{z1}} & \mathbf{A_z B_{z1}} & \mathbf{A_z}^2\mathbf{B_{z1}} & \dots & \mathbf{A}^{n-1}\mathbf{B_{z1}} \end{bmatrix}$;
   - $\mathbf{T} = \mathbf{P_z}\mathbf{P}^{-1}$;
   - check that: $\det \mathbf{T} \neq 0$:
     - if $\det \mathbf{T} = 0$, change $\mathbf{B}$ and $\mathbf{B_z}$ column selection.
6. calculate: $\mathbf{C_z} = \mathbf{C}\mathbf{T}^{-1}$;

For a tidier representation, the three subsystems' matrices are listed in A.3. The three transformed MISO subsystems take the form:

$$\begin{aligned} \mathbf{z_i} &= \mathbf{A_{zi}}\mathbf{z_i} + \mathbf{B_{zi}}\mathbf{\Delta u} \\ y_i &= \mathbf{C_{zi}}\mathbf{z_i} \end{aligned} \quad | \, i = 1, 2, 3$$

NLESO Design

After the transformation performed in the previous section, considering:

- number of inputs: $p = 2$;
- $\mathbf{B_z} = \begin{bmatrix} B_{z11} & B_{z12} \\ B_{z21} & B_{z22} \\ ... & ... \\ B_{zn1} & B_{zn2} \end{bmatrix}$;

each MISO subsystem has now the form:

$$\begin{cases} \dot{z_1} = z_2 + B_{z11}u_1 + B_{z12}u_2; \\ \dot{z_2} = z_3 + B_{z21}u_1 + B_{z22}u_2; \\ ... \\ \dot{z_n} = f\left(z_1, z_2, ..., z_n\right) + B_{zn1}u_1 + B_{zn2}u_2; \\ y = z_1 \end{cases} \tag{3.25}$$

where $n = n_1 = 6$ for subsystem 1 and $n = n_2 = n_3 = 5$ for subsystem 2 and 3. Defining the extended state:

$$f(z_1, z_2, ..., z_n) = z_{n+1}$$

the extended-state system takes the following form:

$$\begin{cases} \dot{z_1} = z_2 + B_{z11}u_1 + B_{z12}u_2; \\ \dot{z_2} = z_3 + B_{z21}u_1 + B_{z22}u_2; \\ ... \\ \dot{z_n} = z_{n+1} + B_{zn1}u_1 + B_{zn2}u_2; \\ \dot{z_{n+1}} = h; \\ y = z_1 \end{cases} \tag{3.26}$$

For this type of system, the NLESO is defined as:

$$\begin{cases} \dot{\widehat{z_1}} = \widehat{z_2} + B_{z11}u_1 + B_{z12}u_2 - \beta_1 g(\widehat{y} - y); \\ \dot{\widehat{z_2}} = \widehat{z_3} + B_{z11}u_1 + B_{z12}u_2 - \beta_2 g(\widehat{y} - y); \\ ... \\ \dot{\widehat{z_n}} = \widehat{z_{n+1}} + B_{z11}u_1 + B_{z12}u_2 - \beta_n g(\widehat{y} - y); \\ \dot{\widehat{z_{n+1}}} = \widehat{h} - g(\widehat{y} - y); \\ \widehat{y} = \widehat{z_1} \end{cases} \tag{3.27}$$

where the $\hat{z}_i$ represent the state estimations and β_i are the observer gain coefficients, with $i = 1, ..., n, n + 1$.
Following the definition of observation error from (1.14), the observer correction term

is chosen as the product between the β coefficients and the nonlinear function $g()$:

$$g\left(\widehat{y}-y\right)=g\left(\widehat{z}_1-z_1\right)=g\left(e_1\right)=fal(\alpha,\delta,e_1)=\begin{cases}\frac{e_1}{\delta^{1-\alpha}} & for \quad |e_1|\leq\delta\\ |e_1|^{\alpha}\,\text{sign}(e_1) & for \quad |e_1|>\delta\end{cases} \quad |\ \alpha,\delta\in\mathbb{R}^{+} \tag{3.28}$$

The choice of α and δ is completely arbitrary: since good NLESO performances were found in [27] choosing:

- $\alpha = 0.65$;
- $\delta = 0.9$;

these values are kept; the fal-function plot can be seen in Figure 3.2.

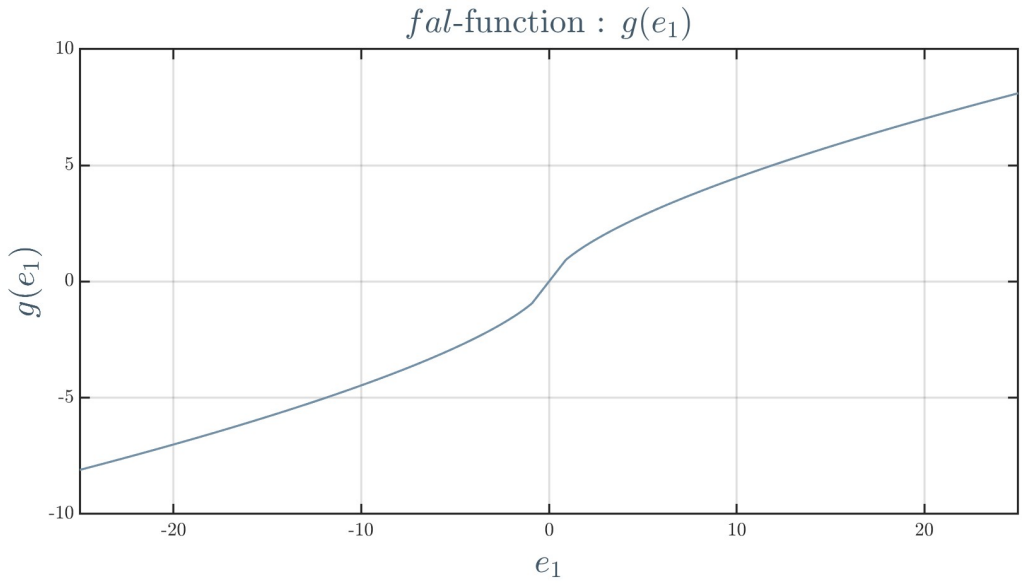

Figure 3.2: Plot of the fal-function, with $\alpha = 0.65$ and $\delta = 0.9$

The observation error dynamic is represented by:

$$\begin{cases}\dot{e_1}=e_2-\beta_1 g\left(e_1\right)\\ \dot{e_2}=e_3-\beta_2 g\left(e_1\right)\\ \dot{e_n}=e_{n+1}-\beta_n g\left(e_1\right)\\ \dot{e_{n+1}}=\left(\widehat{h}-h\right)-\beta_{n+1} g\left(e_1\right)\\ \hat{y}-y=e_1\end{cases} \tag{3.29}$$

Clearly, all the $\beta_i \quad |i=1,...,n,n+1$ coefficients must be identified in order to get a stable observer, which guarantees an asymptotic decay of the observation error towards

zero. In order to accomplish this, let us start by introducing:

$$\Gamma(e_1) = g(e_1) - e_1 \tag{3.30}$$

whose trend can be seen in Figure 3.3.

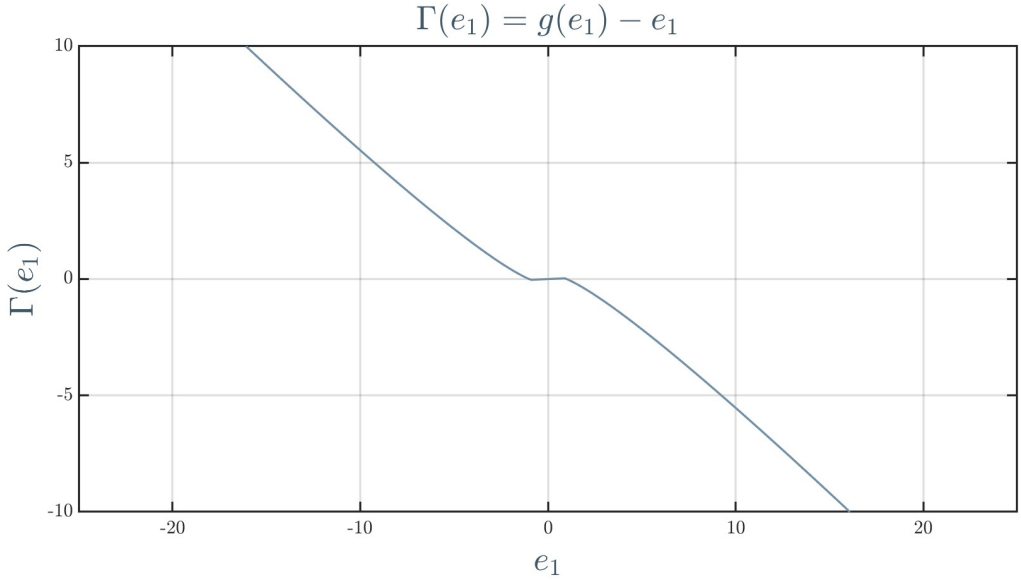

Figure 3.3: Plot of $\Gamma(e_1) = g(e_1) - e_1$

Adding and subtracting $\beta_i e_1$ accordingly in each equation of (3.29), the following system can be found:

$$\begin{cases} \dot{e_1} = e_2 - \beta_1 e_1 + \beta_1 \left(-\Gamma\left(e_1\right)\right) \\ \dot{e_2} = e_3 - \beta_2 e_1 + \beta_2 \left(-\Gamma\left(e_1\right)\right) \\ \cdots \\ \dot{e_n} = e_{n+1} - \beta_n e_1 + \beta_n \left(-\Gamma\left(e_1\right)\right) \\ e_{n+1} = (\hat{h} - h) - \beta_{n+1} e_1 + \beta_{n+1} \left(-\Gamma\left(e_1\right)\right) \\ \hat{y} - y = e_1 \end{cases} \tag{3.31}$$

Considering now:

$$u_e = -\Gamma(e_1)$$

and substituting it in (3.31), the system in matrix form can be seen as[1]:

$$\begin{bmatrix} \dot{e_1} \\ \dot{e_2} \\ \dots \\ \dot{e_n} \\ \dot{e_{n+1}} \end{bmatrix} = \underbrace{\begin{bmatrix} -\beta_1 & 1 & \cdot & 0 & 0 \\ -\beta_2 & 0 & \cdot & 0 & 0 \\ - & \cdot & \cdot & \cdot & \cdot \\ -\beta_n & 0 & \cdot & 1 & 0 \\ -\beta_{n+1} & 0 & \cdot & 0 & 0 \end{bmatrix}}_{[A_e]} \begin{bmatrix} e_1 \\ e_2 \\ \dots \\ e_n \\ e_{n+1} \end{bmatrix} + \underbrace{\begin{bmatrix} \beta_1 \\ \beta_2 \\ \dots \\ \beta_n \\ \beta_{n+1} \end{bmatrix}}_{[B_e]} u_e$$

$$[\widehat{y} - y] = \underbrace{\begin{bmatrix} 1 & 0 & \dots & 0 & 0 \end{bmatrix}}_{[C_e]} \begin{bmatrix} e_1 \\ e_2 \\ \cdots \\ e_n \\ e_{n+1} \end{bmatrix} \tag{3.32}$$

Before moving on, let us introduce some new concept.
Considering the generic linear system of the form:

$$\dot{\mathbf{x}} = \mathbf{A}\mathbf{x} + \mathbf{B}\mathbf{u}$$
$$\mathbf{y} = \mathbf{C}\mathbf{x} + \mathbf{D}\mathbf{u}$$

where $\mathbf{A} \in \mathbb{R}^{nxn}$, $\mathbf{B} \in \mathbb{R}^{nxp}$, $\mathbf{C} \in \mathbb{R}^{qxn}$ and $\mathbf{D} \in \mathbb{R}^{qxp}$, the pair $(\mathbf{A}, \mathbf{B})$ is said to be controllable if [1]:

$$\text{rank}\,(\mathbf{M_c}) = n \tag{3.33}$$

where $\mathbf{M_c}$ is the controllability matrix defined as:

$$\mathbf{M_C} = \begin{bmatrix} \mathbf{B} & \mathbf{AB} & \mathbf{A^2B} & \dots & \mathbf{A^{n-1}B} \end{bmatrix} \tag{3.34}$$

A generic function $f : \mathbb{R} \to \mathbb{R}$ is said to satisfy a Lipschitz condition if there exist a scalar $\gamma \in \mathbb{R}$ such that:

$$\frac{|f(x_1) - f(x_2)|}{|x_1 - x_2|} \leq \gamma \quad \forall x_1, x_2 \in \mathbb{R}\,,\ x_1 \neq x_2 \tag{3.35}$$

[1] we assume that the extended state z_{n+1} rate of change h is bounded, and so its observation error $\hat{h} - h$: hence, its contribute does not affect the system's stability and it will be neglected in the following.

Moreover, function f satisfies a sector condition $[a, b]$ for a finite domain $\mathbb{X} \subset \mathbb{R}$ if there exist $a, b \in \mathbb{R} \mid a < b$ such that:

$$[f(x) - a * x]\,[b * x - f(x)] \geq 0 \quad \forall x \in \mathbb{X} \tag{3.36}$$

Now, if:

- $\Gamma(e_1)$ is a Lipschitz nonlinearity that satisfies a sector condition;
- the β-coefficients for each MISO subsystem's observer (see (3.32)) are chosen such that:
  - $(\mathbf{A_e}, \mathbf{B_e})$ controllable:
  - $(\mathbf{C_e}, \mathbf{A_e})$ observable;

the observation error system is a Lur'e problem and then the absolute stability can be guaranteed applying the Circle Criterion[2] [12].
The choice of the β-coefficients can be done by following the next steps (please refer to Appendix A.4 for each observation error system's matrices):

1. find the β-coefficients such that $\mathbf{A_e}$ is a Hurwitz matrix[3], thus solving:
   - $\det(s\mathbf{I} - A_e) = (s + \alpha_0)^{n+1}$;
   - $\alpha_0 = 10 * \omega_{cI} \mid \omega_{cI} =$ control current loop cut-off angular frequency $= 30\left[\frac{rad}{s}\right]$;
     - the poles of each observation error system can be chosen ten times faster than the current loop cut-off frequency (see Section 2.1): in this way, the design of the observer would be suitable for future implementation in the system control loop [4].

[2] see more in Appendix B.2
[3] a matrix is said to be Hurwitz if all its eigenvalues have negative real part.
[4] it must be noticed how, following all the design steps, the choice of β-coefficients does not depend on the specific subsystem's matrices' values; this is a peculiarity of this observer.

- **Subsystem 1** : $\det(s\mathbf{I} - A_e) = (s+\alpha_0)^{n+1} \mid n = n_1 = 6$:

$$\begin{bmatrix} \beta_1 \\ \beta_2 \\ \beta_3 \\ \beta_4 \\ \beta_5 \\ \beta_6 \\ \beta_7 \end{bmatrix} = \begin{bmatrix} 2,10 * 10^3 \\ 1,89 * 10^6 \\ 9,45 * 10^8 \\ 2,83 * 10^{11} \\ 5,10 * 10^{13} \\ 5,10 * 10^{15} \\ 2,19 * 10^{17} \end{bmatrix} \tag{3.37}$$

- **Subsystem 2 and 3** : $\det(s\mathbf{I} - A_e) = (s+\alpha_0)^{n+1} \mid n = n_2 = n_3 = 5$:

$$\begin{bmatrix} \beta_1 \\ \beta_2 \\ \beta_3 \\ \beta_4 \\ \beta_5 \\ \beta_6 \end{bmatrix} = \begin{bmatrix} 1,80 * 10^3 \\ 1,35 * 10^6 \\ 5,40 * 10^8 \\ 1,21 * 10^{11} \\ 1,46 * 10^{13} \\ 7,29 * 10^{14} \end{bmatrix} \tag{3.38}$$

2. for each subsystem, check that:
   - (A_e, B_e) controllable:
     - **Subsystem 1**:

$$\mathbf{M_{Ce1}} = \begin{bmatrix} \mathbf{B_{e1}} & \mathbf{A_{e1}B_{e1}} & \mathbf{A_{e1}}^2\mathbf{B_{e1}} & \dots & \mathbf{A_{e1}}^{(n_1+1)-1}\mathbf{B_{e1}} \end{bmatrix}$$
$$\rightarrow \text{rank}(\mathbf{M_{Ce1}}) = 7 = n_1 + 1$$

     - **Subsystem 2 and 3**:

$$\mathbf{M_{Ce2}} = \begin{bmatrix} \mathbf{B_{e2}} & \mathbf{A_{e2}B_{e2}} & \mathbf{A_{e2}}^2\mathbf{B_{e2}} & \dots & \mathbf{A_{e2}}^{(n_2+1)-1}\mathbf{B_{e2}} \end{bmatrix} = \mathbf{M_{Ce3}}$$
$$\rightarrow \text{rank}(\mathbf{M_{Ce2}}) = \text{rank}(\mathbf{M_{Ce3}}) = 6 = n_2 + 1 = n_3 + 1$$

   - (C_e, A_e) observable:

– **Subsystem 1**:

$$\mathbf{M_{Oe1}} = \begin{bmatrix} \mathbf{C_{e1}} \\ \mathbf{C_{e1}A_{e1}} \\ \mathbf{C_{e1}A_{e1}}^2 \\ \dots \\ \mathbf{C_{e1}A_{e1}}^{(n_1+1)-1} \end{bmatrix}$$
$$\rightarrow \text{ rank}(\mathbf{M_{Oe1}}) = 7 = n_1 + 1$$

– **Subsystem 2 and 3**:

$$\mathbf{M_{Oe2}} = \begin{bmatrix} \mathbf{C_{e1}} \\ \mathbf{C_{e1}A_{e1}} \\ \mathbf{C_{e1}A_{e1}}^2 \\ \dots \\ \mathbf{C_{e1}A_{e1}}^{(n_2+1)-1} \end{bmatrix} = \mathbf{M_{Oe3}}$$
$$\rightarrow \text{ rank}(\mathbf{M_{Oe2}}) = \text{rank}(\mathbf{M_{Oe3}}) = 6 = n_2 + 1 = n_3 + 1;$$

3. $\Gamma(e_1)$ is defined as:

$$\Gamma(e_1) = \begin{cases} \frac{e_1}{\delta^{1-\alpha}} - e_1 & for \quad |e_1| \leq \delta \\ |e_1|^\alpha \,\text{sign}(e_1) - e_1 & for \quad |e_1| > \delta \end{cases}$$

Its derivative can be defined as:

$$\frac{d\Gamma(e_1)}{d\, e_1} = \begin{cases} \frac{1}{\delta^{1-\alpha}} - 1 & for \quad |e_1| \leq \delta \\ \alpha e_1^{\alpha-1} - 1 & for \quad |e_1| > \delta \text{ and } e_1 > 0 \\ \alpha |e_1|^{\alpha-1} \,\text{sign}(e_1) - 1 & for \quad |e_1| > \delta \text{ and } e_1 < 0 \end{cases}$$

Hence, its derivative is always bounded with $\alpha = 0.65$ and $\delta = 0.9$; a constant γ satisfying the Lipschitz condition can always be found.

4. find $a, b \in \mathbb{R}$ such that: $\Gamma(e_1)$ satisfies the sector condition $[a, b] \,|\, \forall e_1 \in \mathbb{E} \subset \mathbb{R}$ (finite domain) [12]:

- based on the Γ-function: $\Gamma(e_1) = g(e_1) - e_1$ (see Figure 3.3), with $g(e_1)$ defined in (3.28), the upper bound b of the sector condition can be chosen through

the following:

$$b = \left.\frac{d\Gamma\left(e_1\right)}{de_1}\right|_{e_1=0} = \left.\frac{1}{\delta^{1-\alpha}}\right|_{e_1=0} = 0.038 \quad ;$$

In fact, $\Gamma\left(e_1\right)$ crosses the line $b * e_1$ only in the origin, and it lies below the latter one for $e_1 > 0$ and above it for $e_1 < 0$.

- a chosen such that the circle criterion is satisfied (for a finite domain):
  - the circle defined as the disk D whose diameter is the segment connecting the real points $\left(-\frac{1}{a}; -\frac{1}{b}\right)$ must contain the transfer function of system (3.31) $|G_{ei}(j\omega)|$ with $i = 1, 2, 3$, in the Nyquist plane;
    - $|G_{ei}(j\omega)| = |\mathbf{C_{ei}}\left(s\mathbf{I} - \mathbf{A_{ei}}\right)^{-1}\mathbf{B_{ei}}|$
  - a found through a graphical trial and error approach, in this case valid for all the subsystems: $a = -0.65$;

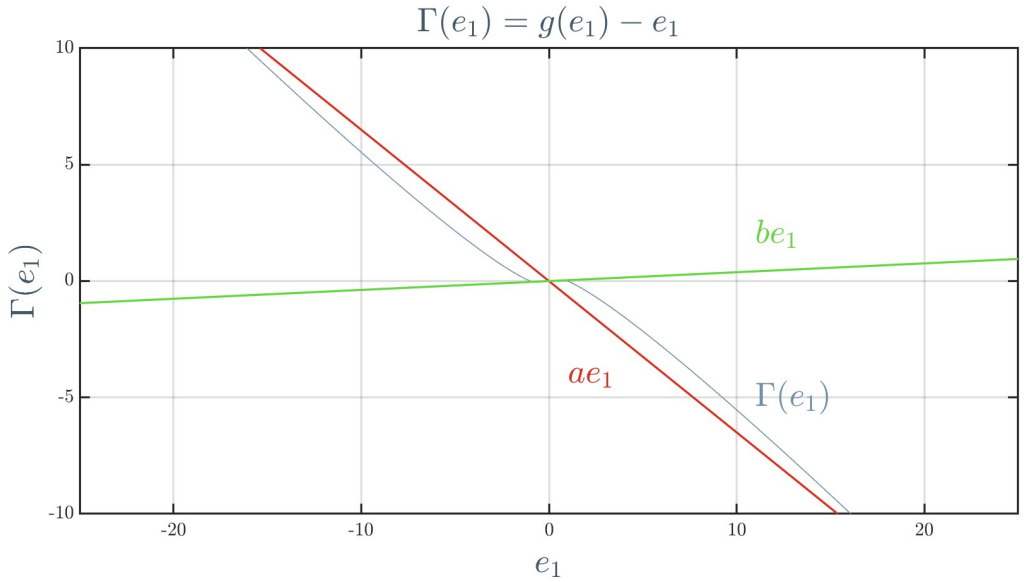

Figure 3.4: Sector condition for $\Gamma(e_1)$: as it can be seen, the function lies inside the region defined by ae_1 and be_1 curves.

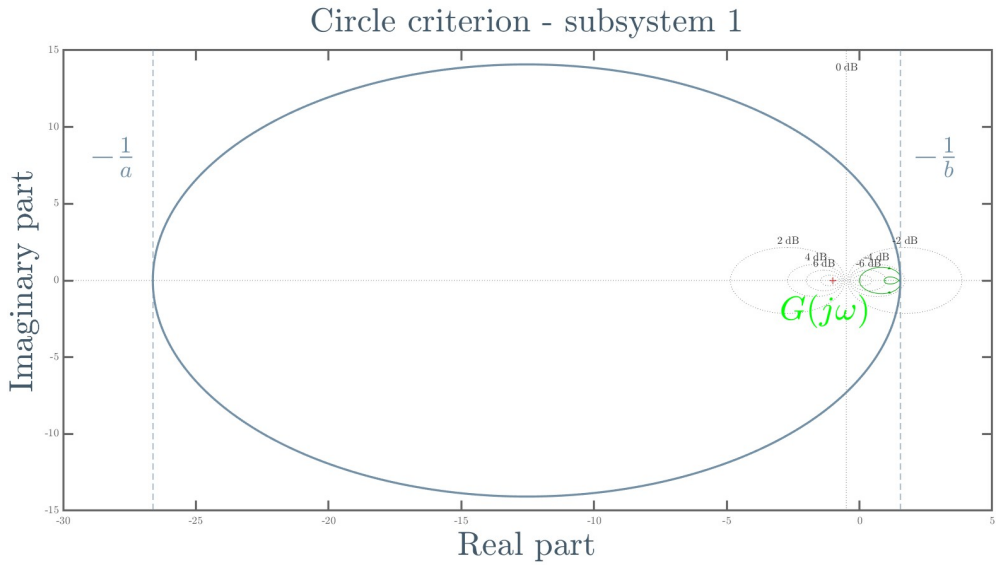

Figure 3.5: Circle criterion applied to subsystem 1, for which, based on the previous selection of the β coefficients, a and b parameters, it results satisfied.

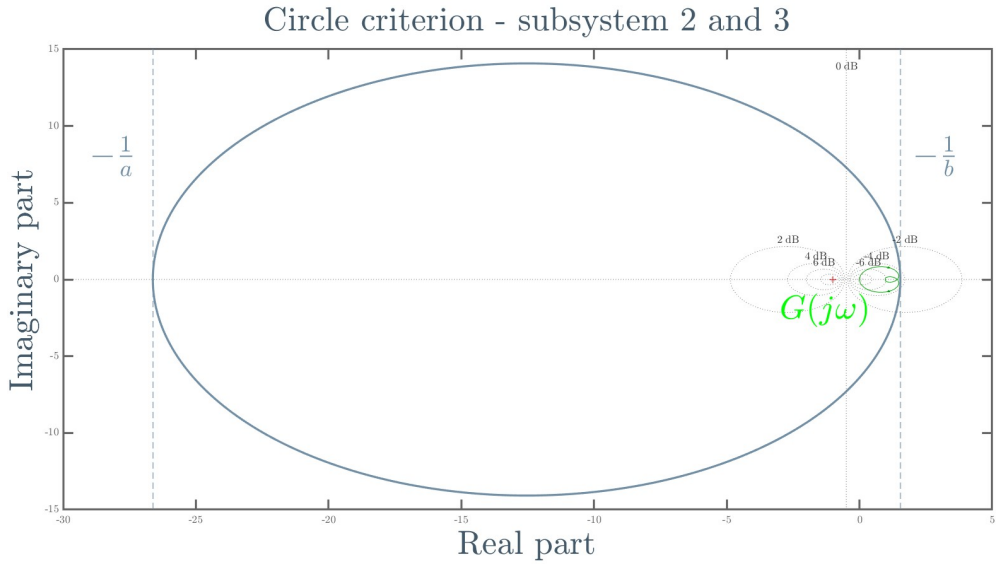

Figure 3.6: Circle criterion applied to subsystem 2 and 3, for which, based on the previous selection of the β coefficients, a and b parameters, it results satisfied.

5. the absolute stability is guaranteed only for $e_1 \in \mathbb{E}$ (finite domain), indeed the sector condition $[-0.65, 0.038]$ for the nonlinear function $\Gamma(e_1)$ is satisfied only locally:
   - $\Gamma(e_1)$ lies inside the sector defined by the two lines $a * e_1$ and $b * e_1$ only for

a limited value of e_1;

- $\mathbb{E} = [-e_{max}\ ;\ e_{max}]$;
- e_{max} is the maximum value of $e_1 > 0$ for which $\Gamma(e_1) > a * e_1$:
  - $a * e_{max} = \Gamma(e_{max}) = g(e_{max}) - e_{max} \quad \rightarrow\ e_{max} = 20.07$
  - $\mathbb{E} = [-20.07\ ;\ 20.07]$

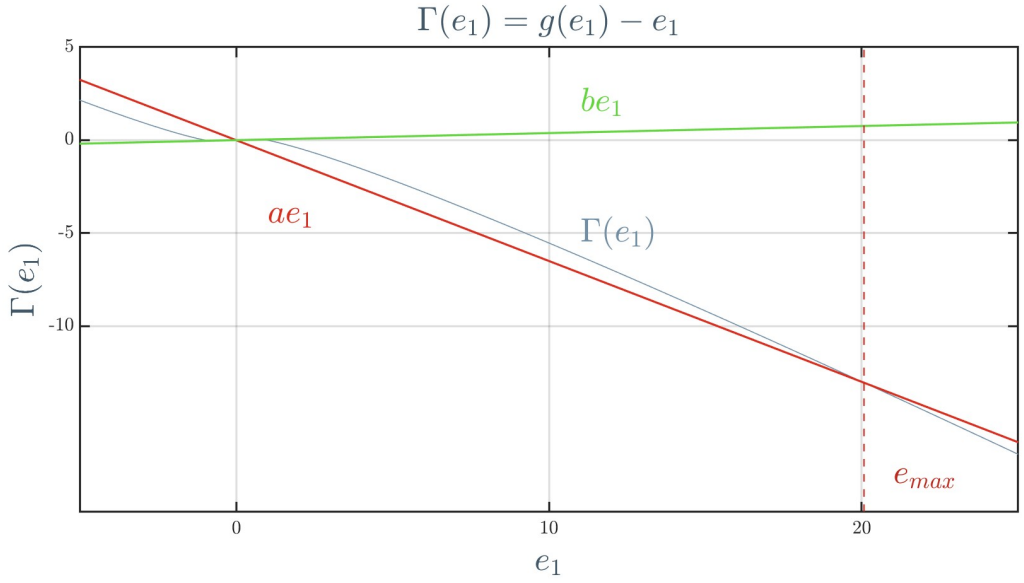

Figure 3.7: Sector condition for $\Gamma(e_1)$: e_{max} is highlighted.

From these last steps, it is clear that the absolute stability depends mainly on the choice of the β-coefficients and it is guaranteed only for a limited magnitude of e_1: thus, the $p.u.$ transformation performed in Section 2.2.2 is beneficial also for the observer stability, keeping a low magnitude value of the state variables and so of the related observation errors.

3.2. NLESO Simulation

3.2.1. Simulation setup

The main objective of the simulation is to assess the estimation performance of the state observer when the mechanical system is subject to torsional vibrations.
The simulation model is divided into several blocks and replicates the control system of a WECS; the model is implemented in a Simulink environment.
Being the aim mainly to validate the state observer's performance, several simplifications are adopted. Starting from the converter's model, it is represented with a unitary gain time delay block assuming a converter operation at a constant switching frequency of $f_{sw} = 1000\ [Hz]$: therefore, the stator voltage output coming from the control system is assumed to be equal to the actual stator voltage applied to the machine, shifted by a small time delay. This simplification represents an ideal condition where no undesirable harmonics are injected by the converter. Hence, the stator voltage harmonics have to be added manually to the control output, through a voltage harmonic injection, in order to induce a resonant condition and properly test the observer's performance; a simple block scheme of this action can be seen in Figure 3.8.

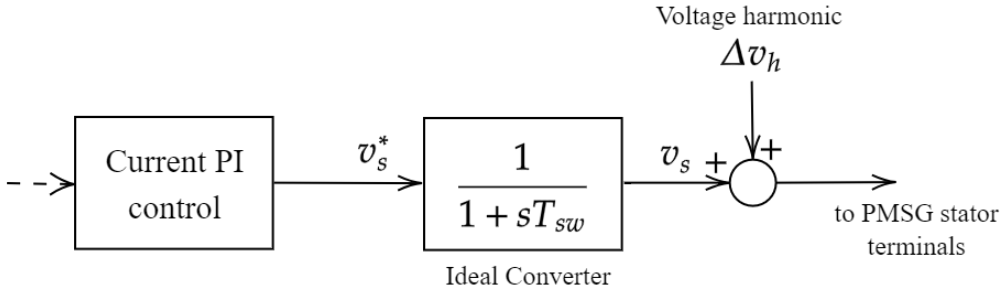

Figure 3.8: simple block scheme of the voltage harmonic Δv_h added to the output of the ideal inverter v_s.

For this reason, the simulation analysis is divided into three steps:

1. operation in ideal conditions, i.e. no voltage harmonic injection;
2. operation in perturbed conditions through the injection of a voltage harmonic at a frequency f_{dist} far from the system's natural frequency;
3. operation in perturbed conditions through the injection of a voltage harmonic at

a frequency f_{res} that excites the system's natural frequency;

In this way, it is possible to evaluate the accuracy of the state estimation and analyze the influence of the resonant condition on the observer operation at steady state.
Recalling the analysis carried out in Section 2.2.3, considering a PWM VSC with $m_f = 33$, the following voltage harmonic orders are able to generate a torque harmonic exciting the resonance frequency in the operating region of the system:

- $h_v = 31, 29 \rightarrow h_T = 30$;
- $h_v = 37, 35 \rightarrow h_T = 36$;
- $h_v = 67, 65 \rightarrow h_T = 66$.

Based on these results, it was decided to inject one voltage component of order $h_v = 35$ and evaluate the system behavior at steady state with a rotor mechanical angular speed:

$$\omega_1^* = \omega_{ref} = 9.69\,[rpm]$$

In this way, a torque harmonic component exciting the system's natural frequency is induced and the observer's performance in this condition can be evaluated.
Regarding the voltage harmonic at a frequency f_{dist} far from the system's natural frequency, the voltage harmonic of order $h_v = 65$ that creates a torque component of order $h_T = 66$ was injected, which at the simulation reference angular speed ω_{ref} correspond to a frequency of:

$$f_{dist} = h_T \frac{p\,\omega_{ref}}{4\pi} = 551.7\ [Hz]\ >\ f_{res} = 302.45\ [H_z]$$

Considering that $V_{n,phase} = 435[V]$ for the PMSG under consideration, to properly excite the system a magnitude $V_{35} = V_{65} = 300\,[V]$ was selected. This choice is arbitrary and it provides a good mechanical vibrations' excitation to the system, needed to properly assess the observer dynamics. Finally, it must be noticed that the direct and quadrature component of the voltage harmonic injected represent respectively inputs Δv_{sd} and Δv_{sq} of each subsystem.
Each NLESO needs for its operation the related output Δy, which are:

- $\Delta\theta_1$ for Subsystem 1;
- Δi_{sd} for Subsystem 2;
- Δi_{sq} for Subsystem 3.

These last quantities are the oscillating term of the homonymous measured state vari-

ables. In order to extract their values during the simulation, an High-Pass (HP) Filter is designed and applied to the measured quantities, so to:

- θ_1;
- i_{sd};
- i_{sq}.

A simple block scheme of the filter can be seen in Figure 3.9; the design of the filter can be found in Appendix A.5.

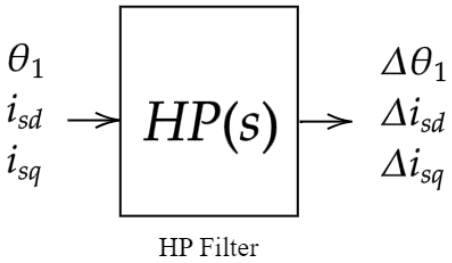

Figure 3.9: simple block scheme of the High-Pass (HP) Filter applied to each measured state variables in order to extract their oscillating term information.

The simulation is initialized with the system rotating at ω_{ref}, providing all the initial values to the system state variables and Proportional-Integral (PI) regulator integral blocks to guarantee a steady state operation from the beginning.

3.2.2. Simulation Results

The scheme comprising the ideal inverter, the voltage harmonic injection, the PMSG and the wind turbine is shown in Figure 3.10.

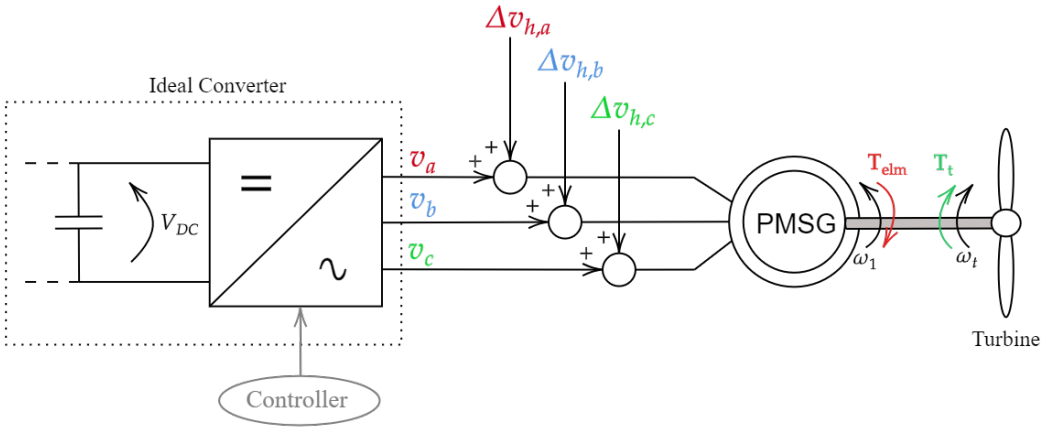

Figure 3.10: overall setup; starting from the left: ideal converter, voltage harmonic injection, PMSG directly coupled with the wind turbine.

The turbine and PMSG rotor angular speed trends and the reference ω_{ref} are displayed in Figure 3.11.

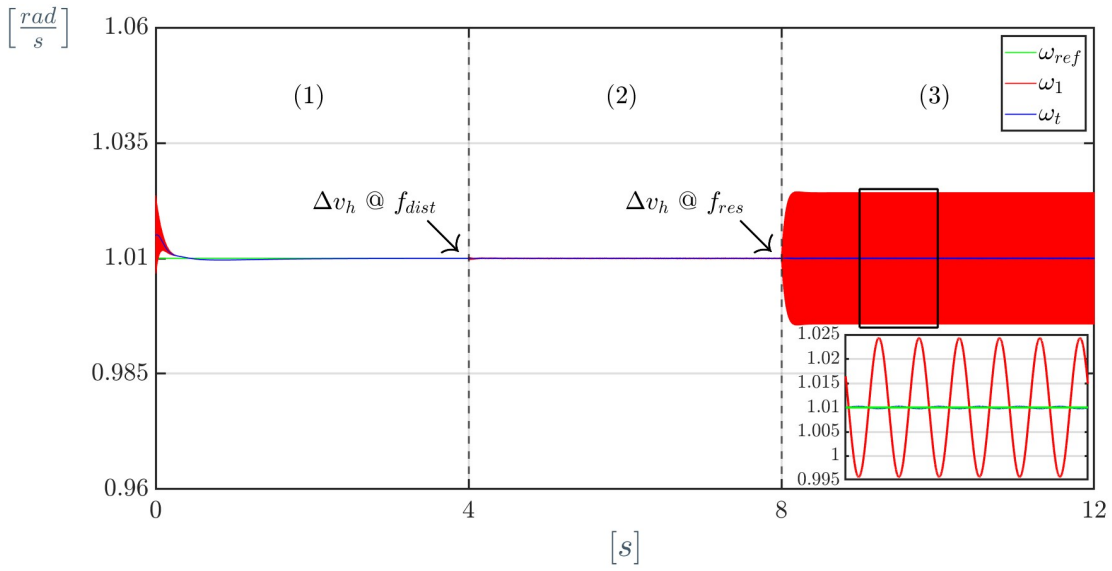

Figure 3.11: Simulation speeds' trends

As can be seen, the simulation is divided into three parts $(1), (2), (3)$ characterized by three different voltage harmonic injections: the voltage harmonic at f_{dist} is injected between seconds 4 and 8 of the simulation, while the voltage harmonic leading to the mechanical resonant condition is present between seconds 8 and 12. The 3-phase stator voltage waveforms in each simulation part before and after the voltage harmonic injection can be seen in Figure 3.12.

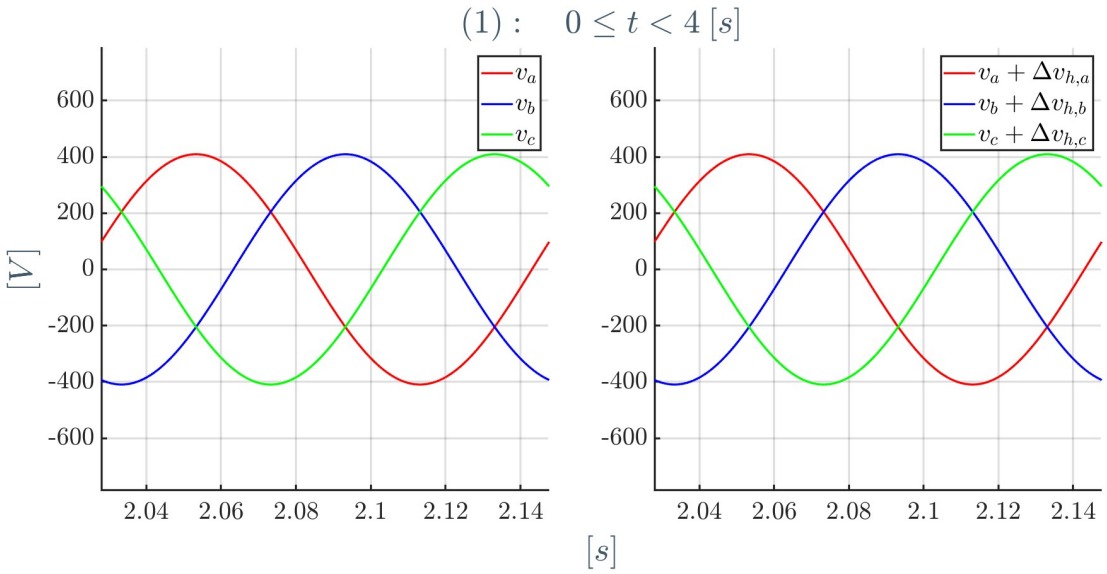
(1) : 0 ≤ t < 4 [s]
v_a
v_b
v_c
v_a + Δv_h,a
v_b + Δv_h,b
v_c + Δv_h,c
600
400
200
0
-200
-400
-600
[V]
2.04
2.06
2.08
2.1
2.12
2.14
[s]

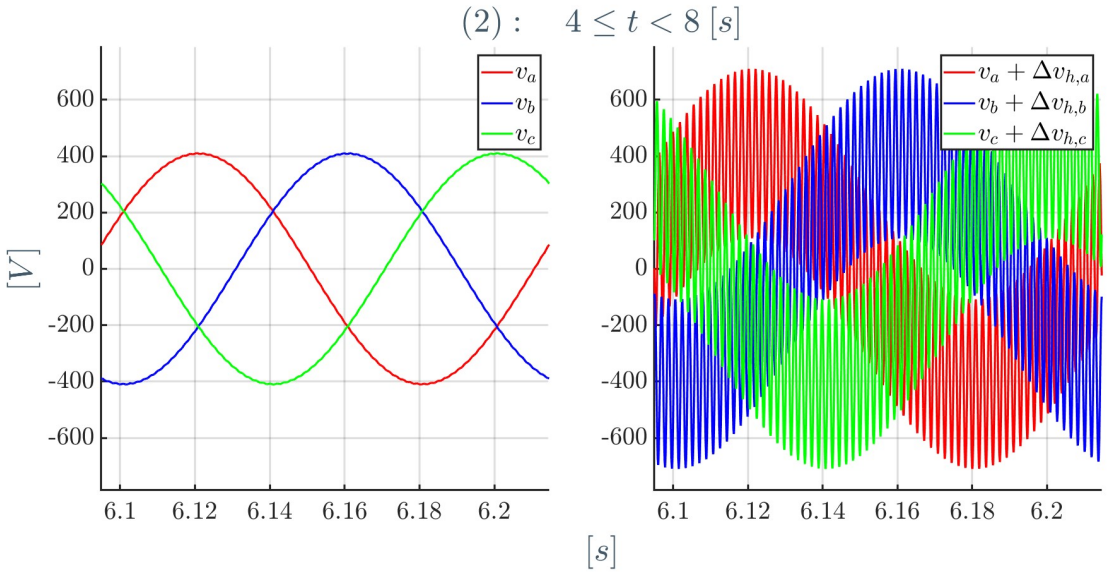
(2) : 4 ≤ t < 8 [s]
v_a
v_b
v_c
v_a + Δv_h,a
v_b + Δv_h,b
v_c + Δv_h,c
600
400
200
0
-200
-400
-600
[V]
6.1
6.12
6.14
6.16
6.18
6.2
[s]

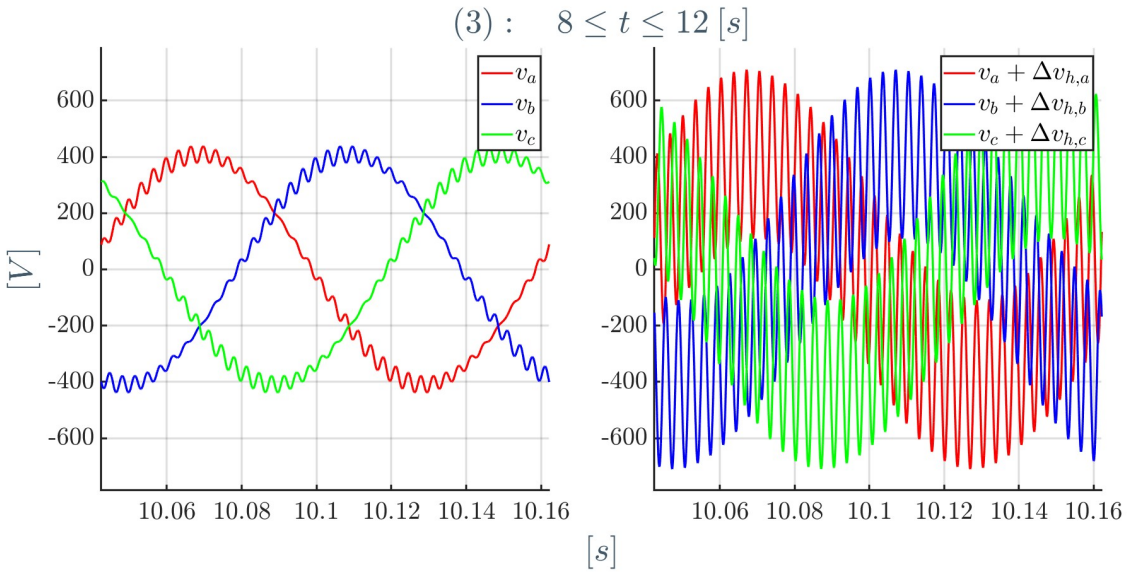

Figure 3.12: stator voltage waveforms before and after the voltage harmonic injection in simulation part (1) (top), (2) (middle), and (3) (bottom)

The distortion in the 3-phase voltage waveforms v_{abc} at the output of the ideal inverter that can be seen in (3) and little in (2) are due to the action of the current control loop. In fact, the current PI regulators' cut-off frequency is set at $\omega_{cI} = 30\,[\frac{rad}{s}]$, which is much lower than the harmonic injections' angular frequencies, located at:

- (2): $f_{dist} = 551.70\,[Hz] \rightarrow \omega_{dist} = 2\pi f_{dist} = 3466.4\,[\frac{rad}{s}]$;
- (3): $f_{res} = 302.45\,[Hz] \rightarrow \omega_{res} = 2\pi f_{res} = 1900.3\,[\frac{rad}{s}]$.

Therefore, the current control loops' response to the voltage harmonic injections is limited in magnitude, i.e. it is not able to damp the action of the disturbance $\Delta v_{h,abc}$, but it is not null. The voltage distortion is more evident for (3) since ω_{res} is lower than ω_{dist} and so closer to ω_{cI}.
The state observer's estimation accuracy for the generic system state variable x_i will be analyzed through the following plots:

- a set of plots showing x_i and its estimate $\hat{x}_i$ at the beginning of each simulation phase ((1), (2), and (3));
- a set of plots showing x_i, $\hat{x}_i$, and the observation error $e_i = x_i - \hat{x}_i$ [5] at steady-state operation in each simulation phase ((1), (2), and (3));

[5] from a results' analysis point of view, this definition has the same meaning of $e_i = \hat{x}_i - x_i$ used previously

These two sets of plots are sufficient to evaluate the state observers' performance: in fact, the generic state variable's estimate $\hat{x}_i$ shows an overshoot when facing a change of operating conditions, which is the case of the simulation beginning or change of Δv_{abc} , and then it tends to a steady-state observation error $x_i - \hat{x}_i$ throughout the simulation.
Starting from the angular position $\Delta\theta_t$ and $\Delta\theta_1$, the plots are shown in Figure 3.13 and 3.14.

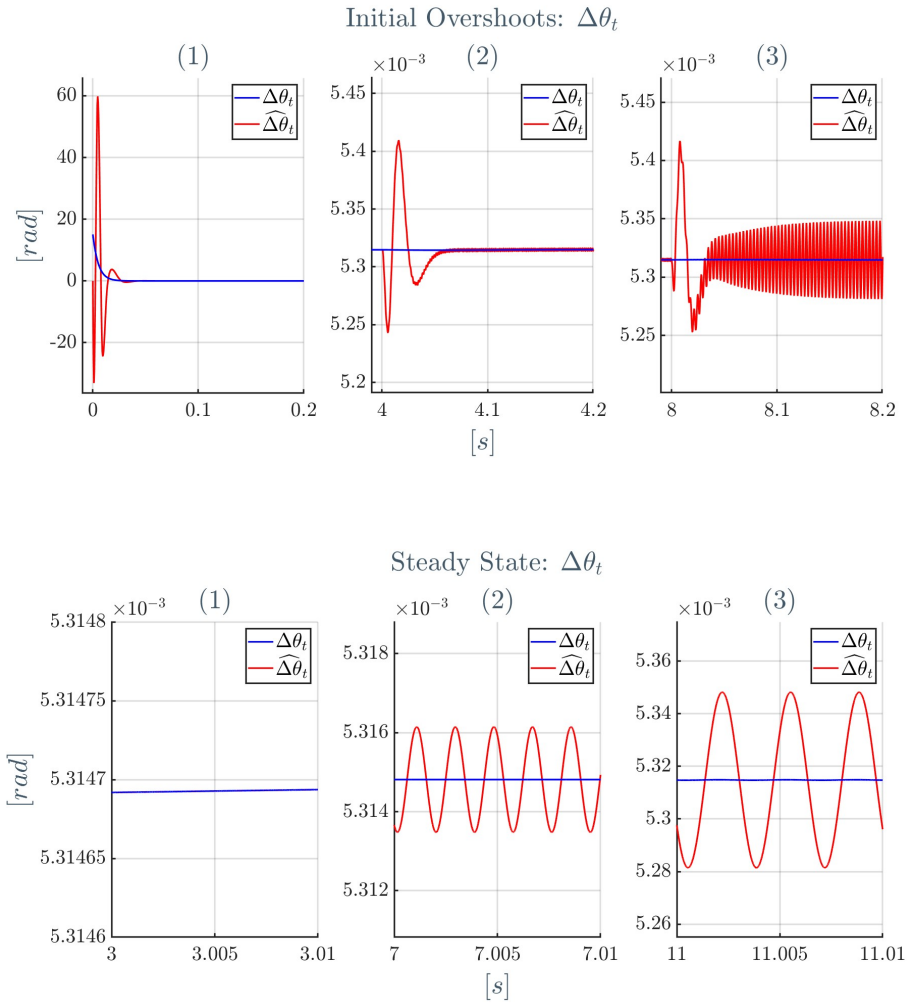

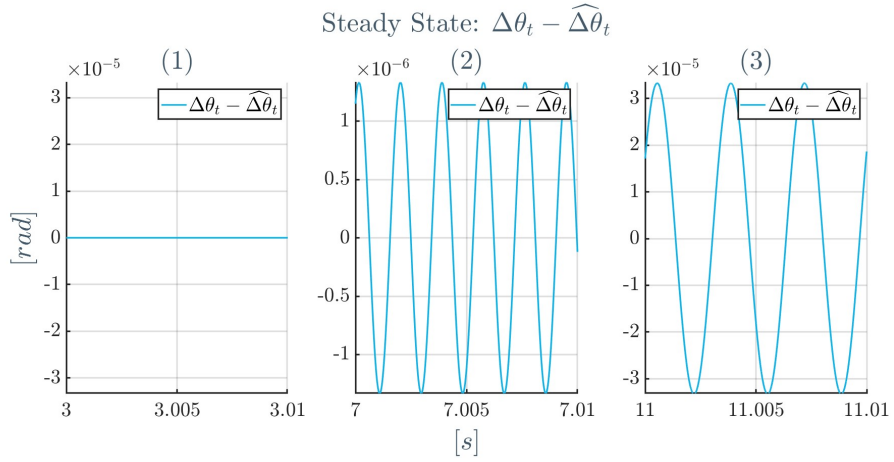

Figure 3.13: $\Delta\theta_t$ true value and estimate during the initial overshoot at the beginning of each simulation phase ((1)-(2)-(3)) (top); $\Delta\theta_t$ true value and estimate at steady state in each simulation phase (middle); observation error $e_1 = \Delta\theta_t - \widehat{\Delta\theta_t}$ at steady state in each simulation phase (bottom)

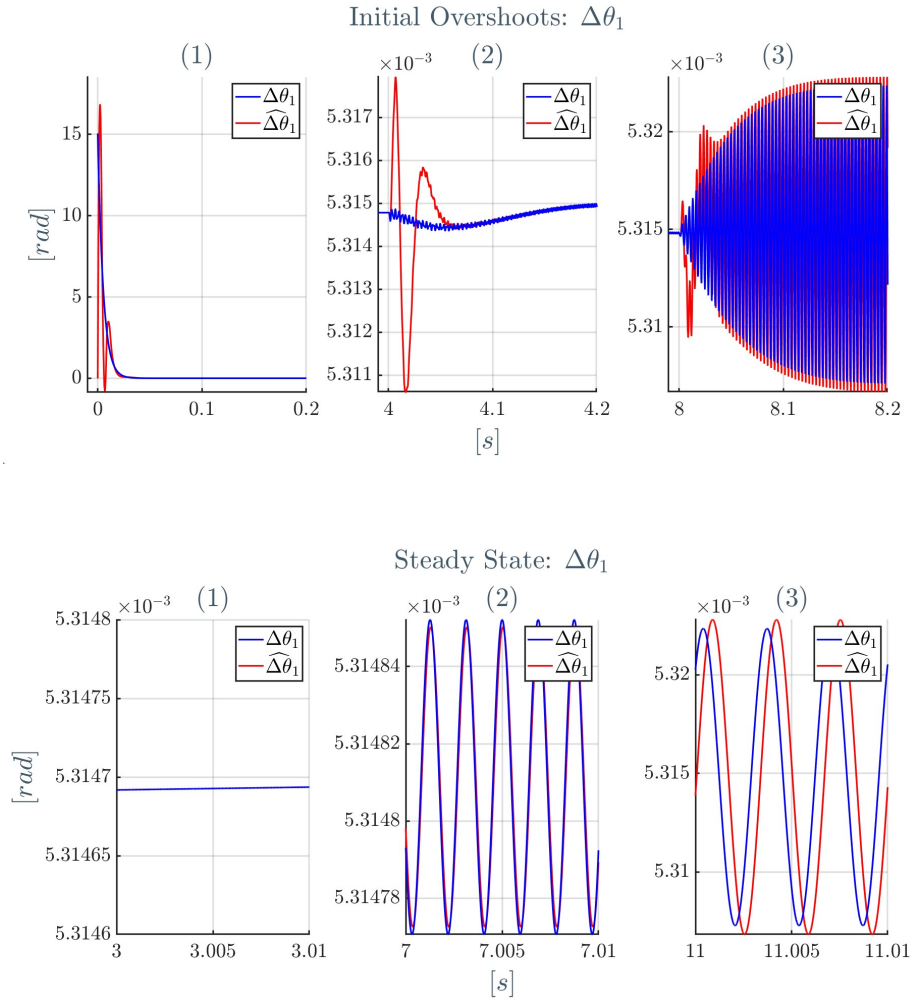

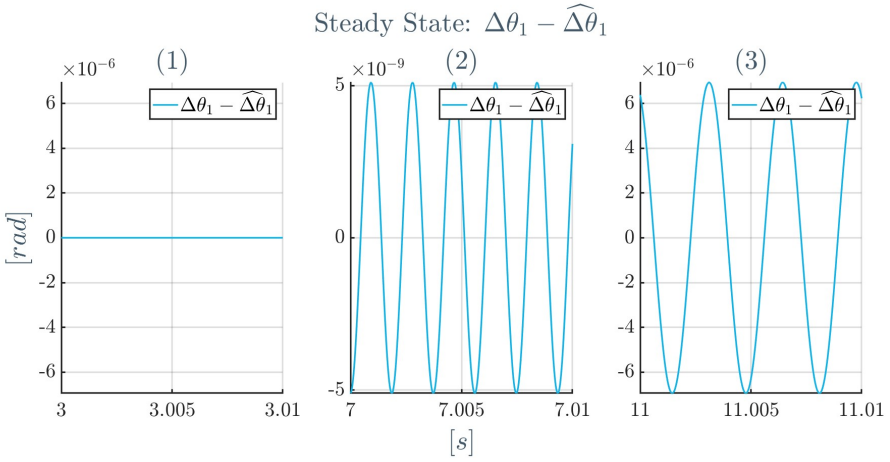

Figure 3.14: $\Delta\theta_1$ true value and estimate during the initial overshoot at the beginning of each simulation phase ((1)-(2)-(3)) (top); $\Delta\theta_1$ true value and estimate at steady state in each simulation phase (middle); observation error $e_2 = \Delta\theta_1 - \widehat{\Delta\theta_1}$ at steady state in each simulation phase (bottom)

The estimation for $\Delta\theta_t$ provided by the NLESO is characterized by a relatively big estimation error: the estimated variable has strong oscillations which are not present in the real value. On the other hand, the estimation of $\Delta\theta_1$ appears to be more accurate, probably because this state variable is Subsystem 1's observer input. However, during mechanical resonance condition, so in simulation phase (3), the phase shift between $\Delta\theta_1$ and its estimate increases, leading to a greater observation error. Both $\Delta\theta_t$ and $\Delta\theta_1$ show a null observation error at simulation phase (1), which is expected since no voltage harmonic injection is present. Of course, this last statement is valid for the other state variables too.
The estimation of the angular positions allows calculating the shaft torque's oscillating component ΔT_{sh}, defined as:

$$\Delta T_{sh} = K_1(\Delta\theta_t - \Delta\theta_1) \tag{3.39}$$

This quantity represents the oscillating part of the torque arising between the two rotating masses, i.e. the wind turbine and the PMSG rotor, due to the difference between θ_t and θ_1, which represents the relative torsional motion, as explained in Section 2.2.1. By using the angular positions' estimates, $\widehat{\Delta T_{sh}}$ can be defined as:

$$\widehat{\Delta T_{sh}} = K_1(\widehat{\Delta\theta_t} - \widehat{\Delta\theta_1}) \tag{3.40}$$

The graphs related to the shaft torque oscillating component and its estimate can be found in Figure 3.15.

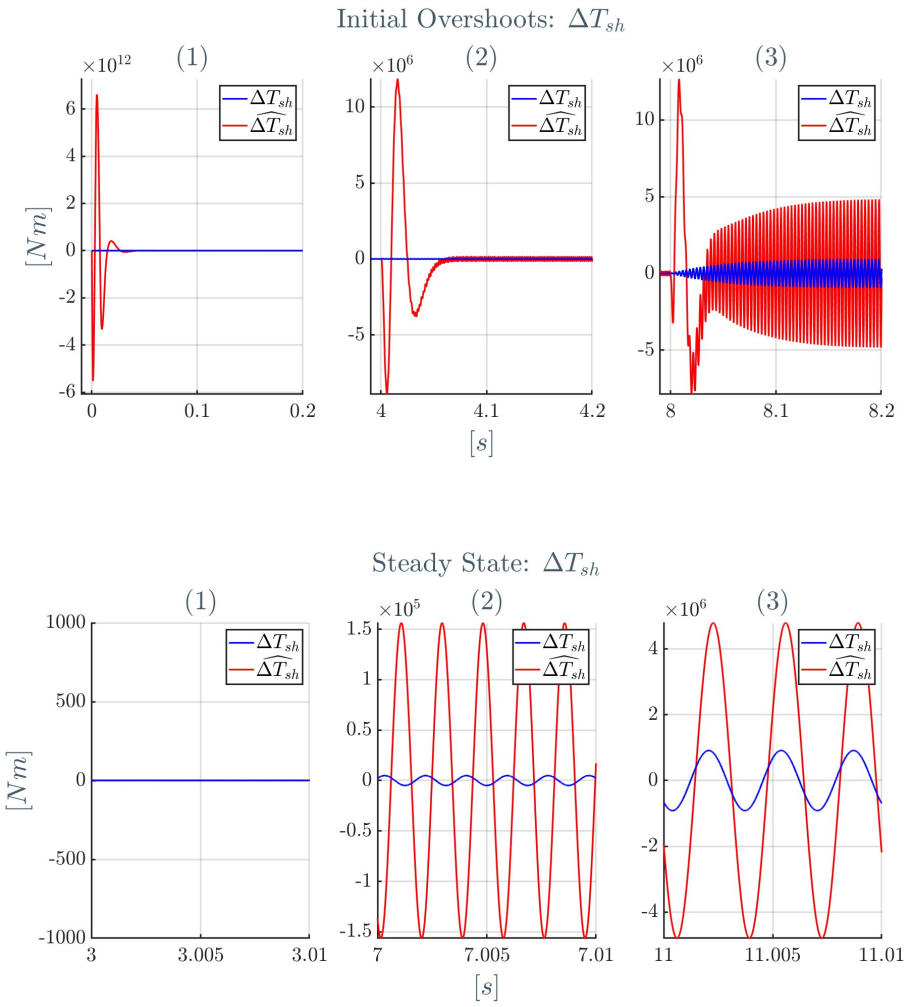

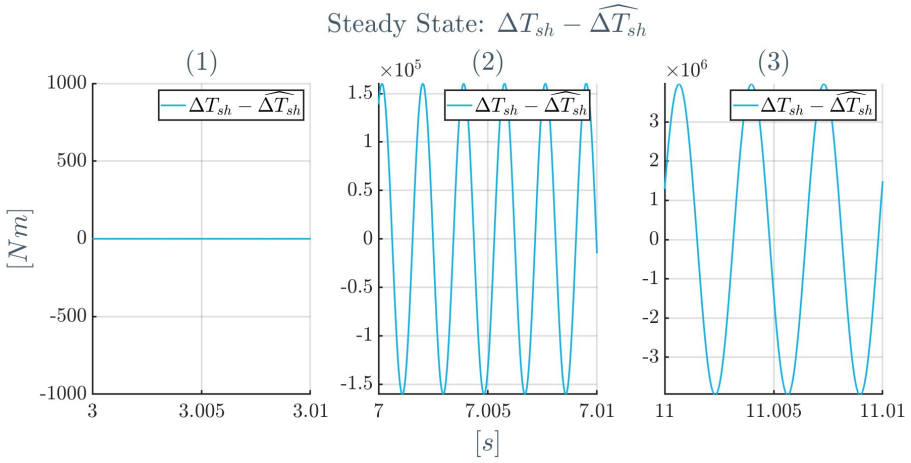

Figure 3.15: ΔT_{sh} true value and estimate during the initial overshoot at the beginning of each simulation phase ((1)-(2)-(3)) (top); ΔT_{sh} true value and estimate at steady state in each simulation phase (middle); observation error $\Delta T_{sh} - \widehat{\Delta T_{sh}}$ at steady state in each simulation phase (bottom)

As can be seen, the inaccuracy in the estimation of $\Delta\theta_t$ and $\Delta\theta_1$ leads to a big error in the estimation of the shaft torque. In simulation phase (2), $\widehat{T_{sh}}$ shows a big phase shift with respect to T_{sh}, qualitatively of $180\ [deg]$, while it does not in (3). Moreover, the estimation error's magnitude in both parts of the simulation is very high and entails a misleading shaft torque estimation.
For what concerns the angular speeds $\Delta\omega_t$ and $\Delta\omega_1$, their graphs are shown in Figure 3.16 and 3.17.

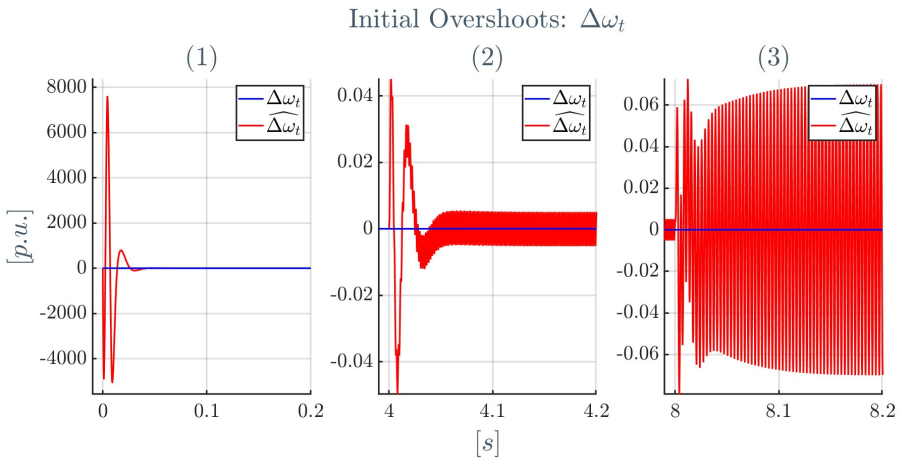

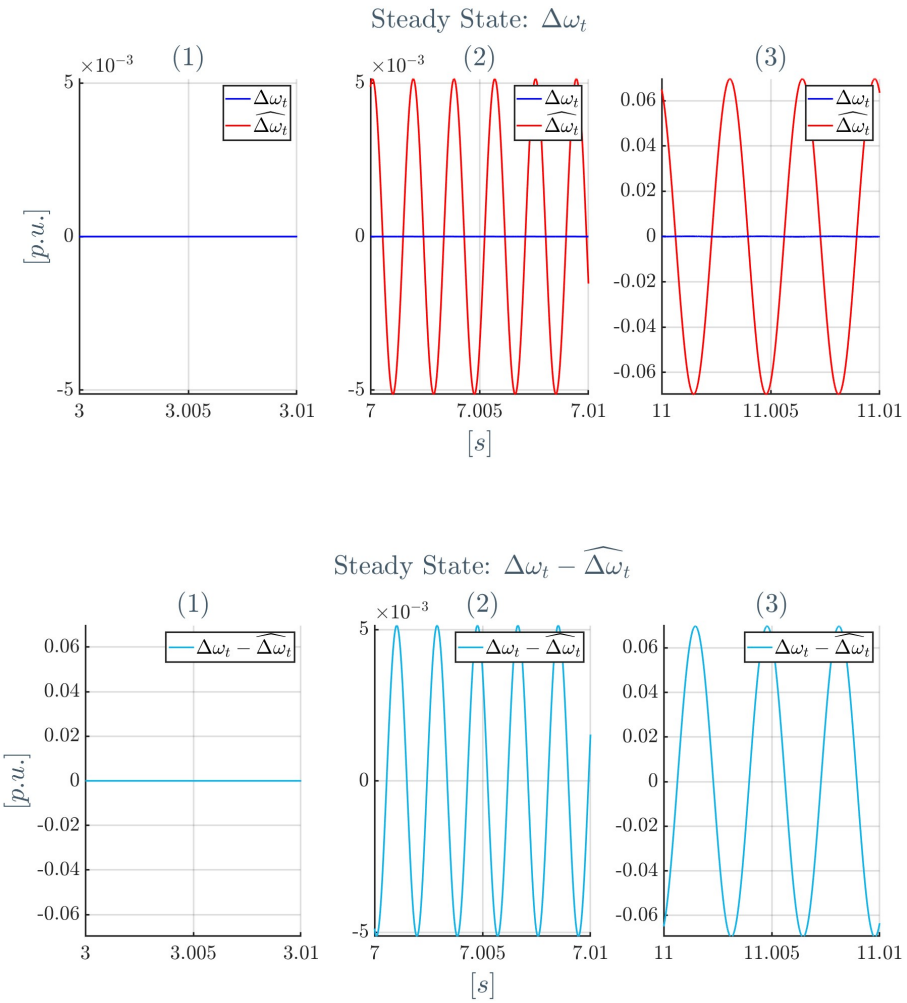

Figure 3.16: $\Delta\omega_t$ true value and estimate during the initial overshoot at the beginning of each simulation phase ((1)-(2)-(3)) (top); $\Delta\omega_t$ true value and estimate at steady state in each simulation phase (middle); observation error $e_3 = \Delta\omega_t - \widehat{\Delta\omega_t}$ at steady state in each simulation phase (bottom)

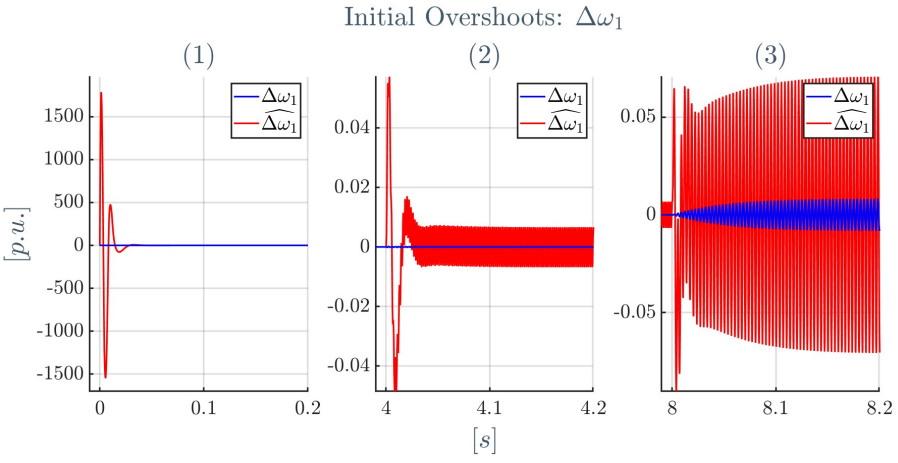

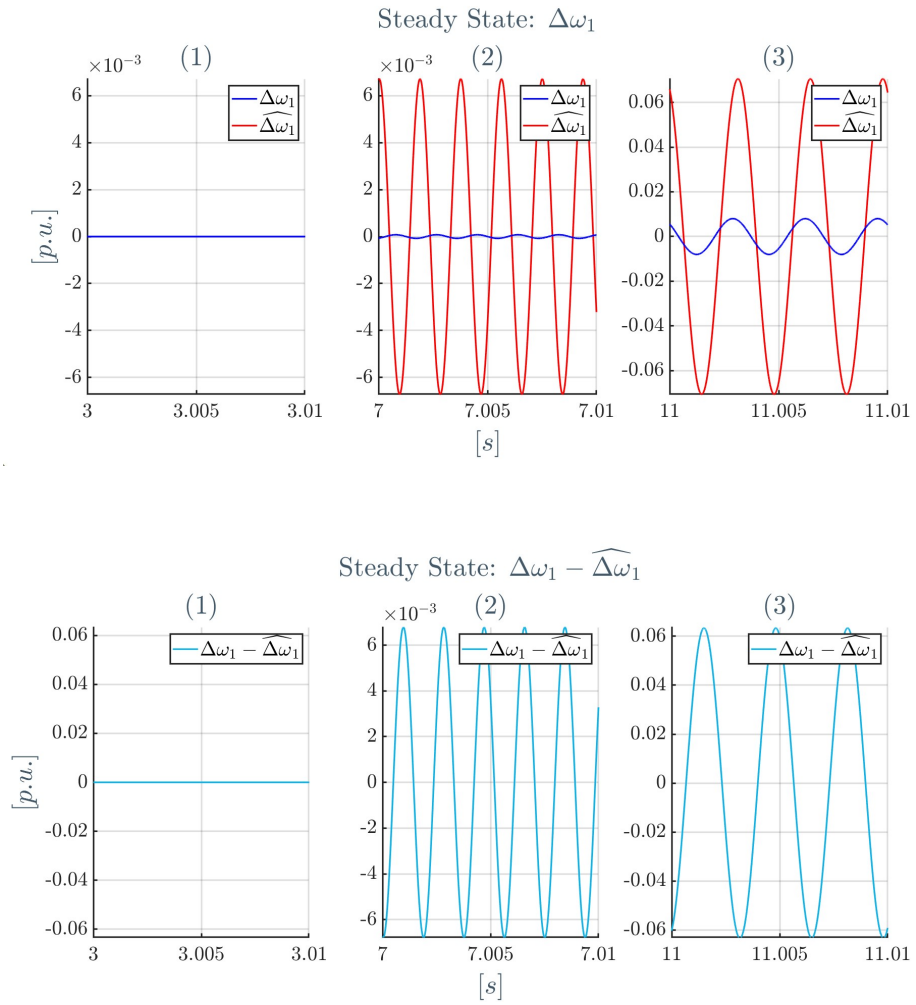

Figure 3.17: $\Delta\omega_1$ true value and estimate during the initial overshoot at the beginning of each simulation phase ((1)-(2)-(3)) (top); $\Delta\omega_1$ true value and estimate at steady state in each simulation phase (middle); observation error $e_4 = \Delta\omega_1 - \widehat{\Delta\omega_1}$ at steady state in each simulation phase (bottom)

Both estimations are characterized by a high level of inaccuracy. The bad estimation of $\Delta\theta_t$ is reflected in $\Delta\omega_t$, which is its derivative. Also from a mechanical point of view, the result is not consistent, since the wind turbine's torsional vibrations should be limited by its high inertia. In simulation phase (2), $\widehat{\Delta\omega_1}$ overestimates $\Delta\omega_1$ and it is almost out of phase with respect to it; in (3), the phase shift decreases but the difference in magnitude is still important.
The graphs related to the oscillating term of the stator currents direct and quadrature components, i.e. Δi_{sd} and Δi_{sq}, are presented in Figures 3.18 and 3.19.

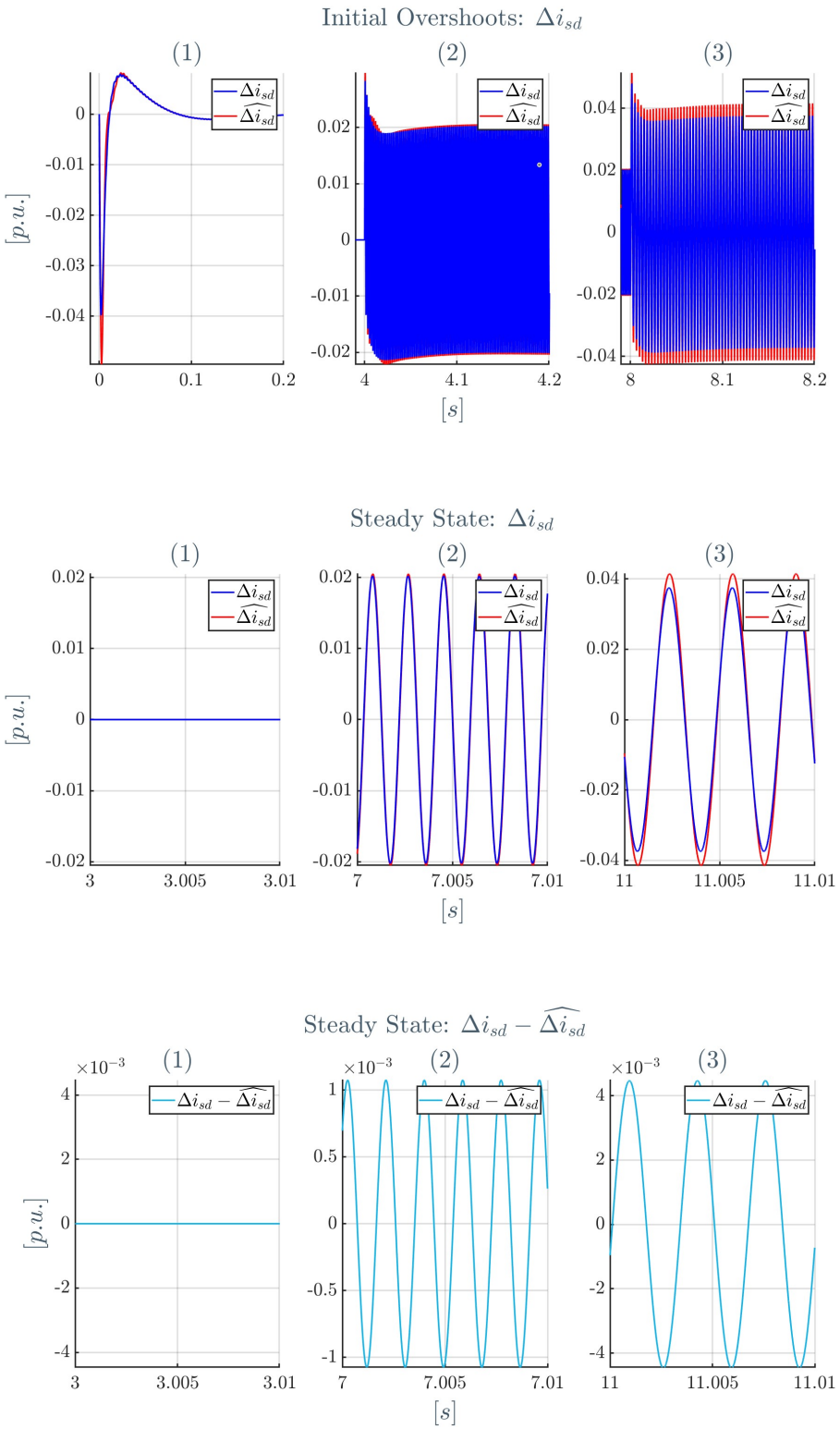

Figure 3.18: Δi_{sd} true value and estimate during the initial overshoot at the beginning of each simulation phase ((1)-(2)-(3)) (top); Δi_{sd} true value and estimate at steady state in each simulation phase (middle); observation error $e_5 = \Delta i_{sd} - \widehat{\Delta i_{sd}}$ at steady state in each simulation phase (bottom)

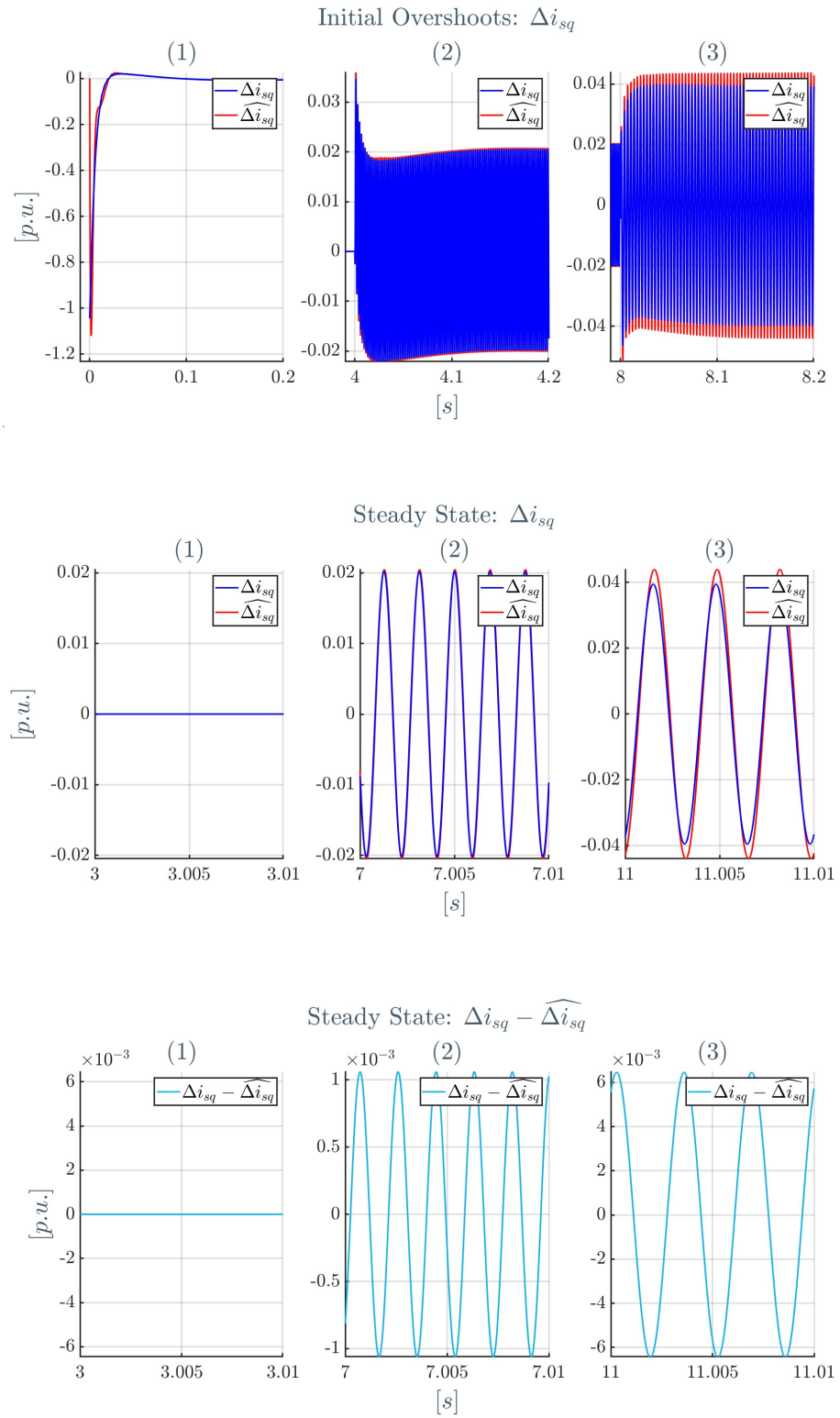

Figure 3.19: Δi_{sq} true value and estimate during the initial overshoot at the beginning of each simulation phase ((1)-(2)-(3)) (top); Δi_{sq} true value and estimate at steady state in each simulation phase (middle); observation error $e_6 = \Delta i_{sq} - \widehat{\Delta i_{sq}}$ at steady state in each simulation phase (bottom)

In this case, the observer provides accurate estimates, both in terms of observation error and phase shift between the true value and its estimate: indeed, as in $\Delta\theta_1$ case, these two state variables represent Subsystem 2 and 3's observers' inputs. In each simulation phase the initial overshoot is limited for both Δi_{sd} and Δi_{sq}, and the observation error tends quickly to a steady-state value.
Some final considerations can be made about the NLESO. First of all, the overall state observer is stable: even under strong perturbations, as in mechanical resonance condition, each observation error reaches a bounded steady state oscillating value around zero. Moreover, the NLESO provides the most accurate estimates for the state variables that are also the subsystems' observers' inputs, so for $\Delta\theta_1$, Δi_{sd} and Δi_{sq}. On the other hand, the NLESO's estimation performance is highly influenced by the presence of disturbances, as it is shown by the high observation errors when a voltage harmonic is injected; the estimation inaccuracy is higher in the case of mechanical resonance condition. From a state observer design point of view, the analytical derivation represents another disadvantage, being quite cumbersome and working on a linearized model of the system only. In addition, the computational burden required to estimate several state variables for three different subsystems can be considered another limiting factor. Due to the above consideration, in the next chapter another state observer type is analyzed and its performance is evaluated and compared to the NLESO.

4 | Luenberger-based Lipschitz Observer

In this chapter, the design of a Luenberger-based state observer for the system already defined is performed. After an initial definition of the observer's main characteristics, the main results from the simulation model will be discussed and compared to the results obtained with the NLESO in Chapter 3. This observer deals directly with the nonlinear system, allowing an easier design compared to the NLESO case, where a small-variation analysis is needed.

4.1. State Observer definition

4.1.1. System definition

Recalling (2.19), the 2-DOF system is represented by:

$$\begin{cases} \dot{\theta}_t = \omega_{b,mech}\omega_t \\ \dot{\theta}_1 = \omega_{b,mech}\omega_1 \\ \dot{\omega}_t = -\frac{B_1\omega_{b,mech}}{2H_tT_n}(\omega_t - \omega_1) - \frac{K_1}{2H_tT_n}(\theta_t - \theta_1) + \frac{T_t}{2H_tT_n} \\ \dot{\omega}_1 = \frac{B_1\omega_{b,mech}}{2H_1T_n}(\omega_t - \omega_1) + \frac{K_1}{2H_1T_n}(\theta_t - \theta_1) - \frac{T_{elm}}{2H_1T_n} \\ \dot{i_{sd}} = -r_s\frac{\omega_b}{l_s}i_{sd} + \omega_b i_{sq}\omega_1 + \frac{\omega_b}{l_s}v_{sd} \\ \dot{i_{sq}} = -r_s\frac{\omega_b}{l_s}i_{sq} - \omega_b i_{sd}\omega_1 - \frac{\omega_b}{l_s}\psi_{PM}\omega_1 + \frac{\omega_b}{l_s}v_{sq} \\ y_1 = \theta_1 \\ y_2 = i_{sd} \\ y_3 = i_{sq} \end{cases} \tag{4.1}$$

Neglecting the damping torque contribution and grouping all the non-linear terms inside a unique vector $\mathbf{\Phi}(\mathbf{x}, t) \in \mathbb{R}^n$, the system can be expressed in matrix form as:

$$\underbrace{\begin{bmatrix} \dot{\theta}_t \\ \dot{\theta}_1 \\ \dot{\omega}_t \\ \dot{\omega}_1 \\ \dot{i}_{sd} \\ \dot{i}_{sq} \end{bmatrix}}_{\dot{\mathbf{x}}} = \underbrace{\begin{bmatrix} 0 & 0 & \omega_{b,mech} & 0 & 0 & 0 \\ 0 & 0 & 0 & \omega_{b,mech} & 0 & 0 \\ -\frac{K_1}{2H_tT_n} & \frac{K_1}{2H_tT_n} & 0 & 0 & 0 & 0 \\ \frac{K_1}{2H_1T_n} & -\frac{K_1}{2H_1T_n} & 0 & 0 & 0 & -\frac{n_p(I_b\psi_b)\psi_{PM}}{2H_1T_n} \\ 0 & 0 & 0 & 0 & -r_s\frac{\omega_b}{l_s} & 0 \\ 0 & 0 & 0 & -\frac{\omega_b}{l_s}\psi_{PM} & 0 & -r_s\frac{\omega_b}{l_s} \end{bmatrix}}_{\mathbf{A}} \underbrace{\begin{bmatrix} \theta_t \\ \theta_1 \\ \omega_t \\ \omega_1 \\ i_{sd} \\ i_{sq} \end{bmatrix}}_{\mathbf{x}} +$$

$$+ \underbrace{\begin{bmatrix} 0 \\ 0 \\ 0 \\ 0 \\ \omega_b i_{sq}\omega_1 \\ -\omega_b i_{sd}\omega_1 \end{bmatrix}}_{\mathbf{\Phi}(\mathbf{x},t)} + \underbrace{\begin{bmatrix} 0 & 0 & 0 \\ 0 & 0 & 0 \\ \frac{1}{2H_tT_n} & 0 & 0 \\ 0 & 0 & 0 \\ 0 & \frac{\omega_b}{l_s} & 0 \\ 0 & 0 & \frac{\omega_b}{l_s} \end{bmatrix}}_{\mathbf{B}} \underbrace{\begin{bmatrix} T_t \\ v_{sd} \\ v_{sq} \end{bmatrix}}_{\mathbf{u}}$$

$$\underbrace{\begin{bmatrix} y_1 \\ y_2 \\ y_3 \end{bmatrix}}_{\mathbf{y}} = \underbrace{\begin{bmatrix} 0 & 1 & 0 & 0 & 0 & 0 \\ 0 & 0 & 0 & 0 & 1 & 0 \\ 0 & 0 & 0 & 0 & 0 & 1 \end{bmatrix}}_{\mathbf{C}} \underbrace{\begin{bmatrix} \theta_t \\ \theta_1 \\ \omega_t \\ \omega_1 \\ i_{sd} \\ i_{sq} \end{bmatrix}}_{\mathbf{x}} \tag{4.2}$$

where $\mathbf{x} \in \mathbb{R}^n$, $\mathbf{y} \in \mathbb{R}^q$, $\mathbf{A} \in \mathbb{R}^{nxn}$, $\mathbf{B} \in \mathbb{R}^{nxp}$ and $\mathbf{C} \in \mathbb{R}^{qxn}$, with $n = 6$, $p = 3$ and $q = 3$. Now, $\mathbf{\Phi}(\mathbf{x}, t) : \mathbb{R}^n \to \mathbb{R}^n$ is a continuous nonlinear function that satisfies the Lipschitz condition for a given subset $\mathbb{X} \subset \mathbb{R}^n$:

$$||\mathbf{\Phi}(\mathbf{x_1}, t) - \mathbf{\Phi}(\mathbf{x_2}, t)|| \leq \gamma \, ||\mathbf{x_1} - \mathbf{x_2}|| \quad | \, \forall \mathbf{x_1}, \mathbf{x_2} \in \mathbb{X} \, , \, \forall t \in \mathbb{R} \tag{4.3}$$

for some Lipschitz constant $\gamma > 0 | \gamma \in \mathbb{R}$. Indeed, ω_1, i_{sd}, and i_{sq} are bounded variables, i.e. their values do not go infinite.
In [15] a method to design a Luenberger-based observer for this type of nonlinear system is proposed.

Let us consider the system defined in (4.2) in the form:

$$\begin{aligned}\dot{\mathbf{x}} =& \mathbf{A}\mathbf{x} + \mathbf{\Phi}(\mathbf{x}, t) + \mathbf{B}\mathbf{u} \\ \mathbf{y} =& \mathbf{C}\mathbf{x}\end{aligned} \tag{4.4}$$

under the hypothesis that:

- $\mathbf{\Phi}(\mathbf{x}, t)$ Lipschitz function with Lipschitz constant γ;
- the pair $(\mathbf{C}, \mathbf{A})$ is observable.

For this system, a Luenberger state observer can be defined as[1]:

$$\begin{aligned}\dot{\hat{\mathbf{x}}} &= \mathbf{A}\hat{\mathbf{x}} + \mathbf{B}\mathbf{u} + \mathbf{\Phi}(\hat{\mathbf{x}}, t) + \mathbf{L}\mathbf{C}\left(\mathbf{x} - \hat{\mathbf{x}}\right) \\ \hat{\mathbf{y}} &= \mathbf{C}\hat{\mathbf{x}}\end{aligned} \tag{4.5}$$

where $\mathbf{L} \in \mathbb{R}^{nxq}$ is the observer gain matrix. The observation error dynamics can be defined by:

$$\dot{\mathbf{e}} = \dot{\mathbf{x}} - \dot{\hat{\mathbf{x}}} = \mathbf{A}\mathbf{x} + \mathbf{\Phi}(\mathbf{x}, t) + \mathbf{B}\mathbf{u} - \left[\mathbf{A}\hat{\mathbf{x}} + \mathbf{B}\mathbf{u} + \mathbf{\Phi}(\hat{\mathbf{x}}, t) + \mathbf{L}\mathbf{C}\left(\mathbf{x} - \hat{\mathbf{x}}\right)\right] \tag{4.6}$$

that results in:

$$\dot{\mathbf{e}} = \underbrace{\left(\mathbf{A} - \mathbf{L}\mathbf{C}\right)}_{\mathbf{A_e}}\mathbf{e} + \underbrace{\left[\mathbf{\Phi}(\mathbf{x}, t) - \mathbf{\Phi}(\hat{\mathbf{x}}, t)\right]}_{\mathbf{\Phi_e}(\hat{\mathbf{x}}, \mathbf{x}, t)} = \mathbf{A_e}\mathbf{e} + \mathbf{\Phi_e}(\hat{\mathbf{x}}, \mathbf{x}, t) \tag{4.7}$$

Based on [15], $\mathbf{L}$ can be computed as:

$$\mathbf{L} = \mathbf{P}^{-1}\mathbf{C}^T$$

where $\mathbf{P} = \mathbf{P}^T > 0 \mid \mathbf{P} \in \mathbb{R}^{nxn}$ is obtained solving the following Lyapunov equation:

$$\left[\mathbf{A}^T + \beta\mathbf{I}\right]\mathbf{P} + \mathbf{P}\left[\mathbf{A}^T + \beta\mathbf{I}\right]^T = -2\mathbf{C}^T\mathbf{C}$$

In this way, $\mathbf{L}$ assigns all the eigenvalues of $\mathbf{A_e} = \mathbf{A} - \mathbf{L}\mathbf{C}$ in the left half plane with real part equal to $-\beta$, where the scalar β satisfies:

$$\beta > \max\left\{\left|\mathfrak{Re}\left[\lambda\left(\mathbf{A}\right)\right]\right|_{max}\ ,\ \gamma\frac{\lambda_{max}\left(\mathbf{P}\right)}{\lambda_{min}\left(\mathbf{P}\right)}\right\}$$

[1] the formulation, in this case, involves $\mathbf{e} = \mathbf{x} - \hat{\mathbf{x}}$, and not $\mathbf{e} = \hat{\mathbf{x}} - \mathbf{x}$ as it is defined in Section 1.3; however, this is just an arbitrary choice that has to be set at the beginning and then respected throughout the analysis. Here, the first definition is used to be consistent with the derivation found in [15]

where $|\mathfrak{Re}\left[\lambda\left(\mathbf{A}\right)\right]|_{max}$ represents the maximum real part of the eigenvalues of $\mathbf{A}$, γ is the Lipschitz constant, and $\lambda_{max}\left(\mathbf{P}\right)$ and $\lambda_{min}\left(\mathbf{P}\right)$ refer to the maximum and minimum eigenvalues of $\mathbf{P}$. However, a remark in [15] claims that for sparse nonlinear functions the latter inequality is relaxed to $\beta > \gamma$: being $\mathbf{\Phi}(\mathbf{x}, t)$ sparse, this simplified inequality will be used in the following. Eventually, this calculation of $\mathbf{L}$ guarantees that the estimation error $\mathbf{e} = \mathbf{x} - \hat{\mathbf{x}}$ converges asymptotically to zero [15].
Basically, the method permits the calculation of $\mathbf{L}$ such that the linear part of the observer is stable, guaranteed by the direct pole placement through the parameter β that becomes the magnitude of the negative real part of the eigenvalues of $\mathbf{A_e}$. Thus, neglecting the presence of the nonlinear terms, selecting a high β implies a fast decay of the observation error $\mathbf{e} \to 0$. However, the observer gain matrix $\mathbf{L}$ parameters' magnitude increases as β increases, which could lead to a chattering phenomenon at steady state of the observer estimates.
Summarizing, the following passages are taken to calculate the observer gain matrix $\mathbf{L}$ for (4.5):

1. check that the pair $(\mathbf{C}, \mathbf{A})$ is observable:
   - $$\mathbf{M_O} = \begin{bmatrix} \mathbf{C} \\ \mathbf{CA} \\ \mathbf{CA}^2 \\ \dots \\ \mathbf{CA}^{n-1} \end{bmatrix} \quad | \, n = 6 \, ;$$
   - $\rho = \text{rank}\left(\mathbf{M_O}\right) = 6 = n \;\rightarrow$ the pair $(\mathbf{C}, \mathbf{A})$ is observable.
2. find the Lipschitz constant γ for the non-linear function $\mathbf{\Phi}(\hat{\mathbf{x}}, t)$ [12]:

- find the Jacobian $\mathbf{J} = \left[\frac{\partial \mathbf{\Phi}}{\partial \mathbf{x}}\right]$:

$$\mathbf{J} = \left[\frac{\partial \mathbf{\Phi}}{\partial \mathbf{x}}\right] = \begin{bmatrix} \frac{\partial \Phi_1}{\partial x_1} & \frac{\partial \Phi_1}{\partial x_2} & \dots & \dots & \dots & \frac{\partial \Phi_1}{\partial x_n} \\ \frac{\partial \Phi_2}{\partial x_1} & 0 & 0 & 0 & 0 & 0 \\ \dots & \dots & \dots & \dots & \dots & \dots \\ \dots & \dots & \dots & \dots & \dots & \dots \\ \dots & \dots & \dots & \dots & \dots & \dots \\ \frac{\partial \Phi_n}{\partial x_1} & \dots & \dots & \dots & \dots & \frac{\partial \Phi_n}{\partial x_n} \end{bmatrix} = \tag{4.8}$$

$$= \begin{bmatrix} 0 & 0 & 0 & 0 & 0 & 0 \\ 0 & 0 & 0 & 0 & 0 & 0 \\ 0 & 0 & 0 & 0 & 0 & 0 \\ 0 & 0 & 0 & 0 & 0 & 0 \\ 0 & 0 & 0 & \omega_b i_{sq} & 0 & \omega_b \omega_1 \\ 0 & 0 & 0 & -\omega_b i_{sd} & -\omega_b \omega_1 & 0 \end{bmatrix}$$

- find the norm of $\mathbf{J}$:

$$||\mathbf{J}|| = \left|\left|\frac{\partial \mathbf{\Phi}}{\partial \mathbf{x}}\right|\right| = \max_{1 \le i \le n} \sum_{j=1}^{n} |J_{ij}| \quad | \; J_{ij} = \text{element of } \mathbf{J} \text{ in row i and column j}$$

  - $||\mathbf{J}||_\infty = \left|\left|\frac{\partial \mathbf{\Phi}}{\partial \mathbf{x}}\right|\right|_\infty = \max\left\{|\omega_b i_{sq}| + |\omega_b \omega_1| \quad , \quad |\omega_b i_{sd}| + |\omega_b \omega_1|\right\}$
  - The state variables can be considered bounded, in fact:
    - $i_{sq,max} = \frac{Tn}{n_p \psi_{PM}(\psi_b I_b)} = 1.07\,[pu]$;
    - $i_{sd,max} \approx 1\,[pu]$;
    - $\omega_{1,max} = \omega_{b,mech} = 1\,[pu]$
  - $||\mathbf{J}||_\infty = \left|\left|\frac{\partial \mathbf{\Phi}}{\partial \mathbf{x}}\right|\right|_\infty =$
    $= \max\left\{|\omega_b i_{sq,max}| + |\omega_b \omega_{1,max}| \quad , \quad |\omega_b i_{sd,max}| + |\omega_b \omega_{1,max}|\right\} = 189.80[\frac{rad}{s}]$;
- $\gamma = 189.80$.

3. choose $\beta > \gamma$:
   - $\beta = 190\,[\frac{rad}{s}]$.
4. define the estimation error system $\mathbf{e} = \mathbf{x} - \hat{\mathbf{x}}$:
   - $\dot{\hat{\mathbf{x}}} = \mathbf{A}\hat{\mathbf{x}} + \mathbf{B}\mathbf{u} + \mathbf{\Phi}(\hat{\mathbf{x}}, t) + \mathbf{L}\mathbf{C}\,(\mathbf{x} - \hat{\mathbf{x}})$;
   - $\dot{\mathbf{x}} = \mathbf{A}\mathbf{x} + \mathbf{\Phi}(\mathbf{x}, t) + \mathbf{B}\mathbf{u}$;

- $\dot{\mathbf{e}} = \underbrace{(\mathbf{A} - \mathbf{LC})}_{\mathbf{A_e}}\mathbf{e} + \underbrace{[\mathbf{\Phi}(\mathbf{x},t) - \mathbf{\Phi}(\hat{\mathbf{x}},t)]}_{\mathbf{\Phi_e}(\hat{\mathbf{x}},\mathbf{x},t)} = \mathbf{A_e}\mathbf{e} + \mathbf{\Phi_e}(\hat{\mathbf{x}},\mathbf{x},t)$;

5. $\mathbf{\Phi_e}(\hat{\mathbf{x}},\mathbf{x},t) = \begin{bmatrix} 0 \\ 0 \\ 0 \\ 0 \\ \omega_b i_{sq}\omega_1 - \omega_b \widehat{i_{sq}}\widehat{\omega_1} \\ -\omega_b i_{sd}\omega_1 + \omega_b \widehat{i_{sd}}\widehat{\omega_1} \end{bmatrix}$;

6. solve the Lyapunov $\left[\mathbf{A}^T + \beta\mathbf{I}\right]\mathbf{P} + \mathbf{P}\left[\mathbf{A}^T + \beta\mathbf{I}\right]^T = -2\mathbf{C}^T\mathbf{C}$:
   - use the Matlab function $lyap()$;
   - $$\mathbf{P} = \begin{bmatrix} 48.91 & -48.91 & -0.16 & -0.0065 & 0 & -0.41 \\ -48.91 & 48.91 & 0.16 & 0.0065 & 0 & 0.41 \\ -0.16 & 0.16 & 0.0015 & 0 & 0 & 0.0020 \\ -0.0065 & 0.0065 & 0 & 0 & 0 & 0.0001 \\ 0 & 0 & 0 & 0 & 0.0054 & 0 \\ -0.41 & 0.41 & 0.0020 & 0.0001 & 0 & 0.0054 \end{bmatrix}$$

7. calculate $\mathbf{L} = \mathbf{P}^{-1}\mathbf{C}^T$.

Eventually, the observer gain matrix $\mathbf{L}$ is found to be:

$$\mathbf{L} = \begin{bmatrix} 190.03 & 0 & -2.65 \\ 190.09 & 0 & -7.01 \\ 5.97 & 0 & -488.12 \\ 36.85 & 0 & -2990.41 \\ 0 & 186.62 & 0 \\ -7.01 & 0 & 756.54 \end{bmatrix} \tag{4.9}$$

In this way a Luenberger-based Lipschitz Observer is defined for (4.2). Differently from the NLESO, in this case the observer deals directly with the nonlinear system, hence no linearization and small-variations analysis is required: this represents a good advantage, resulting in a much simpler observer design.

4.1.2. Observer BIBO stability

Although [15] claims that, to guarantee the observer stability, condition:

$$\beta > \max\left\{ \left|\mathfrak{Re}\left[\lambda\left(\mathbf{A}\right)\right]\right|_{max} \ , \ \gamma\frac{\lambda_{max}\left(\mathbf{P}\right)}{\lambda_{min}\left(\mathbf{P}\right)} \right\}$$

can be reduced to:

$$\beta > \gamma$$

in case of sparse nonlinear functions, it does not provide any satisfactory demonstration to prove it. Moreover, the first condition is not satisfied for $\beta = 190\ [\frac{rad}{s}]$, leaving some space to debate the simpler proposed condition's effectiveness. For this reason, a deeper analysis of the observation error dynamics is needed to assess whether the system is at least Bounded Input Bounded Output (BIBO) stable, so to ensure that the response of the observation error system to the nonlinear term $\mathbf{\Phi_e}(\hat{\mathbf{x}}, \mathbf{x}, t)$ is limited, i.e. does not go infinite. In this way, it is possible to check if the observer has an unstable behavior due to the nonlinear terms impact and, in addition to the claim in [15], to provide a better overview of the observer dynamics.
Let us consider again the observation error system:

$$\dot{\mathbf{e}} = \mathbf{A_e}\mathbf{e} + \mathbf{\Phi_e}(\hat{\mathbf{x}}, \mathbf{x}, t)$$

By looking at the nonlinear term $\mathbf{\Phi_e}(\hat{\mathbf{x}}, \mathbf{x}, t)$ as an input disturbance, it can be seen as:

$$\mathbf{\Phi_e}(\hat{\mathbf{x}}, \mathbf{x}, t) = \begin{bmatrix} 0 \\ 0 \\ 0 \\ 0 \\ \omega_b i_{sq}\omega_1 - \omega_b\widehat{i_{sq}\omega_1} \\ -\omega_b i_{sd}\omega_1 + \omega_b\widehat{i_{sd}\omega_1} \end{bmatrix} = \mathbf{B_{\Phi_e}}\mathbf{u_{\Phi_e}} = \begin{bmatrix} 0 & 0 \\ 0 & 0 \\ 0 & 0 \\ 0 & 0 \\ \omega_b & 0 \\ 0 & \omega_b \end{bmatrix} \begin{bmatrix} i_{sq}\omega_1 - \widehat{i_{sq}\omega_1} \\ -i_{sd}\omega_1 + \widehat{i_{sd}\omega_1} \end{bmatrix}$$

(4.10)

Evaluating the observation error transfer function, defined as:

$$\mathbf{G_e}(s) = \frac{\mathbf{e}(s)}{\mathbf{u_{\Phi_e}}(s)} = (s\mathbf{I} - \mathbf{A_e})^{-1}\,\mathbf{B_{\Phi_e}} = \begin{bmatrix} G_{e,11} & G_{e,12} \\ G_{e,21} & G_{e,22} \\ G_{e,31} & G_{e,32} \\ G_{e,41} & G_{e,42} \\ G_{e,51} & G_{e,52} \\ G_{e,61} & G_{e,62} \end{bmatrix} \tag{4.11}$$

which results in:

$$\mathbf{G_e}(s) = \begin{bmatrix} G_{e,11} & G_{e,12} \\ G_{e,21} & G_{e,22} \\ G_{e,31} & G_{e,32} \\ G_{e,41} & G_{e,42} \\ G_{e,51} & G_{e,52} \\ G_{e,61} & G_{e,62} \end{bmatrix} = \begin{bmatrix} 0 & G_{e,12} \\ 0 & G_{e,22} \\ 0 & G_{e,32} \\ 0 & G_{e,42} \\ G_{e,51} & 0 \\ 0 & G_{e,62} \end{bmatrix} \tag{4.12}$$

The complete expression of $\mathbf{G_e}(s)$ can be found running the Matlab script in Appendix A.6. In Figure 4.1, the plot of $\mathbf{G_e}(s)$ in the frequency domain is shown.

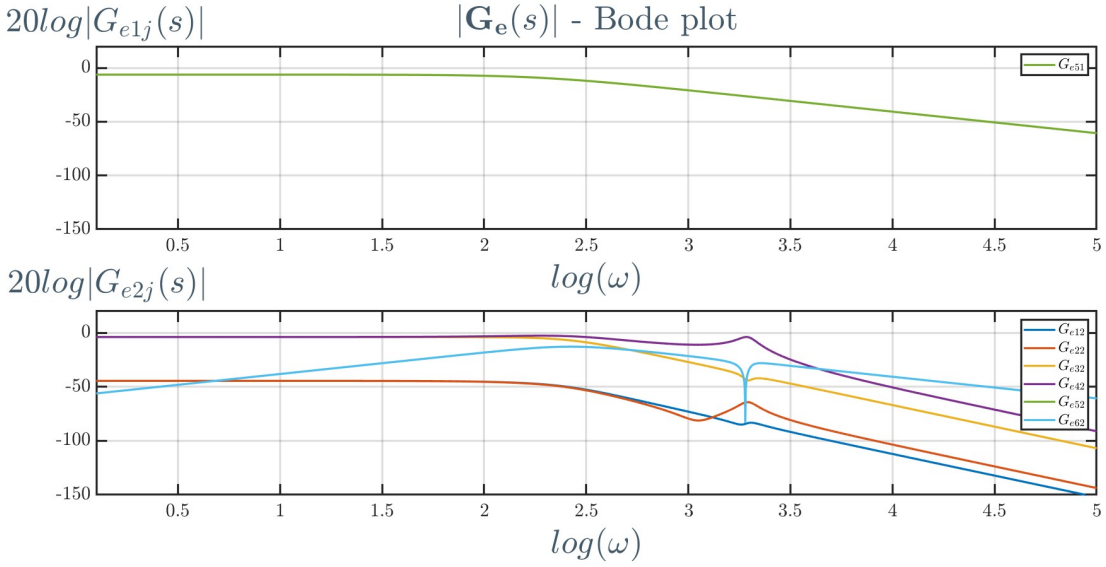

Figure 4.1: Bode plot (magnitude) of the observation error transfer function $\mathbf{G_e(s)}$

Now, recalling the BIBO stability property of a system [6], the observation error dynamics system is BIBO stable if a bounded input $\mathbf{u_{\Phi_e}}$ leads to a bounded output $\mathbf{y_e} = \mathbf{e}$. Considering that:

- the input $\mathbf{u}_{\mathbf{\Phi_e}}$ consists of the subtraction of the same Lipschitz function operating with two different variables, i.e. $\mathbf{x}$ and $\widehat{\mathbf{x}}$, which belong to a bounded domain given by the operating region of the system;
- $\lim_{\widehat{\mathbf{x}}\to\mathbf{x}} \mathbf{u}_{\mathbf{\Phi_e}} = \lim_{\widehat{\mathbf{x}}\to\mathbf{x}} \mathbf{\Phi_e}\left(\mathbf{x}, \widehat{\mathbf{x}}\right) \to 0$;
- the magnitude of each element of $\mathbf{G_e}(s)$ is bounded in the frequency domain;

the observation error dynamics system can be assumed BIBO stable.

4.2. Lipschitz system's state observer simulation

4.2.1. Simulation setup

To properly compare the two state observers defined in this thesis, the two simulation setups are kept the same: in this way, each observer is tested with the same operating conditions, allowing an easier analysis and performance comparison. Therefore, the setup defined in Section 3.2.1 is still valid in this chapter.
Now the state observer operates directly on the state variable and not on its small perturbation term, so the HP filter is no more needed.

4.2.2. Simulation results

Let us refer to the scheme comprising the ideal converter, the voltage harmonic injection, the PMSG and the wind turbine in Figure 3.10, defined in Section 3.2.2.
The turbine and PMSG rotor angular speeds' trends are shown in Figure 4.2, with the reference speed being constant at $\omega_{ref} = 9.69\,[rpm]$ to represent a steady-state operation. As was done for the NLESO in Section 3.2.2, the simulation is divided into three phases: the voltage harmonic at f_{dist} is injected between seconds 4 and 8 of the simulation, while the voltage harmonic leading to the mechanical resonant condition is present between seconds 8 and 12.

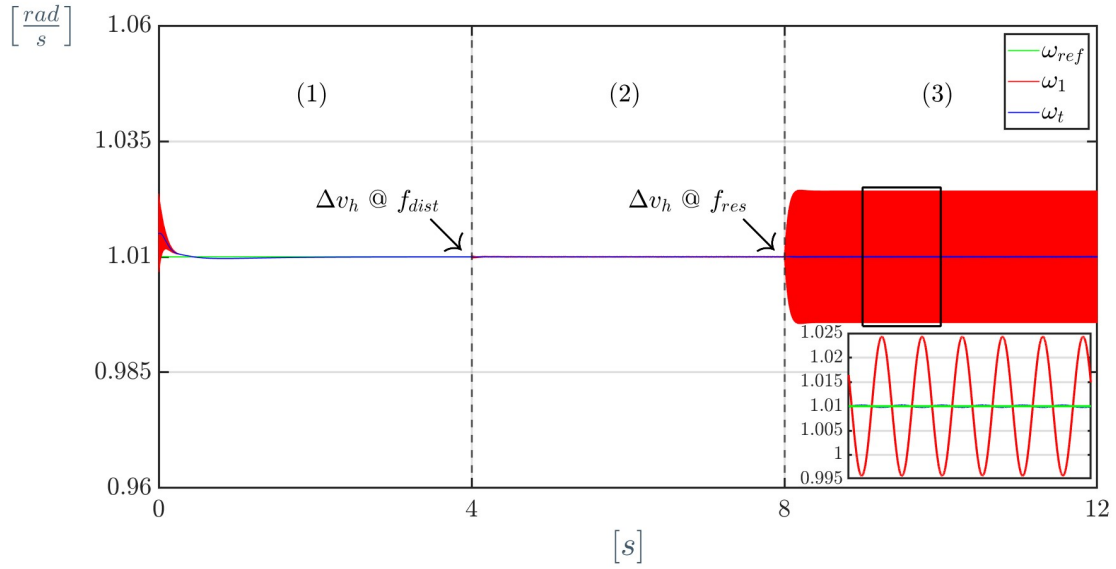

Figure 4.2: Speeds used in Lipschitz observer's simulation

The 3-phase stator voltage waveforms in each simulation part before and after the

voltage harmonic injection can be seen in Figure 4.3.

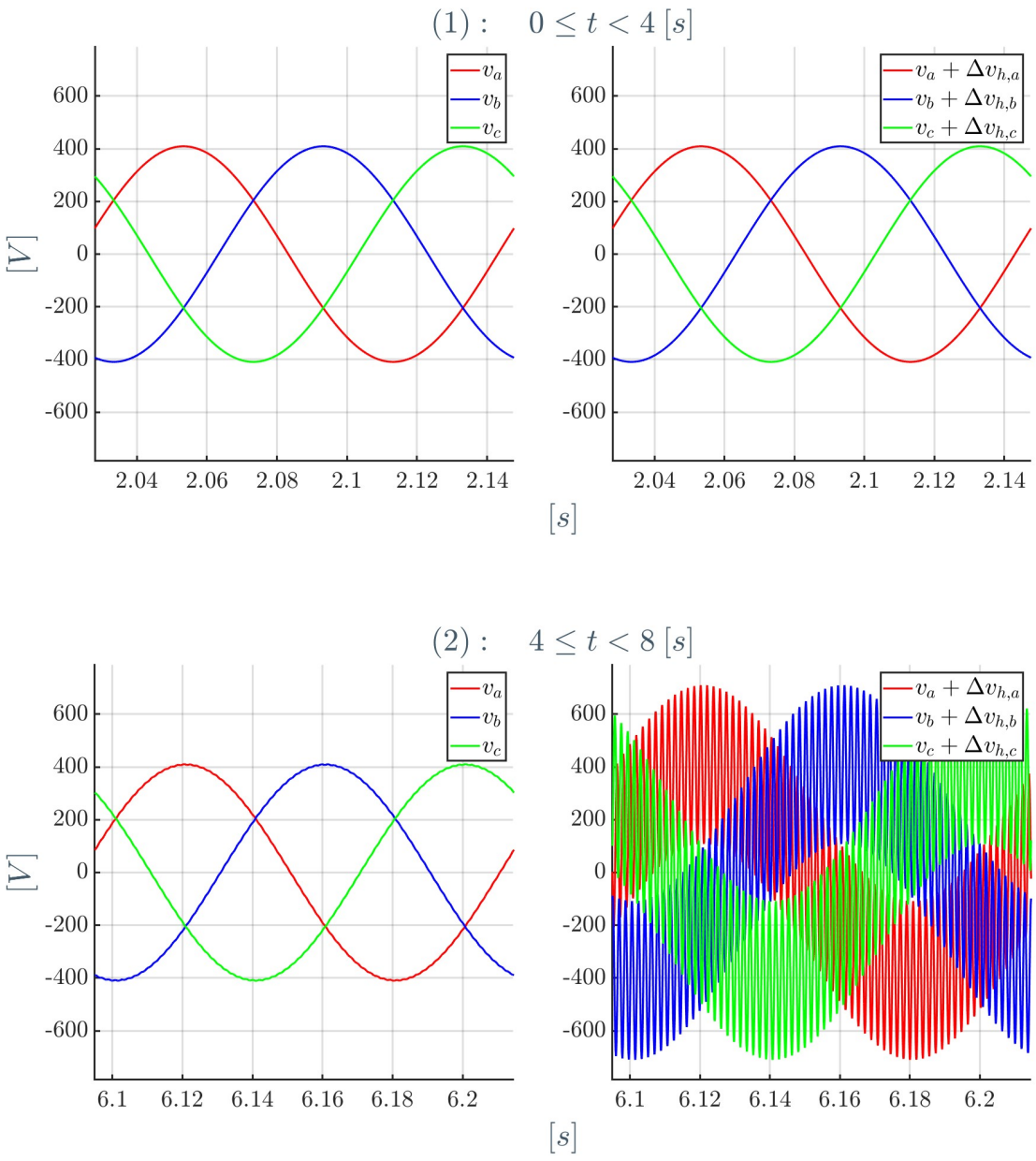

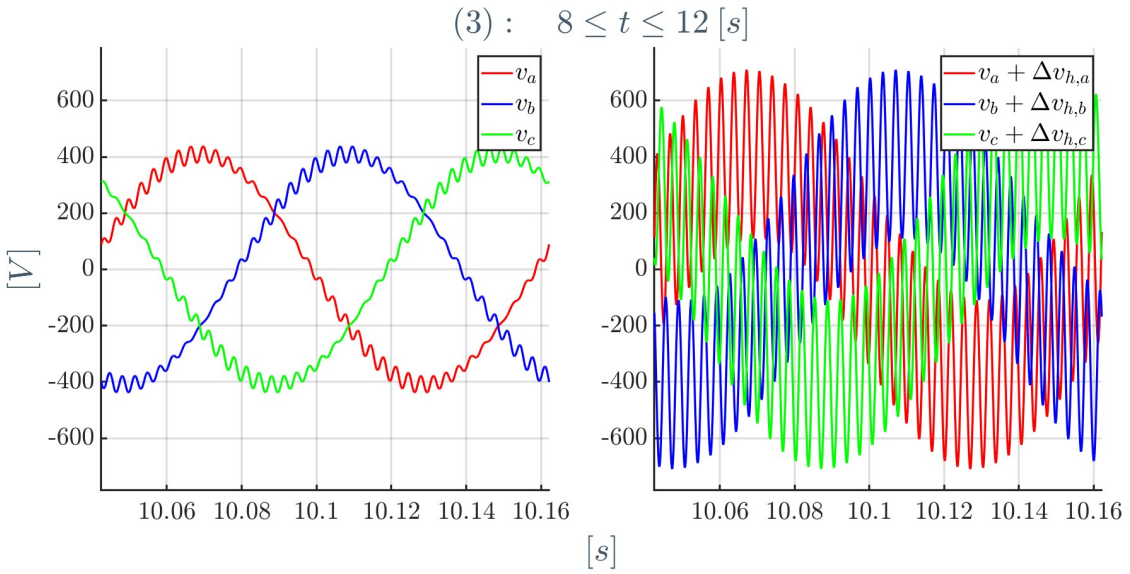

Figure 4.3: stator voltage waveforms before and after the voltage harmonic injection in Lipschitz observer's simulation part (1) (top), (2) (middle), and (3) (bottom)

As expected, the same trends shown in Section 3.2.2 are obtained here, since the two simulation setups are kept the same. The same plots used to evaluate the NLESO's performance will be used: in this way, the comparison of the two observers' results is easier.
Starting from the angular positions θ_t and θ_1, their graphs are shown in Figure 4.4 and 4.5.

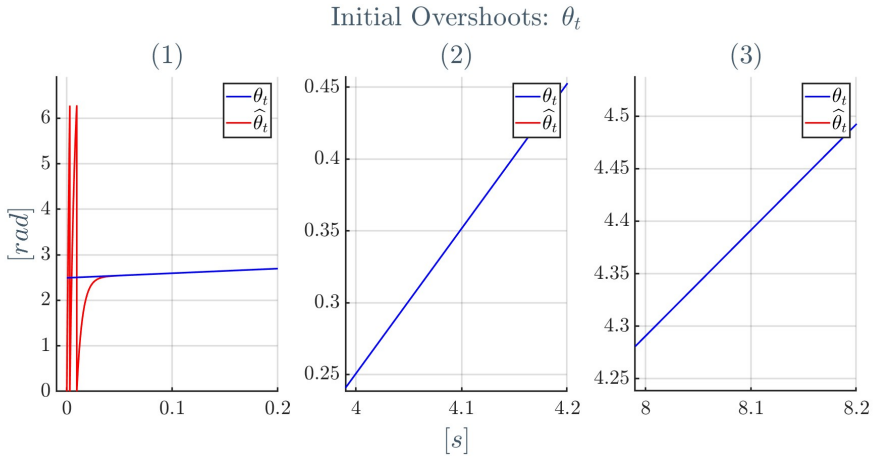

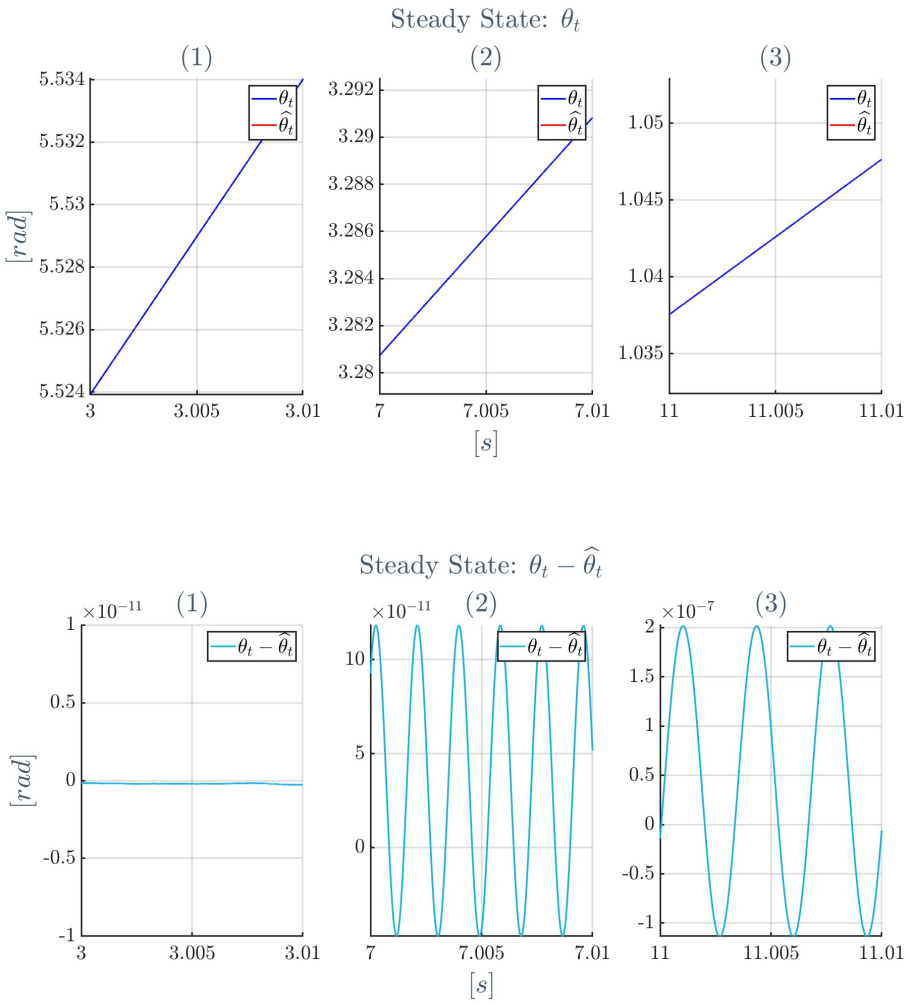

Figure 4.4: θ_t true value and estimate during the initial overshoot at the beginning of each simulation phase ((1)-(2)-(3)) (top); θ_t true value and estimate at steady state in each simulation phase (middle); observation error $e_1 = \theta_t - \widehat{\theta}_t$ at steady state in each simulation phase (bottom)

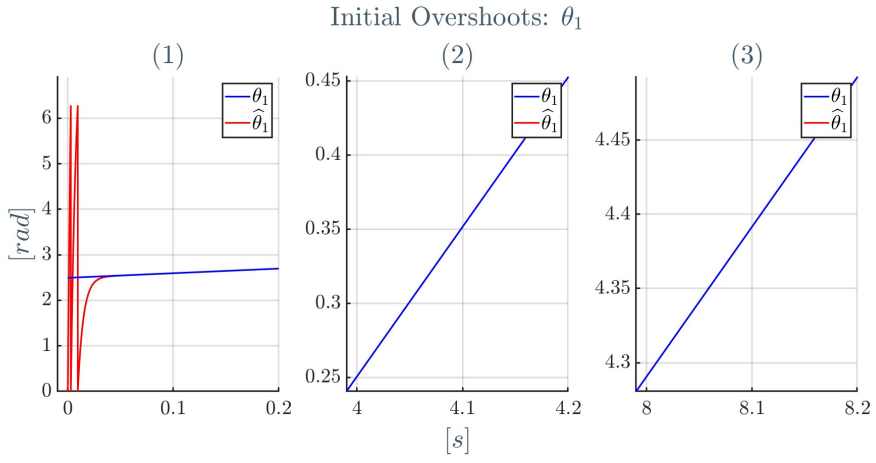

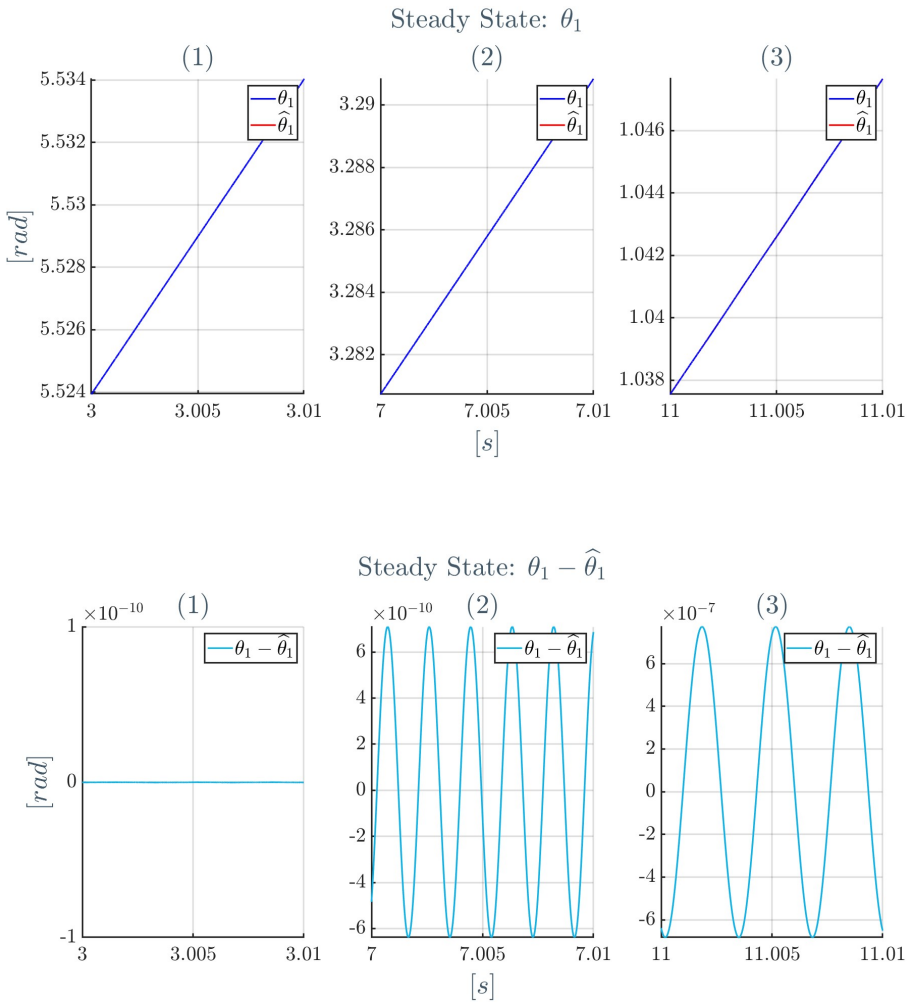

Figure 4.5: θ_1 true value and estimate during the initial overshoot at the beginning of each simulation phase ((1)-(2)-(3)) (top); θ_1 true value and estimate at steady state in each simulation phase (middle); observation error $e_2 = \theta_1 - \widehat{\theta}_1$ at steady state in each simulation phase (bottom)

As it is shown in Figures 4.4 and 4.5, the observation error for both the state variables θ_t and θ_1 tends quickly to a small value that oscillates around zero. The overshoot is present only in simulation phase (1), while it is not when a voltage harmonic Δv_{abc} is injected: this is true also for the other state variables; so, this observer is not affected by changes in the operating conditions. The worst estimation is given in mechanical resonance condition, with a small error at steady state. Even if θ_1 is one of the state observer's inputs, the best estimation performance is provided for θ_t, which shows an observation error at steady state of one order of magnitude less compared to θ_1 case in mechanical resonance conditions ((3)): this can be due to the relatively low oscillations occurring on the turbine compared to those of the PMSG rotor. Indeed, the

wind turbine has a high inertia J_t which naturally limits vibrations.
An important datum that can be derived from these two state variables is the shaft torque T_{sh}, defined as:

$$T_{sh} = K_1(\theta_t - \theta_1) \tag{4.13}$$

Let us define the estimate of this last quantity as:

$$\widehat{T_{sh}} = K_1(\widehat{\theta_t} - \widehat{\theta_1}) \tag{4.14}$$

In Figure 4.6 the shaft torque real value and estimates comparison together with the observation error are shown.

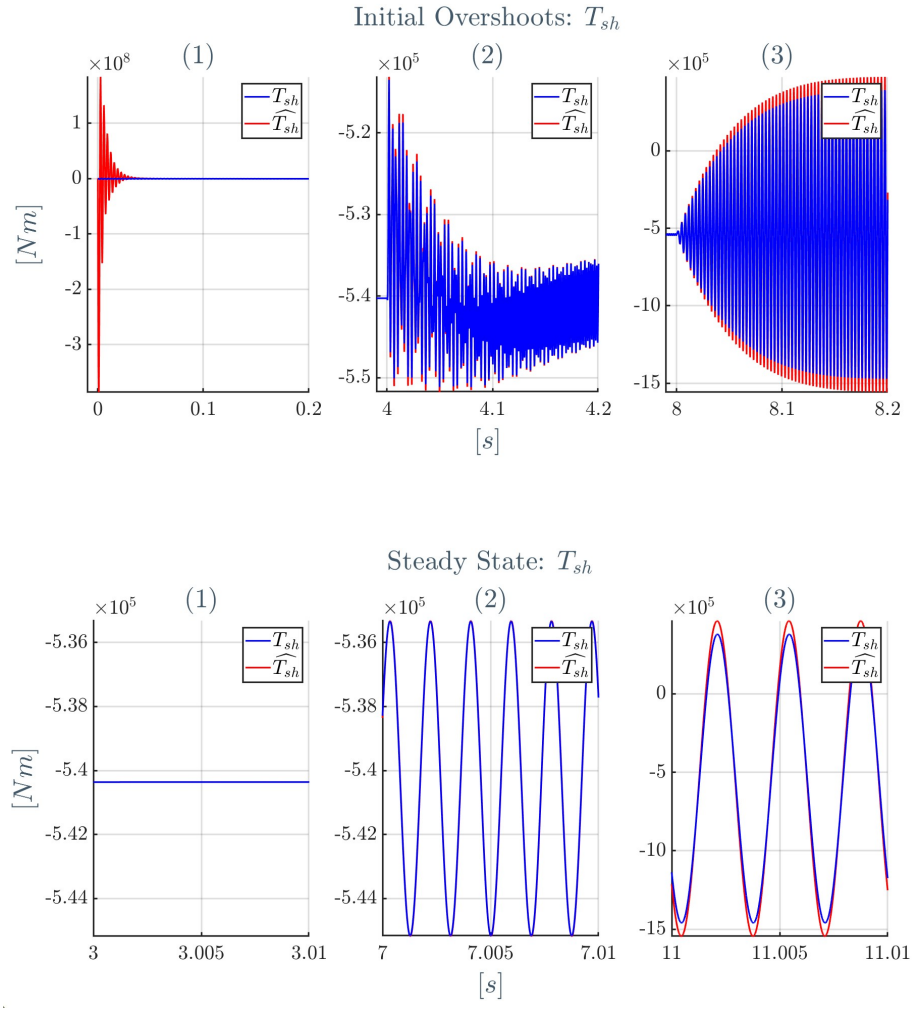

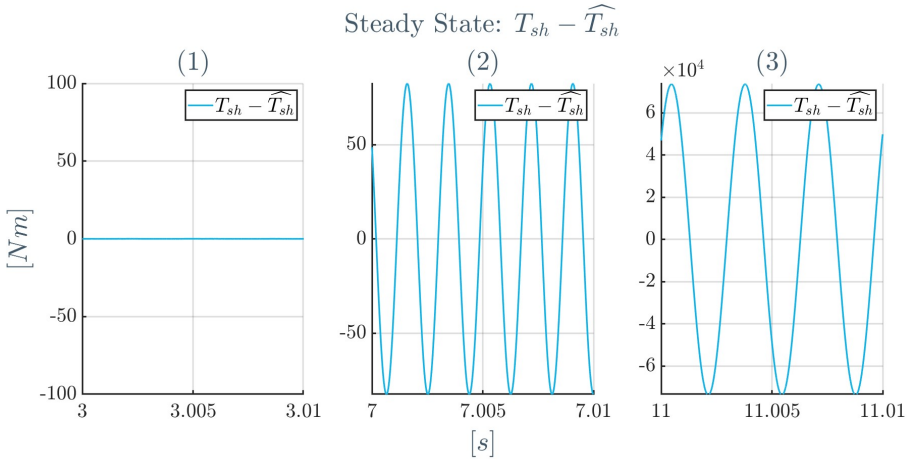

Figure 4.6: T_{sh} true value and estimate during the initial overshoot at the beginning of each simulation phase ((1)-(2)-(3)) (top); T_{sh} true value and estimate at steady state in each simulation phase (middle); observation error $T_{sh} - \widehat{T_{sh}}$ at steady state in each simulation phase (bottom)

As can be seen, the shaft torque can be estimated with good accuracy with $\widehat{\theta}_t$ and $\widehat{\theta}_1$, with an observation error during the resonance condition one order of magnitude smaller than the true value T_{sh}. Different from the NLESO, it can be concluded that this observer is able to provide a good estimation of the shaft torque.
The graphs related to the turbine and PMSG rotor angular speeds are shown in Figure 4.7 and 4.8.

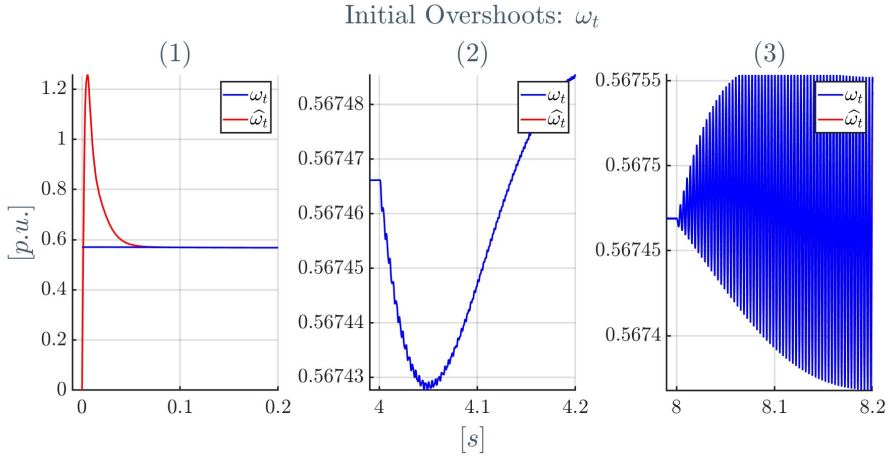

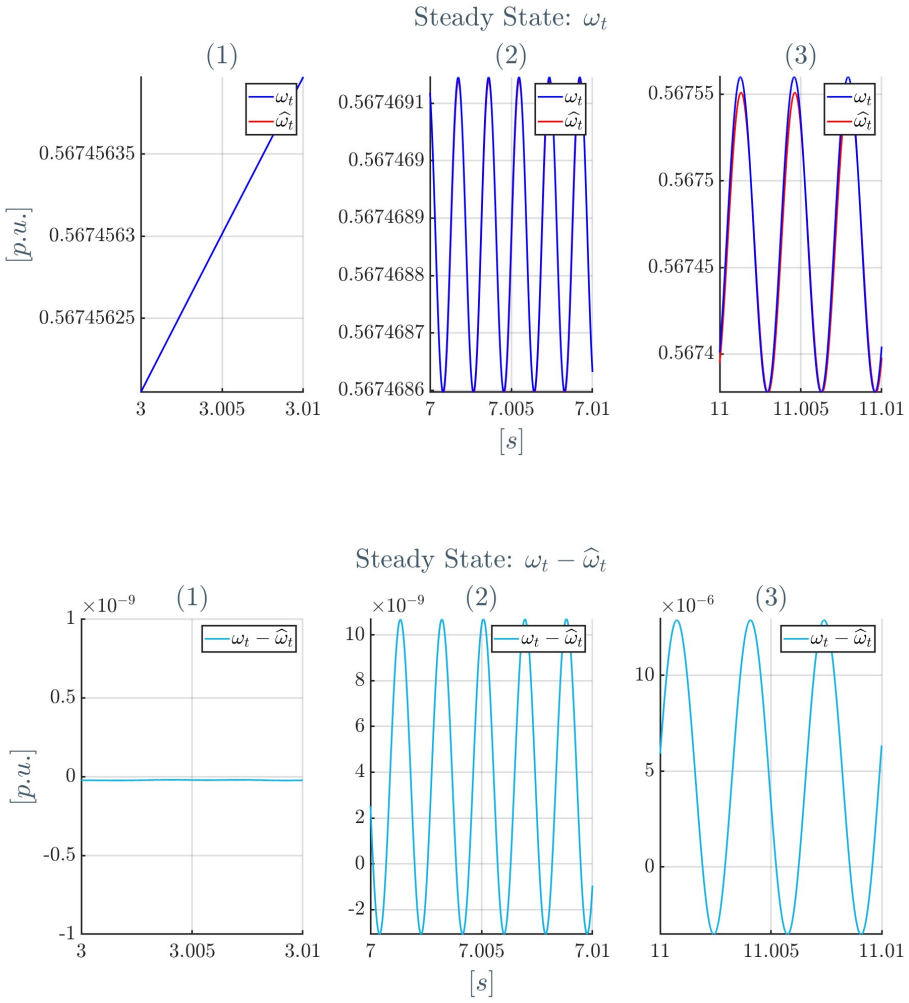

Figure 4.7: $\Delta\omega_t$ true value and estimate during the initial overshoot at the beginning of each simulation phase ((1)-(2)-(3)) (top); $\Delta\omega_t$ true value and estimate at steady state in each simulation phase (middle); observation error $e_3 = \omega_t - \widehat{\omega}_t$ at steady state in each simulation phase (bottom)

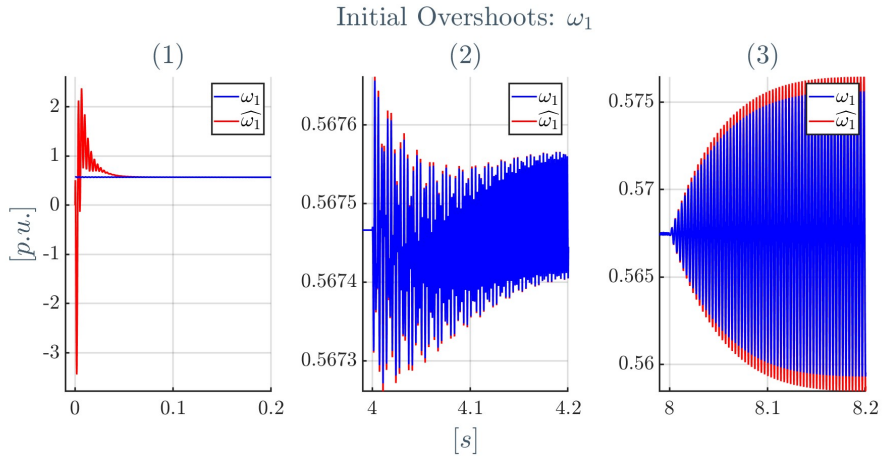

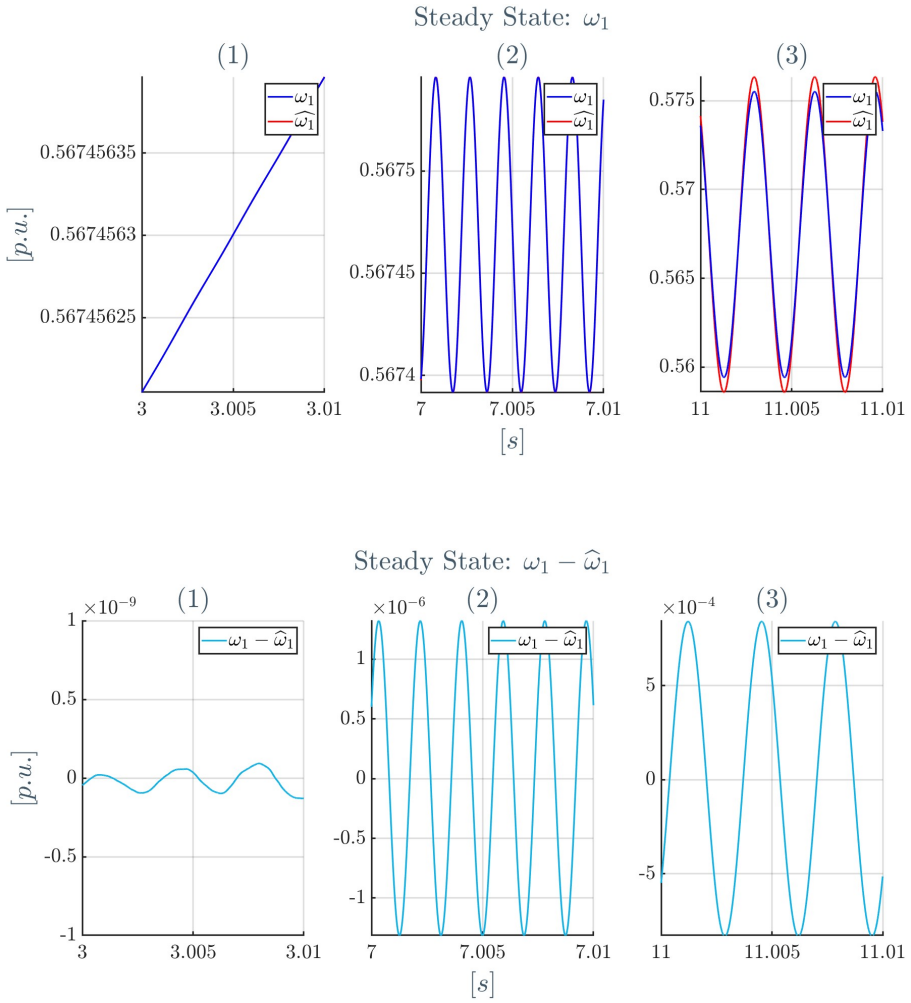

Figure 4.8: ω_1 true value and estimate during the initial overshoot at the beginning of each simulation phase ((1)-(2)-(3)) (top); ω_1 true value and estimate at steady state in each simulation phase (middle); observation error $e_4 = \omega_1 - \widehat{\omega_1}$ at steady state in each simulation phase (bottom)

The estimation of ω_t appears to be more accurate than the one of ω_1: indeed, the wind turbine is characterized by smaller torsional vibrations, as it was explained previously. The last estimated state variables are the direct and quadrature stator currents i_{sd} and i_{sq}[2], which are also state observer's inputs; their trends are presented in Figure 4.9 and 4.10.

[2]the value of i_{sq} in the simulation is negative: this is due to a simulation setup in which the wind turbine is treated as a load and the PMSG as a motor. Being just a matter of conventions, the observer's performance's evaluation is not affected.

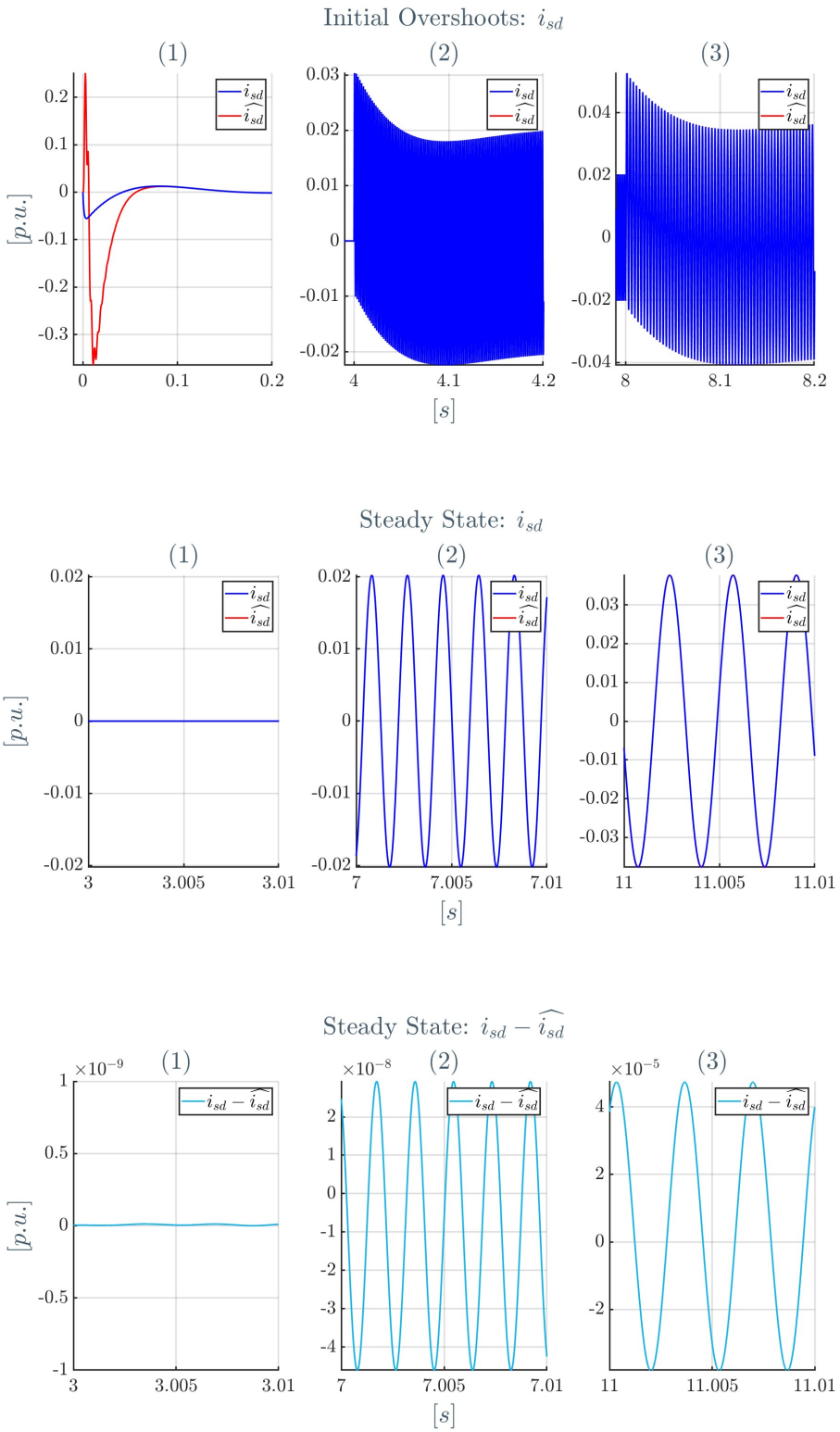

Figure 4.9: i_{sd} true value and estimate during the initial overshoot at the beginning of each simulation phase ((1)-(2)-(3)) (top); i_{sd} true value and estimate at steady state in each simulation phase (middle); observation error $e_5 = i_{sd} - \widehat{i_{sd}}$ at steady state in each simulation phase (bottom)

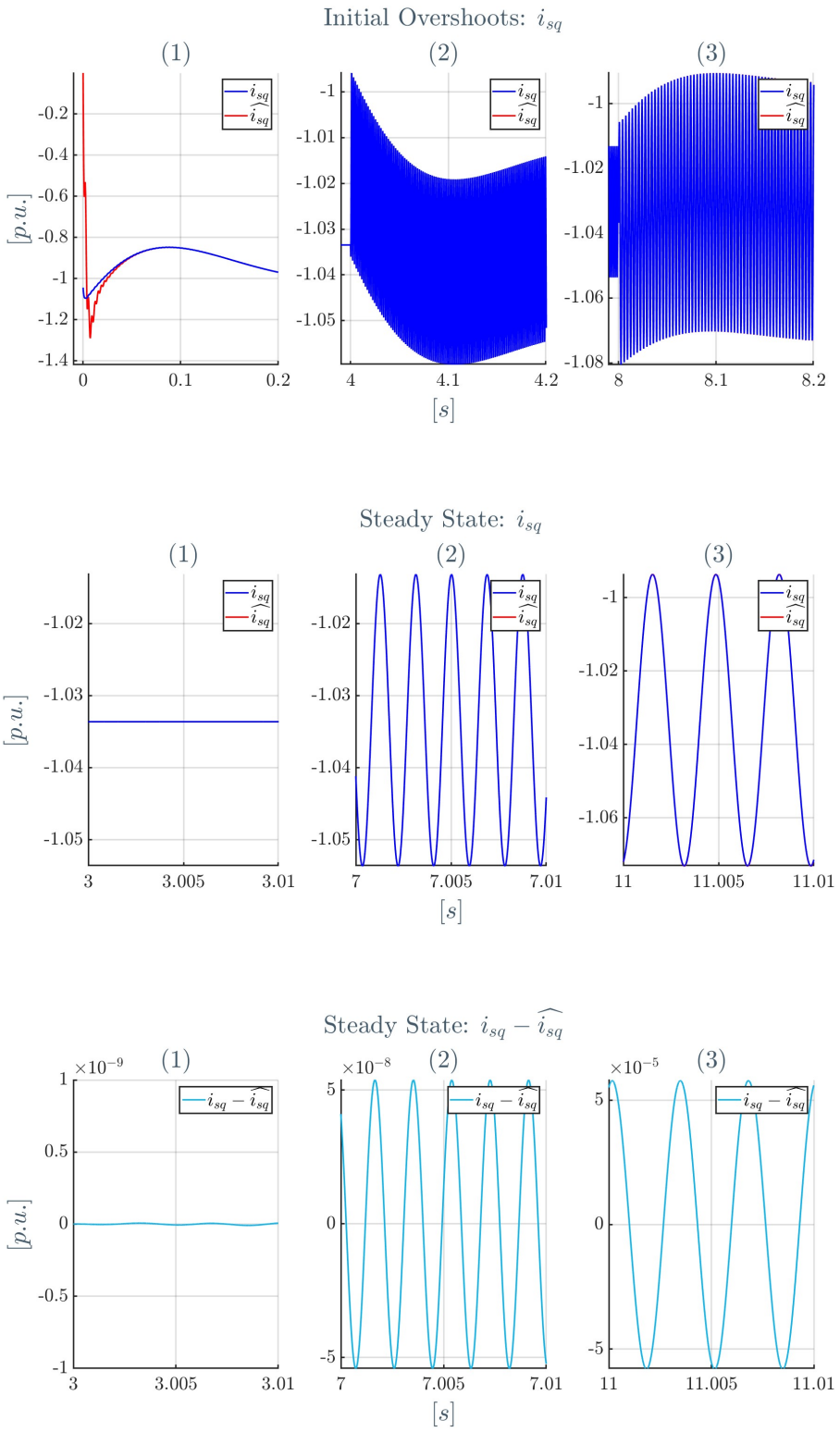

Figure 4.10: i_{sq} true value and estimate during the initial overshoot at the beginning of each simulation phase ((1)-(2)-(3)) (top); i_{sq} true value and estimate at steady state in each simulation phase (middle); observation error $e_6 = i_{sq} - \widehat{i_{sq}}$ at steady state in each simulation phase (bottom)

The observation error is very small for i_{sd} and i_{sq}, which confirms the tendency of the state observer to provide good estimates for its input state variables.
Based on the simulation results, some final remarks can be made. Also in this case the state observer is stable, but now more accurate estimates are provided for all the state variables compared to the NLESO case. The overshoots of the state estimates are present only in simulation phase (1), in which the steady-state error shows the littlest value, almost equal to 0. The observer performance decreases during mechanical resonance conditions, while it is less affected by a generic disturbance such as the voltage harmonic injection at frequency f_{dist}. In this case, the state observer design is much easier than the NLESO: it deals with the nonlinear MIMO system without any subsystem decomposition and variable transformation, reducing also the online computational burden. Moreover, the state observer's outputs are the complete state variables now, while in the previous case only the oscillating term was provided.
However, a deeper analysis regarding the observer stability is required, in order to provide a design that can be reliable for other applications or operating conditions.

5 | Conclusions and future developments

Multi-Modular Axial-Flux Permanent Magnet (MMAFPM) machines can represent a good alternative to Radial-Flux ones in Wind Energy Conversion Systems (WECS), especially for applications that demand high torque densities and low aspect ratios. However, the interaction of voltage and current harmonics produced by the Variable Frequency Drive (VFD) creates torque harmonics at different frequencies, which lead to torsional vibrations inside the machine. A method to damp torsional vibrations is to design a so-called PI State Space (SS) control, in which the complete information of the state variables of the system is needed: a state observer can be designed for this task.
A two Degree-of-Freedom (DOF), comprising a Permanent Magnet Synchronous Generator (PMSG) directly connected to a Wind Turbine, was considered in this thesis. Two different state observers were presented, considering as measured variables only the PMSG rotor position and the stator current direct and quadrature components. When considering the electrical model of the system, some nonlinear terms appear regarding the direct and quadrature stator current's components and the machine speed: the system model becomes nonlinear and a state observer design results more complex. This study provides two state observers for the nonlinear Multi-Input Multi-Output (MIMO) system.
First, a Non-Linear Extended State Observer (NLESO) working on a linearized model of the system was proposed. The results can be summarized as follows:

- the design of this observer type, which involves a Multi-Input Single-Output (MISO) subsystem decomposition and state variables transformation, appears to be quite complex and cumbersome, although it was possible to prove the absolute stability of the observation error;
- the estimates have a low level of accuracy, especially in highly perturbed operating condition, such as during torsional vibrations.

Then, a Luenberger-based Lipschitz Observer was proposed:

- its design is less complex than the previous observer and it deals directly with the nonlinear system. Further investigation regarding its stability is required;
- the observer can provide accurate estimates of all the state variables and it is more robust to generic disturbances, while its performance is still affected in mechanical resonance condition.

Starting from this thesis work, further research is required to extend the state observer design to an MMAFPM machine, still using the available mechanical angular position and stator currents measurements. Mainly, it will be interesting to:

- test the effectiveness of the proposed observers on a real laboratory setup, starting from a simple two-DOF system, and assess the impact of external disturbances on the estimates' accuracy;
- design a Luenberger-based Lipschitz Observer for a multi-mass system comprising an MMAFPM machine, assessing its stability properties and observation performance;
- analyze and implement a control loop which, based on the system state estimates, effectively damps torsional oscillations.

Bibliography

[1] P. Bolzern, R. Scattolini, and N. Schiavoni. *Fondamenti di controlli automatici*. Collana di istruzione scientifica. McGraw-Hill Companies, 2008. ISBN 9788838664342.

[2] M. Bramanti, C. Pagani, and S. Salsa. *Analisi matematica 1. Con elementi di algebra lineare*. Zanichelli, 2014. ISBN 9788808254214.

[3] A. Cavagnino, M. Lazzari, F. Profumo, and A. Tenconi. A comparison between the axial flux and the radial flux structures for pm synchronous motors. *IEEE Transactions on Industry Applications*, 38(6):1517–1524, 2002. doi: 10.1109/TIA.2002.805572.

[4] L. Chen, H. Xu, and J. Wenske. Active damping of torsional vibrations in the drive train of a dfig wind turbine. *Renewable Energy and Power Quality Journal*, pages 270–275, 04 2014. doi: 10.24084/repqj12.309.

[5] J. Dilys, V. Stankevič, and K. Łuksza. Implementation of extended kalman filter with optimized execution time for sensorless control of a pmsm using arm cortex-m3 microcontroller. *Energies*, 14(12), 2021. ISSN 1996-1073. doi: 10.3390/en14123491.

[6] O. Grasselli, L. Menini, and S. Galeani. *Sistemi dinamici*. Hoepli, 2007. ISBN 9788820337032.

[7] B.-Z. Guo and Z. liang Zhao. On the convergence of an extended state observer for nonlinear systems with uncertainty. *Systems and Control Letters*, 60(6):420–430, 2011. ISSN 0167-6911. doi: https://doi.org/10.1016/j.sysconle.2011.03.008.

[8] B.-Z. Guo and Z. Zhao. *Active Disturbance Rejection Control for Nonlinear Systems: An Introduction*. 10 2016. ISBN 9781119239925. doi: 10.1002/9781119239932.ch2.

[9] M. E. Haque, M. Negnevitsky, and K. M. Muttaqi. A novel control strategy for a variable-speed wind turbine with a permanent-magnet synchronous generator.

IEEE Transactions on Industry Applications, 46(1):331–339, 2010. doi: 10.1109/TIA.2009.2036550.

[10] M. J. K. Jacek F. Gieras, Rong-Jie Wang. *Axial Flux Permanent Magnet Brushless Machines*. Springer Dordrecht, 2008.

[11] L. W.-W. Y. e. a. Jiang, S. Study on electromechanical coupling torsional resonance characteristics of gear system driven by pmsm: a case on shearer semi-direct drive cutting transmission system. *International Journal of Vehicle Mechanics and Mobility - Vehicle System Dynamics*, 104:1205–1225, 2021. doi: 10.1007/s11071-021-06364-9.

[12] H. Khalil. *Nonlinear Systems*. Pearson Education. Prentice Hall, 2002. ISBN 9780130673893.

[13] H. Kim, J. Son, and J. Lee. A high-speed sliding-mode observer for the sensorless speed control of a pmsm. *IEEE Transactions on Industrial Electronics*, 58(9):4069–4077, 2011. doi: 10.1109/TIE.2010.2098357.

[14] S. Kim. *Electric Motor Control: DC, AC, and BLDC Motors*. Elsevier Science, 2017. ISBN 9780128123195.

[15] P. C. Papageorgiou and A. T. Alexandridis. A direct pole placement-based approach for the design of nonlinear lipschitz observers. In *2020 European Control Conference (ECC)*, pages 1520–1525, 2020. doi: 10.23919/ECC51009.2020.9143649.

[16] N. Radwan-Pragłowska, T. Węgiel, and D. Borkowski. Modeling of axial flux permanent magnet generators. *Energies*, 13(21), 2020. ISSN 1996-1073. doi: 10.3390/en13215741.

[17] S. Rao and P. Griffin. *Mechanical Vibrations*. Pearson, 2017. ISBN 9781292178608.

[18] Y. Shtessel, C. Edwards, L. Fridman, and A. Levant. *Sliding Mode Control and Observation*, pages 291–320. 01 2014. ISBN 978-0-8176-4892-3. doi: 10.1007/978-0-8176-4893-0_8.

[19] K. Sitapati and R. Krishnan. Performance comparisons of radial and axial field, permanent-magnet, brushless machines. *IEEE Transactions on Industry Applications*, 37(5):1219–1226, 2001. doi: 10.1109/28.952495.

[20] J. Song-Manguelle, G. Ekemb, S. Schröder, T. Geyer, J.-M. Nyobe-Yome, and R. Wamkeue. Analytical expression of pulsating torque harmonics due to pwm drives. In *2013 IEEE Energy Conversion Congress and Exposition*, pages 2813–2820, 2013. doi: 10.1109/ECCE.2013.6647066.

[21] U. Spangenberg. Variable frequency drive harmonics and interharmonics exciting axle torsional vibration resulting in railway wheel polygonisation. *International Journal of Vehicle Mechanics and Mobility - Vehicle System Dynamics*, 58(3):404–424, 2020. doi: 10.1080/00423114.2019.1581235.

[22] S. Thomsen, N. Hoffmann, and F. W. Fuchs. Pi control, pi-based state space control, and model-based predictive control for drive systems with elastically coupled loads—a comparative study. *IEEE Transactions on Industrial Electronics*, 58(8): 3647–3657, 2011. doi: 10.1109/TIE.2010.2089950.

[23] A. Ulutaş and T. Duru. Variable-speed direct-drive permanent magnet synchronous generator wind turbine modeling and simulation. *Kocaeli Journal of Science and Engineering*, 2(1):21 – 27, 2019. doi: 10.34088/kojose.515467.

[24] W. Wang and Z. Gao. A comparison study of advanced state observer design techniques. 6:4754–4759 vol.6, 2003. doi: 10.1109/ACC.2003.1242474.

[25] X. Xi, H. Geng, G. Yang, S. Li, and F. Gao. Torsional oscillation damping control for dfig-based wind farm participating in power system frequency regulation. *IEEE Transactions on Industry Applications*, 54(4):3687–3701, 2018. doi: 10.1109/TIA.2018.2814559.

[26] X. Yin, K. Arulmaran, and J. Liu. Subsystem decomposition for distributed state estimation of nonlinear systems. pages 5569–5574, 2016. doi: 10.1109/ACC.2016.7526543.

[27] M. Zaid. *Design and Analysis of Nonlinear Extended State Observer for Suppressing Torsional Vibrations in a Multi-Mass System*. MSc thesis, Politecnico di Milano, 2022.

[28] Z. Zhao, Y. Lu, D. Xie, S. Yu, and W. Wu. Two methods for damping torsional vibrations in dfig-based wind generators using power converters. *IOP Conference Series: Earth and Environmental Science*, 52(1):012021, jan 2017. doi: 10.1088/1742-6596/52/1/012021.

A | Appendix A

A.1. Torque Harmonics

To understand the relationship between voltage harmonics and torque harmonics in a VFD an analysis based on [20] is conducted.
For an AC machine it holds:

- Stator voltage equations (abc frame):

$$v_{s,k} = r_s i_{s,k} + \frac{d\psi_{s,k}}{dt} \quad | \, k = 1, 2, 3$$

- Electromagnetic torque expression (stator $\alpha\beta$ frame, magnitude invariant transformation[1]):

$$T_{elm} = \frac{3}{2} n_p \Im\mathfrak{m} \left\{ \mathbf{i_s} \mathbf{\Psi_s} * \right\} = \frac{3}{2} n_p (\psi_{s\alpha} i_{s,\beta} - \psi_{s,\beta} i_{s,\alpha}) \tag{A.1}$$

where $\mathbf{i_s}$ and $\mathbf{\Psi_s}$ are the stator current and flux linkage space vectors, n_p is the number of pole pairs.
For high power operating regime, resistive losses in the stator can be neglected [20], therefore:

$$v_{s,k} \approx \frac{d\psi_{s,k}}{dt} \quad \rightarrow \; \psi_{s,k} = \int v_{s,k} \, dt \quad | \, k = 1, 2, 3$$

Considering as a fundamental angular frequency $\omega_1 = 2\pi f_1$, the stator voltage can be seen as:

$$v_{s,k} = \widehat{V_1} \cos\left(\omega_1 t - \frac{2\pi}{3}(k-1)\right) + \sum_{h=2}^{+\infty} \widehat{V_h} \cos\left[h\left(\omega_1 t - \frac{2\pi}{3}(k-1)\right) + \varphi_h\right] \, | \, k = 1, 2, 3$$

[1] throughout the work, the power invariant transformation was used; here the magnitude invariant is chosen just for simplicity: the aim of this analysis is to assess how voltage harmonics lead to torque harmonics in the machine. However, the results can be referred to different space-vector transformation just changing the arbitrary transformation constant.

Applying $abc/s\alpha\beta$, or Clarke, transformation:

$$\mathbf{v_s} = \frac{2}{3}\left(v_{s1} + v_{s2}e^{j\frac{2\pi}{3}} + v_{s3}e^{j\frac{4\pi}{3}}\right) = v_{s,\alpha} + jv_{s,\beta}$$

where:

$$\begin{cases} v_{s,\alpha} = \widehat{V_1}\cos(\omega_1 t) + \sum_{h=2}^{+\infty}\widehat{V_h}\cos(h\omega_1 t + \varphi_h) \\ v_{s,\beta} = \widehat{V_1}\sin(\omega_1 t) \pm \sum_{h=2}^{+\infty}\widehat{V_h}\sin(h\omega_1 t + \varphi_h) \end{cases} \begin{cases} + \text{ if } h\omega_1 \text{ is a positive sequence} \\ - \text{ if } h\omega_1 \text{ is a negative sequence} \end{cases}$$

Notice how zero-sequence terms result in a null space vector.
Now, the flux linkage:

$$\mathbf{\Psi_s} = \psi_{s,\alpha} + j\psi_{s,\beta}$$

with:

$$\begin{cases} \psi_{s,\alpha} = \int\left[\widehat{V_1}\cos(\omega_1 t) + \sum_{h=2}^{+\infty}\widehat{V_h}\cos(h\omega_1 t + \varphi_h)\right]dt \\ \psi_{s,\beta} = \int\left[\widehat{V_1}\sin(\omega_1 t) \pm \sum_{h=2}^{+\infty}\widehat{V_h}\sin(h\omega_1 t + \varphi_h)\right]dt \end{cases}$$

$$\begin{cases} \psi_{s,\alpha} = \frac{\widehat{V_1}}{\omega_1}\sin(\omega_1 t) + \sum_{h=2}^{+\infty}\frac{\widehat{V_h}}{h\omega_1}\sin(h\omega_1 t + \varphi_h) \\ \psi_{s,\beta} = -\frac{\widehat{V_1}}{\omega_1}\cos(\omega_1 t) \mp \sum_{h=2}^{+\infty}\frac{\widehat{V_h}}{h\omega_1}\sin(h\omega_1 t + \varphi_h) \end{cases} \begin{cases} - \text{ if } h\omega_1 \text{ is a positive sequence} \\ + \text{ if } h\omega_1 \text{ is a negative sequence} \end{cases}$$

Considering only the fundamental component of the stator current, its space vector is:

$$\mathbf{i_s} = i_{s,\alpha} + ji_{s,\beta} = \begin{cases} i_{s,\alpha} = \widehat{I_1}\cos(\omega_1 t - \varphi_1) \\ i_{s,\beta} = \widehat{I_1}\sin(\omega_1 t - \varphi_1) \end{cases}$$

and recalling the electromagnetic torque T_{elm} expression in Equation A.1:

- $$\psi_{s\alpha}i_{s\beta} = \left[\frac{\widehat{V_1}}{\omega_1}\sin(\omega_1 t) + \sum_{h=2}^{+\infty}\frac{\widehat{V_h}}{h\omega_1}\sin(h\omega_1 t + \varphi_h)\right]\left(\widehat{I_1}\sin(\omega_1 t - \varphi_1)\right) =$$
$$= \frac{\widehat{V_1}\widehat{I_1}}{\omega_1}\sin(\omega_1)\sin(\omega_1 t - \varphi_1) + \sum_{h=2}^{+\infty}\frac{\widehat{V_h}\widehat{I_1}}{h\omega_1}\sin(h\omega_1 t + \varphi_h)\sin(\omega_1 t - \varphi_1)$$

- $$\begin{aligned}\psi_{s\beta} i_{s\alpha} &= \left[-\frac{\widehat{V_1}}{\omega_1}\cos(\omega_1 t) \mp \sum_{h=2}^{+\infty} \frac{\widehat{V_h}}{h\omega_1}\cos(h\omega_1 t + \varphi_h)\right]\left(\widehat{I_1}\cos(\omega_1 t - \varphi_1)\right) \\ &= -\frac{\widehat{V_1}\widehat{I_1}}{\omega_1}\cos(\omega_1)\cos(\omega_1 t - \varphi_1) \mp \sum_{h=2}^{+\infty} \frac{\widehat{V_h}\widehat{I_1}}{h\omega_1}\cos(h\omega_1 t + \varphi_h)\cos(\omega_1 t - \varphi_1)\end{aligned}$$

Substituting the previous ones into T_{elm} expression:

$$\begin{aligned}T_{elm} = \frac{3}{2} n_p \Bigg(&\frac{\widehat{V_1}\widehat{I_1}}{\omega_1}\sin(\omega_1)\sin(\omega_1 t - \varphi_1) + \sum_{h=2}^{+\infty} \frac{\widehat{V_h}\widehat{I_1}}{h\omega_1}\sin(h\omega_1 t + \varphi_h)\sin(\omega_1 t - \varphi_1) \\ &+ \frac{\widehat{V_1}\widehat{I_1}}{\omega_1}\cos(\omega_1 t)\cos(\omega_1 t - \varphi_1) \pm \sum_{h=2}^{+\infty} \frac{\widehat{V_h}\widehat{I_1}}{h\omega_1}\cos(h\omega_1 t + \varphi_h)\cos(\omega_1 t - \varphi_1)\Bigg)\end{aligned} \tag{A.2}$$

Now, considering that:

- $\cos(a)\cos(b) + \sin(a)\sin(b) = \cos(a - b)$;
- $\cos(a)\cos(b) - \sin(a)\sin(b) = \cos(a + b)$;

Equation A.2 becomes:

$$T_{elm} = \frac{3}{2} n_p \left[\frac{\widehat{V_1}\widehat{I_1}}{\omega_1}\cos(\varphi_1) + \begin{cases} \sum_{h=2}^{+\infty} \frac{\widehat{V_h}\widehat{I_1}}{h\omega_1}\cos((h-1)\omega_1 t + \varphi_1 + \varphi_h) & \text{if } h\omega_1 \text{ is a positive seq.} \\ \sum_{h=2}^{+\infty} \frac{\widehat{V_h}\widehat{I_1}}{h\omega_1}\cos((h+1)\omega_1 t - \varphi_1 + \varphi_h) & \text{if } h\omega_1 \text{ is a negative seq.} \end{cases}\right] \tag{A.3}$$

By looking at the expression of Equation A.3, it can be concluded that:

- a DC torque component arises from the interaction between iso-frequencies terms;
- $(h-1)\omega_1$ torque component from the interaction between a positive sequence voltage harmonic of index h and the fundamental current component;
- $(h+1)\omega_1$ torque component from the interaction between a negative sequence voltage harmonic of index h and the fundamental current component;

Considering a generic constant $l \in \mathbb{N}$, the generic voltage harmonic order can be divided in:

- $h = 3l$: zero sequence harmonic;
- $h = 6l + 1$: positive sequence harmonic;

- $h = 6l - 1$: negative sequence harmonic.

Then, the following statements hold true:

- zero sequence voltage harmonics result in a null space vector component: the net flux produced in the machine is null, thus no torque harmonics are produced;
- positive and negative sequence voltage harmonics produce torque harmonics located at $\omega_h = 6l\omega_1$;
- for a given $l^* \in \mathbb{N}$, the interaction between the stator current fundamental component and the two voltage harmonics of order $6l^* + 1$ (positive sequence) and $6l^* - 1$ (negative sequence) produce a torque harmonic at the same frequency $6l^*$.

A.2. Observability matrices

In this section, the observability matrices of the analyzed systems are listed.

NLESO

$$\mathbf{\Delta M_O} = \begin{bmatrix} 0 & 1.0 & 0 & 0 & 0 & 0 \\ 0 & 0 & 0 & 0 & 1.0 & 0 \\ 0 & 0 & 0 & 0 & 0 & 1.0 \\ 0 & 0 & 0 & 1.78 & 0 & 0 \\ 0 & 0 & 0 & 139.0 & -3.38 & 92.6 \\ 0 & 0 & 0 & -141.0 & -92.6 & -3.38 \\ 3.57 * 10^6 & -3.57 * 10^6 & 0 & 0 & 0 & -15.6 \\ 2.8 * 10^8 & -2.8 * 10^8 & 0 & -1.35 * 10^4 & -8550.0 & -1840.0 \\ -2.83 * 10^8 & 2.83 * 10^8 & 0 & -1.24 * 10^4 & 625.0 & -7320.0 \\ 0 & 0 & 6.36 * 10^6 & -6.35 * 10^6 & 1440.0 & 52.5 \\ -2.72 * 10^{10} & 2.72 * 10^{10} & 4.98 * 10^8 & -4.99 * 10^8 & 1.99 * 10^5 & -6.67 * 10^5 \\ -2.49 * 10^{10} & 2.49 * 10^{10} & -5.04 * 10^8 & 5.05 * 10^8 & 6.75 * 10^5 & 1.91 * 10^5 \\ -1.29 * 10^{13} & 1.29 * 10^{13} & 0 & 1.93 * 10^5 & -9720.0 & 5.57 * 10^7 \\ -1.01 * 10^{15} & 1.01 * 10^{15} & -4.84 * 10^{10} & 4.85 * 10^{10} & 6.11 * 10^7 & 4.38 * 10^9 \\ 1.03 * 10^{15} & -1.03 * 10^{15} & -4.44 * 10^{10} & 4.44 * 10^{10} & -2.0 * 10^7 & -4.36 * 10^9 \\ 3.88 * 10^{11} & -3.88 * 10^{11} & -2.29 * 10^{13} & 2.29 * 10^{13} & -5.15 * 10^9 & -1.91 * 10^8 \\ 9.84 * 10^{16} & -9.84 * 10^{16} & -1.8 * 10^{15} & 1.8 * 10^{15} & -4.05 * 10^{11} & -4.33 * 10^{11} \\ 9.01 * 10^{16} & -9.01 * 10^{16} & 1.83 * 10^{15} & -1.82 * 10^{15} & 4.03 * 10^{11} & -3.75 * 10^{11} \end{bmatrix}$$

$$\mathbf{\Delta M_{O1}} = \begin{bmatrix} 0 & 1.0 & 0 & 0 & 0 & 0 \\ 0 & 0 & 0 & 1.78 & 0 & 0 \\ 3.57 * 10^{6} & -3.57 * 10^{6} & 0 & 0 & 0 & -15.6 \\ 0 & 0 & 6.36 * 10^{6} & -6.35 * 10^{6} & 1440.0 & 52.5 \\ -1.29 * 10^{13} & 1.29 * 10^{13} & 0 & 1.93 * 10^{5} & -9720.0 & 5.57 * 10^{7} \\ 3.88 * 10^{11} & -3.88 * 10^{11} & -2.29 * 10^{13} & 2.29 * 10^{13} & -5.15 * 10^{9} & -1.91 * 10^{8} \end{bmatrix}$$

$$\mathbf{\Delta M_{O2}} = \begin{bmatrix} 0 & 0 & 0 & 0 & 1.0 & 0 \\ 0 & 0 & 0 & 139.0 & -3.38 & 92.6 \\ 2.8 * 10^{8} & -2.8 * 10^{8} & 0 & -1.35 * 10^{4} & -8550.0 & -1840.0 \\ -2.72 * 10^{10} & 2.72 * 10^{10} & 4.98 * 10^{8} & -4.99 * 10^{8} & 1.99 * 10^{5} & -6.67 * 10^{5} \\ -1.01 * 10^{15} & 1.01 * 10^{15} & -4.84 * 10^{10} & 4.85 * 10^{10} & 6.11 * 10^{7} & 4.38 * 10^{9} \\ 9.84 * 10^{16} & -9.84 * 10^{16} & -1.8 * 10^{15} & 1.8 * 10^{15} & -4.05 * 10^{11} & -4.33 * 10^{11} \end{bmatrix}$$

$$\mathbf{\Delta M_{O3}} = \begin{bmatrix} 0 & 0 & 0 & 0 & 0 & 1.0 \\ 0 & 0 & 0 & -141.0 & -92.6 & -3.38 \\ -2.83 * 10^{8} & 2.83 * 10^{8} & 0 & -1.24 * 10^{4} & 625.0 & -7320.0 \\ -2.49 * 10^{10} & 2.49 * 10^{10} & -5.04 * 10^{8} & 5.05 * 10^{8} & 6.75 * 10^{5} & 1.91 * 10^{5} \\ 1.03 * 10^{15} & -1.03 * 10^{15} & -4.44 * 10^{10} & 4.44 * 10^{10} & -2.0 * 10^{7} & -4.36 * 10^{9} \\ 9.01 * 10^{16} & -9.01 * 10^{16} & 1.83 * 10^{15} & -1.82 * 10^{15} & 4.03 * 10^{11} & -3.75 * 10^{11} \end{bmatrix}$$

$$\mathbf{\Delta M^{1}_{O2}} = \begin{bmatrix} 0 & 0 & 0 & 1.0 & 0 \\ 0 & 0 & 139.0 & -3.38 & 92.6 \\ 2.8 * 10^{8} & 0 & -1.35 * 10^{4} & -8550.0 & -1840.0 \\ -2.72 * 10^{10} & 4.98 * 10^{8} & -4.99 * 10^{8} & 1.99 * 10^{5} & -6.67 * 10^{5} \\ -1.01 * 10^{15} & -4.84 * 10^{10} & 4.85 * 10^{10} & 6.11 * 10^{7} & 4.38 * 10^{9} \end{bmatrix}$$

$$\mathbf{\Delta M^{1}_{O3}} = \begin{bmatrix} 0 & 0 & 0 & 0 & 1.0 \\ 0 & 0 & -141.0 & -92.6 & -3.38 \\ -2.83 * 10^{8} & 0 & -1.24 * 10^{4} & 625.0 & -7320.0 \\ -2.49 * 10^{10} & -5.04 * 10^{8} & 5.05 * 10^{8} & 6.75 * 10^{5} & 1.91 * 10^{5} \\ 1.03 * 10^{15} & -4.44 * 10^{10} & 4.44 * 10^{10} & -2.0 * 10^{7} & -4.36 * 10^{9} \end{bmatrix}$$

Luenberger-based Lipschitz Observer

$$\mathbf{M_{O}} = \begin{bmatrix} 0 & 1.0 & 0 & 0 & 0 & 0 \\ 0 & 0 & 0 & 0 & 1.0 & 0 \\ 0 & 0 & 0 & 0 & 0 & 1.0 \\ 0 & 0 & 0 & 1.78 & 0 & 0 \\ 0 & 0 & 0 & 0 & -3.38 & 0 \\ 0 & 0 & 0 & -144 & 0 & -3.38 \\ 3.57 * 10^{6}, & -3.57 * 10^{6}, & 0 & 0 & 0 & -15.9 \\ 0 & 0 & 0 & 0 & 11.4 & 0 \\ -2.89 * 10^{8} & 2.89 * 10^{8} & 0 & 487 & 0 & 1300 \\ 0 & 0 & 6.36 * 10^{6} & -6.35 * 10^{6} & 0 & 53.7 \\ 0 & 0 & 0 & 0 & -38.5 & 0 \\ 9.77 * 10^{8} & -9.77 * 10^{8} & -5.15 * 10^{8} & 5.15 * 10^{8} & 0 & -8730 \\ -1.29 * 10^{13} & 1.29 * 10^{13} & 0 & -7740 & 0 & 5.67 * 10^{7} \\ 0 & 0 & 0 & 0 & 130 & 0 \\ 1.04 * 10^{15} & -1.04 * 10^{15} & 1.74 * 10^{9} & -1.74 * 10^{9} & 0 & -4.6 * 10^{9} \\ -1.55 * 10^{10} & 1.55 * 10^{10} & -2.29 * 10^{13} & 2.29 * 10^{13} & 0 & -1.91 * 10^{8} \\ 0 & 0 & 0 & 0 & -439 & 0 \\ -3.53 * 10^{15} & 3.53 * 10^{15} & 1.86 * 10^{15} & -1.86 * 10^{15} & 0 & 3.1 * 10^{10} \end{bmatrix}$$

A.3. MISO Subsystems matrices

The MISO subsystems' transformed matrices are shown in numeric form: indeed, the algebraic form would involve big expressions containing the parameters that are already defined in Section 2.2.1 and Section 2.2.2.

Subsystem 1

$$\mathbf{z_1} = \begin{bmatrix} \Delta\theta_1 \\ 1.78\Delta\omega_1 \\ 3.57 * 10^6(\Delta\theta_t - \Delta\theta_1) - 15.6\Delta i_{sq} \\ 1.44 * 10^3\Delta i_{sd} + 52.5\Delta i_{sq} - 6.35 * 10^6\Delta\omega_1 + 6.36 * 10^6\Delta\omega_t \\ 5.57 * 10^7\Delta i_{sq} - 9.72 * 10^3\Delta i_{sd} + 1.29 * 10^{13}(\Delta\theta_1 - \Delta\theta_t) + 1.93 * 10^5\Delta\omega_1 \\ 3.88 * 10^{11}(\Delta\theta_t - \Delta\theta_1) + 2.29 * 10^{13}(\Delta\omega_1 - \Delta\omega_t) - 1.91 * 10^8\Delta i_{sq} - 5.15 * 10^9\Delta i_{sd} \end{bmatrix}$$

$$\mathbf{A_{z1}} = \begin{bmatrix} 0 & 1.0 & 0 & 0 & 0 & 0 \\ 0 & 0 & 1.0 & 0 & 0 & 0 \\ 0 & 0 & 0 & 1.0 & 0 & 0 \\ 0 & 0 & 0 & 0 & 1.0 & 0 \\ 0 & 0 & 0 & 0 & 0 & 1.0 \\ 0 & 4.68 * 10^9 & -3.09 * 10^{10} & -2.43 * 10^7 & -3.62 * 10^6 & -6.75 \end{bmatrix}$$

$$\mathbf{B_{z1}} = \begin{bmatrix} 0 & 0 \\ 0 & 0 \\ 0 & -2200 \\ 2.03 * 10^5 & 7420 \\ -1.37 * 10^6 & 7.86 * 10^9 \\ -7.28 * 10^{11} & -2.69 * 10^{10} \end{bmatrix}$$

$$\mathbf{C_{z1}} = \begin{bmatrix} 1 & 0 & 0 & 0 & 0 & 0 \end{bmatrix}$$

Subsystem 2

$$\mathbf{z_2} = \begin{bmatrix} \Delta i_{sd} \\ 92.6\Delta i_{sq} - 3.38\Delta i_{sd} + 139\Delta\omega_1 \\ 2.8 * 10^8(\Delta\theta_t - \Delta\theta_1) - 1.35 * 10^4\Delta\omega_1 - 1840\Delta i_{sq} - 8.5 * 10^3\Delta i_{sd} \\ 2.72 * 10^{10}(\Delta\theta_1 - \Delta\theta_t) - 4.98 * 10^8\Delta\omega_t - 4.99 * 10^8\Delta\omega_1 + 1.99 * 10^5\Delta i_{sd} - 6.67 * 10^5\Delta i_{sq} \\ 1.01 * 10^{15}(\Delta\theta_1 - \Delta\theta_t) + 4.85 * 10^{10}\Delta\omega_1 - 4.84 * 10^{10}\Delta\omega_t + 6.11 * 10^7\Delta i_{sd} + 4.38 * 10^9\Delta i_{sq} \end{bmatrix}$$

$$\mathbf{A_{z2}} = \begin{bmatrix} 0 & 1.0 & 0 & 0 & 0 \\ 0 & 0 & 1.0 & 0 & 0 \\ 0 & 0 & 0 & 1.0 & 0 \\ 0 & 0 & 0 & 0 & 1.0 \\ 4.68 * 10^9 & -3.09 * 10^{10} & -2.43 * 10^7 & -3.62 * 10^6 & -6.75 \end{bmatrix}$$

$$\mathbf{B_{z2}} = \begin{bmatrix} 141 & 0 \\ -477.0 & 1.31 * 10^4 \\ -1.21 * 10^6 & -2.6 * 10^5 \\ 2.82 * 10^7 & -9.42 * 10^7 \\ 8.62 * 10^9 & 6.18 * 10^{11} \end{bmatrix}$$

$$\mathbf{C_{z2}} = \begin{bmatrix} 1 & 0 & 0 & 0 & 0 \end{bmatrix}$$

Subsystem 3

$$\mathbf{z_3} = \begin{bmatrix} \Delta i_{sq} \\ -92.6\Delta i_{sd} - 3.38\Delta i_{sq} + 141\Delta\omega_1 \\ 2.83 * 10^8(\Delta\theta_1 - \Delta\theta_t) - 1.24 * 10^4\Delta\omega_1 - 7.32 * 10^3\Delta i_{sq} - 625\Delta i_{sd} \\ 2.49 * 10^{10}(\Delta\theta_1 - \Delta\theta_t) - 5.04 * 10^8\Delta\omega_t + 5.05 * 10^8\Delta\omega_1 + 6.75 * 10^5\Delta i_{sd} + 1.91 * 10^5\Delta i_{sq} \\ 1.03 * 10^{15}(\Delta\theta_t - \Delta\theta_1) + 4.44 * 10^{10}\Delta\omega_1 - 4.44 * 10^{10}\Delta\omega_t - 2.0 * 10^7\Delta i_{sd} - 4.36 * 10^9\Delta i_{sq} \end{bmatrix}$$

$$\mathbf{A_{z3}} = \begin{bmatrix} 0 & 1.0 & 0 & 0 & 0 \\ 0 & 0 & 1.0 & 0 & 0 \\ 0 & 0 & 0 & 1.0 & 0 \\ 0 & 0 & 0 & 0 & 1.0 \\ 4.68 * 10^9 & -3.09 * 10^{10} & -2.43 * 10^7 & -3.62 * 10^6 & -6.75 \end{bmatrix}$$

$$\mathbf{B_{z3}} = \begin{bmatrix} 0 & 141.0 \\ -1.31 * 10^4 & -477.0 \\ 8.82 * 10^4, & -1.03 * 10^6 \\ 9.54 * 10^7 & 2.7 * 10^7 \\ -2.82 * 10^9 & -6.15 * 10^{11} \end{bmatrix}$$

$$\mathbf{C_{z3}} = \begin{bmatrix} 1 & 0 & 0 & 0 & 0 \end{bmatrix}$$

A.4. NLESO Observation error systems' matrices

Subsystem 1:

$$\mathbf{A_{e1}} = \begin{bmatrix} -2100.0 & 1.0 & 0 & 0 & 0 & 0 & 0 \\ -1.89 * 10^{6} & 0 & 1.0 & 0 & 0 & 0, & 0 \\ -9.45 * 10^{8} & 0 & 0 & 1.0 & 0 & 0, & 0 \\ -2.84 * 10^{11} & 0 & 0 & 0 & 1.0 & 0, & 0 \\ -5.1 * 10^{13} & 0 & 0 & 0 & 0 & 1.0 & 0 \\ -5.1 * 10^{15} & 0 & 0 & 0 & 0 & 0 & 1.0 \\ -2.19 * 10^{17} & 0 & 0 & 0 & 0 & 0 & 0 \end{bmatrix} \quad \mathbf{B_{e1}} = \begin{bmatrix} 2100.0 \\ 1.89 * 10^{6} \\ 9.45 * 10^{8} \\ 2.84 * 10^{11} \\ 5.1 * 10^{13} \\ 5.1 * 10^{15} \\ 2.19 * 10^{17} \end{bmatrix} \quad \mathbf{C_{e1}} = \begin{bmatrix} 1 & 0 & 0 & 0 & 0 & 0 & 0 \end{bmatrix}$$

$$\mathbf{M_{Ce1}} = \begin{bmatrix} 2100.0 & -2.52 * 10^{6} & 2.27 * 10^{9} & -1.7 * 10^{12} & 1.12 * 10^{15} & -6.74 * 10^{17} & 3.75 * 10^{20} \\ 1.89 * 10^{6} & -3.02 * 10^{9} & 3.06 * 10^{12} & -2.45 * 10^{15} & 1.68 * 10^{18} & -1.04 * 10^{21} & 5.91 * 10^{23} \\ 9.45 * 10^{8} & -1.7 * 10^{12} & 1.84 * 10^{15} & -1.53 * 10^{18} & 1.08 * 10^{21} & -6.82 * 10^{23} & 3.94 * 10^{26} \\ 2.84 * 10^{11} & -5.44 * 10^{14} & 6.12 * 10^{17} & -5.25 * 10^{20} & 3.79 * 10^{23} & -2.42 * 10^{26} & 1.42 * 10^{29} \\ 5.1 * 10^{13} & -1.02 * 10^{17} & 1.18 * 10^{20} & -1.03 * 10^{23} & 7.58 * 10^{25} & -4.91 * 10^{28} & 2.9 * 10^{31} \\ 5.1 * 10^{15} & -1.05 * 10^{19} & 1.24 * 10^{22} & -1.1 * 10^{25} & 8.18 * 10^{27} & -5.36 * 10^{30} & 3.19 * 10^{33} \\ 2.19 * 10^{17} & -4.59 * 10^{20} & 5.51 * 10^{23} & -4.96 * 10^{26} & 3.72 * 10^{29} & -2.46 * 10^{32} & 1.47 * 10^{35} \end{bmatrix}$$

$$\mathbf{M_{Oe1}} = \begin{bmatrix} 1.0 & 0 & 0 & 0 & 0 & 0 & 0 \\ -2100.0 & 1.0 & 0 & 0 & 0 & 0 & 0 \\ 2.52 * 10^{6} & -2100.0 & 1.0 & 0 & 0 & 0 & 0 \\ -2.27 * 10^{9} & 2.52 * 10^{6} & -2100.0 & 1.0 & 0 & 0 & 0 \\ 1.7 * 10^{12} & -2.27 * 10^{9} & 2.52 * 10^{6} & -2100.0 & 1.0 & 0 & 0 \\ -1.12 * 10^{15} & 1.7 * 10^{12} & -2.27 * 10^{9} & 2.52 * 10^{6} & -2100.0 & 1.0 & 0 \\ 6.74 * 10^{17} & -1.12 * 10^{15} & 1.7 * 10^{12} & -2.27 * 10^{9} & 2.52 * 10^{6} & -2100.0 & 1.0 \end{bmatrix}$$

Subsystem 2 = Subsystem 3:

$$\mathbf{A_{e2}} = \mathbf{A_{e3}} = \begin{bmatrix} -1800 & 1 & 0 & 0 & 0 & 0 \\ -1.35 * 10^{6} & 0 & 1 & 0 & 0 & 0 \\ -5.4 * 10^{8} & 0 & 0 & 1 & 0 & 0 \\ -1.22 * 10^{11} & 0 & 0 & 0 & 1 & 0 \\ -1.46 * 10^{13} & 0 & 0 & 0 & 0 & 1 \\ -7.29 * 10^{14} & 0 & 0 & 0 & 0 & 0 \end{bmatrix} \quad \mathbf{B_{e2}} = \mathbf{B_{e3}} = \begin{bmatrix} 1800 \\ 1.35 * 10^{6} \\ 5.4 * 10^{8} \\ 1.22 * 10^{11} \\ 1.46 * 10^{13} \\ 7.29 * 10^{14} \end{bmatrix} \quad \mathbf{C_{e2}} = \mathbf{C_{e3}} = \begin{bmatrix} 1 & 0 & 0 & 0 & 0 & 0 \end{bmatrix}$$

$$\mathbf{M_{Ce2}} = \mathbf{M_{Ce3}} = \begin{bmatrix} 1.8 * 10^{3} & -1.89 * 10^{6} & 1.51 * 10^{9} & -1.02 * 10^{12} & 6.12 * 10^{14} & -3.37 * 10^{17} \\ 1.35 * 10^{6} & -1.89 * 10^{9} & 1.7 * 10^{12} & -1.22 * 10^{15} & 7.65 * 10^{17} & -4.33 * 10^{20} \\ 5.4 * 10^{8} & -8.5 * 10^{11} & 8.16 * 10^{14} & -6.12 * 10^{17} & 3.94 * 10^{20} & -2.27 * 10^{23} \\ 1.22 * 10^{11} & -2.04 * 10^{14} & 2.04 * 10^{17} & -1.57 * 10^{20} & 1.03 * 10^{23} & -6.06 * 10^{25} \\ 1.46 * 10^{13} & -2.55 * 10^{16} & 2.62 * 10^{19} & -2.07 * 10^{22} & 1.38 * 10^{25} & -8.18 * 10^{27} \\ 7.29 * 10^{14} & -1.31 * 10^{18} & 1.38 * 10^{21} & -1.1 * 10^{24} & 7.44 * 10^{26} & -4.46 * 10^{29} \end{bmatrix}$$

$$\mathbf{M_{Oe2}} = \mathbf{M_{Oe3}} = \begin{bmatrix} 1.0 & 0 & 0 & 0 & 0 & 0 \\ -1800.0 & 1.0 & 0 & 0 & 0 & 0 \\ 1.89 * 10^{6} & -1800.0 & 1.0 & 0 & 0 & 0 \\ -1.51 * 10^{9} & 1.89 * 10^{6} & -1800.0 & 1.0 & 0 & 0 \\ 1.02 * 10^{12} & -1.51 * 10^{9} & 1.89 * 10^{6} & -1800.0 & 1.0 & 0 \\ -6.12 * 10^{14} & 1.02 * 10^{12} & -1.51 * 10^{9} & 1.89 * 10^{6} & -1800.0 & 1.0 \end{bmatrix}$$

A.5. High-Pass (HP) Filter design

Each of the subsystems' NLESO needs as input:

- the oscillating terms of the v_{sd} and v_{sq} inputs: Δv_{sd} and Δv_{sq};
- each subsystem's output: $\Delta y_i = \Delta x_i$, with $i = 1, 2, 3$ (subsystem's number).

What is available from the real system are the measurements of the states, i.e. control system's outputs y_i, and the real value of the control variables v_{sd} and v_{sq}. In order to extract the oscillating term information from each quantity, a High-Pass (HP) Filter is used: its bandwidth should be chosen such that only the oscillating term is extracted from the measured and input variables.
Since the aim is to estimate the system state variables during the mechanical resonance condition, the filter cut-off frequency is chosen such that:

$$\omega_{HP,cut-off} = 2\pi \frac{f_{res}}{10} = 2\pi \frac{302.45}{10} = 190.03 \left[\frac{rad}{s}\right]$$

The filter transfer function in Laplace domain $HP(s)$ is defined as:

$$HP(s) = \frac{\tau s}{1 + \tau s} \tag{A.4}$$

where:

$$\tau = \frac{1}{\omega_{HP,cut-off}}$$

From Equation A.4 it is clear how:

$$|HP(s)| = \begin{cases} \tau s & \text{if} \quad |\tau s| << 1 \quad \rightarrow \quad |s| << \frac{1}{\tau} = \omega_{HP,cut-off} \\ 1 & \text{if} \quad |\tau s| >> 1 \quad \rightarrow \quad |s| >> \frac{1}{\tau} = \omega_{HP,cut-off} \end{cases}$$

The magnitude and phase Bode-diagrams of $HP(j\omega)$ is shown in Figure A.1.

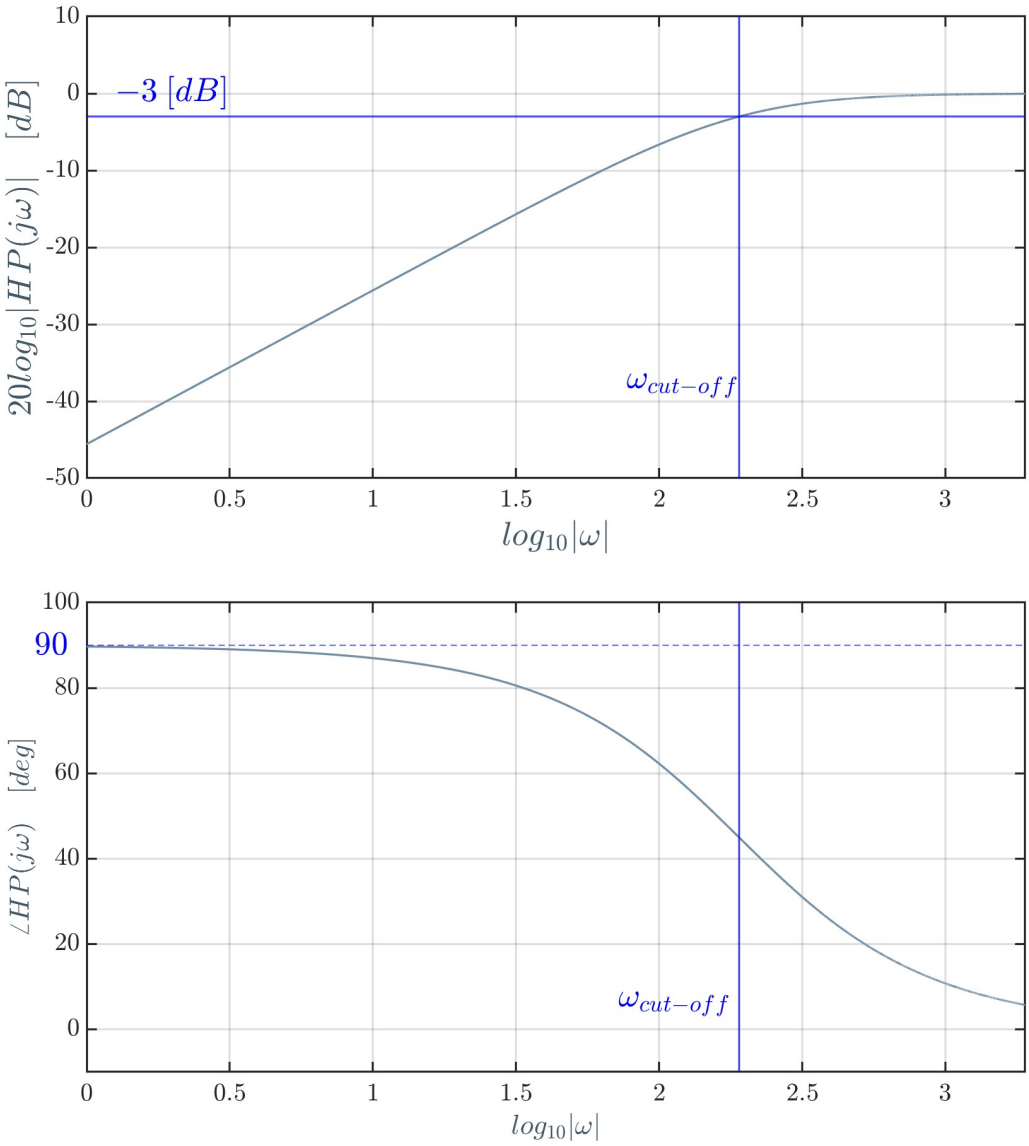

Figure A.1: magnitude (top) and phase (bottom) Bode-diagrams of $HP(s)$

A.6. Luenberger-based Lipschitz Observer script

```
clc
clear all
close all


set(groot,'defaulttextinterpreter','latex');
set(groot, 'defaultAxesTickLabelInterpreter','latex');
```

```
set(groot, 'defaultLegendInterpreter','latex');

%% p.u. base parameters and gamma calculation

Vn = 435; % [V]
Vb = sqrt(3)*Vn;
In = 713; % [A]
Ib = sqrt(3)*In;
fn = 14.73; % [Hz]
wb = 2*pi*fn; % [rad/s]
Zb = Vb/Ib; % [Ohm]
psib = Vb/wb; % [Wb]
Lb = Zb/wb; % [H]

psi_PM = double(8.314/psib); % [pu]
R = double(14.59e-3/Zb);
Ld = double(4.321e-3/Lb);
Lq = Ld;
p = double(104);
np = double(p/2);
jt = double(3e6); % kg*m^2
j1 = double(3.36e4);
k = double(1.2e11); % Nm/rad
wmb = wb/np;
Tn = 561e3; %Nm
Ht = 0.5*(jt*wmb^2)/(Tn*wmb); % [pu]
H1 = 0.5*(j1*wmb^2)/(Tn*wmb);

id_max = 1; % [pu]
iq_max = Tn/(np*Ib*psi_PM*psib);
w_max = 1;
gamma = max([wb*(iq_max+w_max) wb*(id_max+w_max)]);

%% State Space system definition

a13 = wmb;
a24 = wmb;
```

```
a31 = -k/(2*Ht*Tn); a32 = k/(2*Ht*Tn);
a41 = k/(2*H1*Tn); a42 = -k/(2*H1*Tn); a46 = -np*psi_PM*psib*Ib
   /(2*H1*Tn);
a55 = -wb*R/Ld;
a64 = -(psi_PM/Lq)*wb; a66 = -wb*R/Lq;

A = [0 0 a13 0 0 0;
     0 0 0 a24 0 0;
     a31 a32 0 0 0 0;
     a41 a42 0 0 0 a46;
     0 0 0 0 a55 0;
     0 0 0 a64 0 a66];

B = [0 0 0;
     0 0 0;
     1/(2*Ht*Tn) 0 0;
     0 0 0;
     0 wb/Ld 0;
     0 0 wb/Lq];

C = [0 1 0 0 0 0;
     0 0 0 0 1 0;
     0 0 0 0 0 1];

p2 = A*A;
p3 = p2*A;
p4 = p3*A;
p5 = p4*A;

Q = [C;
     C*A;
     C*p2;
     C*p3;
     C*p4;
     C*p5];

rQ = rank(Q,1e-15); % the system is observable
```

```
%% Observer Design Algorithm
% ... = -2CC^T = CtC
C1 = C'*C;
CtC = -2*C1;
% beta = gamma+1;
beta = 190;
% M = A^T+betaI
M = A'+beta*eye(size(A));
% Calculation of P
P = lyap(M,CtC);
P_inv = P\eye(6);
% Calculation of L
L = P_inv*(C');

%% Transfer function of the observation error system
% observation error system definition
Ae = A-L*C;
Be = zeros(6,2);
Be(5,1) = wb;
Be(6,2) = wb;
Ce = eye(6);
D = 0;

Ge = tf(sys); % G_e transfer function
```

B | Appendix B

It may be necessary to include another appendix to better organize the presentation of supplementary material.

B.1. Kernel Calculation

By the definition from [2], the kernel of a linear map $L(\mathbf{x}) : \mathbb{R}^{n'} \rightarrow \mathbb{R}^{m'}$ is the set of vectors $\mathbf{x} \in \mathbb{R}^{n'}$ which have as image the null vector of $\mathbb{R}^{m'}$, i.e.:

$$\ker(L) = \left\{ \mathbf{x} \in \mathbb{R}^{n'} \mid L(\mathbf{x}) = \mathbf{0} \in \mathbb{R}^{m'} \right\}$$

For example, considering [6]:

$$L(\mathbf{x}) : \begin{bmatrix} y_1 \\ y_2 \\ y_3 \end{bmatrix} = \underbrace{\begin{bmatrix} -1 & 0 & 1 \\ 0 & 0 & -1 \\ 0 & 0 & 1 \end{bmatrix}}_{\mathbf{L}} \begin{bmatrix} x_1 \\ x_2 \\ x_3 \end{bmatrix}$$

the kernel of the $\mathbf{L}$ can be calculated as:

$$\ker(\mathbf{L}) = \begin{bmatrix} x_1^* \\ x_2^* \\ x_3^* \end{bmatrix} \text{ such that: } \begin{bmatrix} -1 & 0 & 1 \\ 0 & 0 & -1 \\ 0 & 0 & 1 \end{bmatrix} \begin{bmatrix} x_1^* \\ x_2^* \\ x_3^* \end{bmatrix} = \begin{bmatrix} 0 \\ 0 \\ 0 \end{bmatrix}$$

which results in:

$$\begin{bmatrix} x_1^* \\ x_2^* \\ x_3^* \end{bmatrix} = \begin{bmatrix} 0 \\ 1 \\ 0 \end{bmatrix}$$

B.2. Lur'e Problem and Circle Criterion

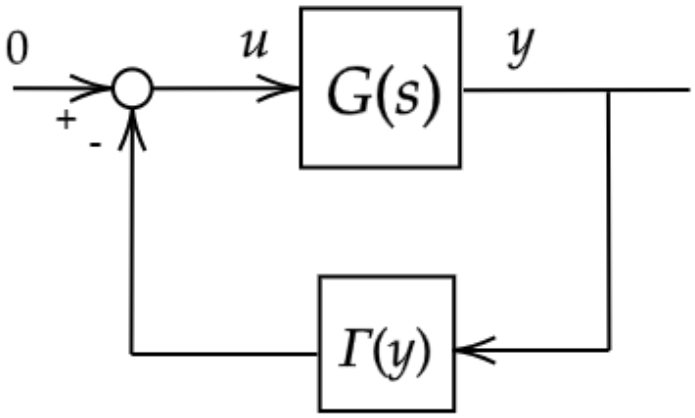

Figure B.1: nonlinear feedback system

Considering a generic linear system of n states $\mathbf{x}(t) \in \mathbb{R}^n$, $\mathbf{u}, \mathbf{y} \in \mathbb{R}^p$:

$$\begin{aligned} \dot{\mathbf{x}} &= \mathbf{A}\mathbf{x} + \mathbf{B}u \\ \mathbf{y} &= \mathbf{C}\mathbf{x} + \mathbf{D}\mathbf{u} \\ \mathbf{u} &= -\Gamma(t, \mathbf{y}) \end{aligned} \tag{B.1}$$

where $\mathbf{A} \in \mathbb{R}^{nxn}$, $\mathbf{B} \in \mathbb{R}^{nxp}$, $\mathbf{C} \in \mathbb{R}^{pxn}$, $\mathbf{D} \in \mathbb{R}^{pxp}$ and $\Gamma(t, .) : \mathbb{R}^p \to \mathbb{R}^p$ is a Lipschitz nonlinear function, possibly time-varying and piecewise continuous in t. Let us assume $\mathbf{D} = 0$ and that $\Gamma(t, \mathbf{y}) = \Gamma(\mathbf{y})$. Let us define the system transfer function:

$$\mathbf{G}(s) = \mathbf{C}\left(s\mathbf{I} - \mathbf{A}\right)^{-1}\mathbf{B} \tag{B.2}$$

If:

- $\Gamma(\mathbf{y})$ satisfies a sector condition (please refer to [12] page 232);
- $(\mathbf{A}, \mathbf{B})$ controllable:
- $(\mathbf{C}, \mathbf{A})$ observable;

then (B.1) represents a Lur'e problem, the origin represent an equilibrium point for the system; its absolute stability can be study applying the Circle Criterion if the system is SISO, thus if $p = 1$. For the theorem and its prove please refer to [12] page 270.

List of Figures

List of Tables

Acknowledgements

Here we are: my student career has come to an end. During these years, several people joined me in this journey and helped me complete it: I want to dedicate this space of my thesis to them.
Thanks to my parents, Attilio Deponti and Roberta Cremonesi, who gave me the possibility to study and supported me in every decision I took.
Thanks to my mentor, Carlo Cremonesi, who motivated me throughout all these years and taught me that there is always time to lend a hand to those who need help.
Thanks to my best friend and Mathematical Engineer Daniel Sima, for all the everlasting study sessions and mutual support.
Thanks to my girlfriend Ruxandra Mantea, to never stop believing in me and for showing me how life is simple after all.
Moreover, I want to express my deep gratitude to Prof. Roberto Perini and Dr. Dejan Pejovski, not only for the precious technical support and motivation but also for teaching me how to encourage others and how to value their work: I sincerely believe that this thesis has helped me grow both as a person and an engineer.